OBJECT-ORIENTED AND PIXEL-BASED IMAGE CLASSIFICATION USING LANDSAT MULTISPECTRAL AND HYPERION HYPERSPECTRAL IMAGERY IN BOREAL CONDITIONS

by

Jevon S. Hagens

A Graduate Thesis Submitted in
Partial Fulfillment of the requirements for the
Degree of Masters of Science in Forestry

Faculty of Forestry and the Forest Environment

Lakehead University

January 2008

Library and
Archives Canada

Published Heritage
Branch

395 Wellington Street
Ottawa ON K1A 0N4
Canada

Bibliothèque et
Archives Canada

Direction du
Patrimoine de l'édition

395, rue Wellington
Ottawa ON K1A 0N4
Canada

Canada

LIBRARY RIGHTS STATEMENT

In presenting this thesis in partial fulfillment of the requirements for the M.Sc.F degree at Lakehead University in Thunder Bay, I agree that the University will make it freely available for inspection.

This thesis is made available by my authority solely for the purpose of private study and research and may not be copied or reproduced in whole or in part (except as permitted by the Copyright Laws) without my written authority.

Signature: _____

Date _____

ABSTRACT

Current environmental trends dictate a need for new methods, initiatives, and technologies that provide reliable, up-to-date forest information. Canada, which is home to ten percent of the Earth's forests, has made national and international commitments to better monitor the sustainable development of its forest ecosystems. In Ontario, the Ministry of Natural Resources monitors its natural resources through the Ontario Land Cover Database (OLCD). The OLCD is a large area land classification that uses Landsat multispectral imagery with a traditional pixel-based classifier. The goal of this thesis is to explore new ways to improve upon large area land classifications such as the OLCD. This thesis evaluates two alternative approaches: (1) it compares Landsat-5 TM multispectral imagery to Hyperion hyperspectral imagery, and (2) it compares a traditional pixel-based classifier to eCognition's object-oriented image classifier. Eight boreal cover classes were used consisting of water, wetland (aggregated marsh, fen and bog), black spruce, jack pine, mixedwood, dense deciduous, sparse deciduous and clearcuts.

The objectives of this study were to: (1) identify the optimal method for reducing image dimensionality, (2) identify wavelength regions that best contribute to the separation between taxonomic groups and species, (3) determine whether a hyperspectral sensor can improve classification accuracy over a multispectral sensor, (4) identify ecological factors that can be used to explain classification error, and (5) explore the potential of eCognition's object-oriented image classifier. Feature selection using six Landsat bands and a discriminant function analysis for Hyperion was a more optimal method in reducing image dimensionality than principal component analysis for both sensors. Hyperion wavelengths used range from 0.50 μm to 2.32 μm. Ecological factors used to explain classification error included age of vegetation, ecosystem type and species composition. Overall accuracy using a pixel-based classifier was 87.82% for Hyperion and 79.69% for Landsat. Overall accuracy using an object-oriented classifier was 87.82% for Hyperion and 85.04% for Landsat. The main finding of this study is that, although hyperspectral imagery can improve classifications, it is not necessary to wait for hyperspectral imagery to become economically feasible in order to improve classifications. For the present time, the most practical method for potentially improving large land cover classification accuracy, such as the OLCD, is to change from a pixel-based to an object-oriented image classifier.

IV

CONTENTS

IX

TABLES

Table   Page

FIGURES

ACKNOWLEDGEMENTS

INTRODUCTION

Current environmental trends dictate a need for new methods, initiatives, and technologies that provide reliable, up-to-date forest information. Canada, which is home to ten percent of the Earth's forests, has made national and international commitments to better monitor the sustainable development of its forest ecosystems (Goodenough *et al.* 2002). International commitments, such as the Kyoto Protocol (United Nations 1998), obligate Canada to provide accurate reports on environmental sustainability. National commitments, such as the Canadian Biodiversity Strategy, acknowledge the need for reliable up-to-date information on biodiversity (Environment Canada 1995). In response to the increasing pressure, the Canadian Forest Service and the Canadian Space Agency developed the Earth Observation for Sustainable Development of Forests (EOSD) initiative. This initiative involves the use and development of space-based technology for land cover mapping, monitoring change, and estimating biomass.

Large-area land cover mapping programs in Canada presently use multispectral satellite imagery with traditional pixel-based image classifiers. The 1995 Land Cover Map of Canada, for example, uses low 1km spatial resolution Advanced Very High Resolution Radiometer (AVHRR) imagery (Cihlar *et al.* 1999). This map was produced by Natural Resources Canada and the Canada Centre for Remote Sensing, and consists of 29 broad land cover classes (Franklin and Wulder 2002). The most detailed provincial wide land cover map in Ontario is the Ontario Land Cover Classification Database (OLCD). It was produced by the Ontario Ministry of Natural Resources

(OMNR), and was derived from medium 30m resolution Landsat imagery, and consists of 27 classes (Spectranalysis 1999).

The newest edition to satellite remote sensing imagery is the hyperspectral sensor, such as Hyperion on the EO-1 spacecraft. This technology has the potential to improve upon the use of multispectral sensors (Goodenough *et al.* 2002). Existing methods and automated tools to deal with hyperspectral imagery, however, are primitive and more research is needed before large-area applications are feasible. In addition to new satellite sensors, new knowledge-based classifiers, such as Definiens' eCognition object-oriented image classifier, have been developed. Although eCognition has potential for improving traditional image classifiers, it is currently not used for large-area land cover classifications in Canada.

This thesis compares the ability of Hyperion hyperspectral and Landsat multispectral satellite imagery to perform large-area land cover classifications similar to that of the OLCD. The use of both a traditional pixel-based and eCognition's object-oriented image classifier are addressed. The focus taxonomic groups and species used in this thesis are found in the upland areas of the boreal forest of northwestern Ontario, an area not yet researched with the Hyperion sensor. If research shows that these new technologies can provide improvements over currently used technology, then it may be worth investing more into new technologies, so that they become more economically feasible for large-area land classification programs in the future, and contribute to Canada's commitments to monitoring the sustainability of its forest ecosystems.

GOALS & OBJECTIVES

This thesis assesses the feasibility of medium resolution multispectral and hyperspectral imagery to perform large-area land classification using pixel-based and object-oriented classifiers. It focuses on upland taxonomic and species classes in the boreal forest. The goal of this thesis is to discover new ways to improve large area land classifications such as the OLCD, using alternative methods applicable for the present time, as well as for in the future when new advances in spatial, spectral and radiometric properties of remotely sensed imagery become available. The specific objectives of this thesis are as follows:

1. Identify the optimal method (principal component analysis or feature selection) for reducing image dimensionality. Current image classifiers perform poorly if too many bands, such as the large number found in hyperspectral imagery, are used in a classification. It is difficult to hypothesize which method will be optimal because of the lack of literature on this subject;

2. Identify the wavelength regions that best contribute to the separation between taxonomic groups and species. Bands located in the infrared region are expected to best contribute to the separation, because infrared is the most sensitive to vegetation;

3. Determine whether a hyperspectral sensor can improve classification accuracy over a multispectral sensor. Since hyperspectral imagery contains more spectral information then multispectral, it is expected that the hyperspectral will produce a more accurate classification. If this is true, then it may be worth investing more into hyperspectral technology for future use;

4. Identify ecological factors that can be used to explain classification error. The understanding of the factors that cause error in a classification is essential for improving future classifications. It is expected that factors such as vegetation age, ecosystem class and species composition will contribute to classification error;

5. Determine whether eCognition's new object-oriented classifier can improve accuracy over a traditional pixel-based classifier. ECognition is expected to provide a more accurate classification because of its ability to also include spatial information into its classification.

LITERATURE REVIEW

3.1 REMOTE SENSING

Remote sensing is the study of an object, area or phenomenon through the use of a data capturing device not in contact with the object, area or phenomenon (Lillesand *et al.* 1994). For the purpose of this thesis, remote sensing refers to sensors from spacecraft and aircraft that capture electromagnetic energy in the form of digital images used for mapping the Earth's surface.

Objects on the earth's surface reflect electromagnetic radiation from the Sun's rays. This reflected energy can be measured by a remote sensor at different wavelengths along the electromagnetic spectrum (Figure 1). The human eye for example, captures reflections within the blue (0.4 - 0.5 μm), green (0.5 - 0.6 *μm*), and red (0.6 - 0.7 *μm*) wavelengths, known as the visible component of the spectrum. Although the human eye cannot detect radiation within infrared range of the electromagnetic spectrum, infrared is optimum for obtaining information on vegetation (Jensen 2005). This study focuses on the remote sensors that record data within the visible and infrared range of the electromagnetic spectrum.
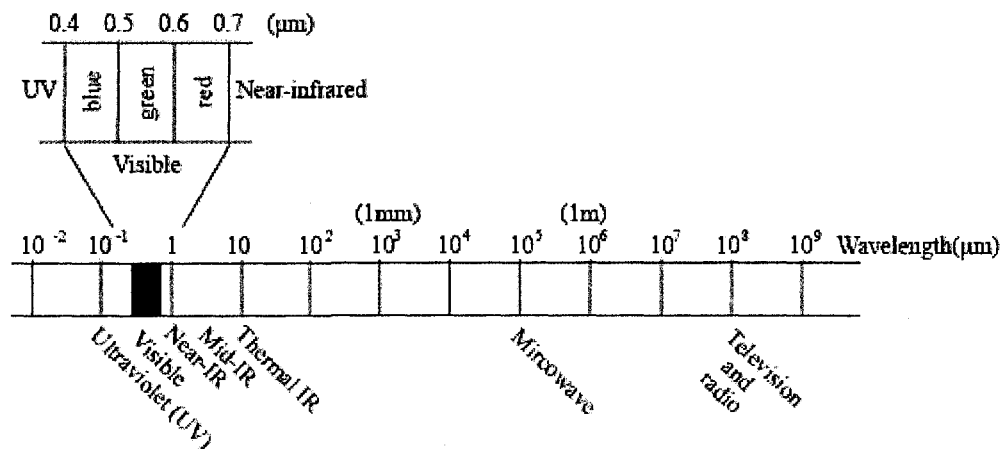
Figure 1. Section of the electromagnetic spectrum measured in micrometers (*μm*) (Lillesand and Kiefer 1994).

3.2 MULTISPECTRAL IMAGERY

Commercial multispectral satellite sensors have been around since 1972, when the first Landsat satellite was launched into space. The term multispectral refers to images from remote sensors that have a few spectral bands covering broad ranges of the electromagnetic spectrum (Jensen 2005). For example, a blue band may record the average wavelength of 0.4-$0.5\mu m$, instead of a more narrow wavelength range of 0.448-$0.458\mu m$. In general, each band represents an average wavelength range.

Since the launch of the first multispectral satellite, Landsat-1, many more multispectral satellite sensors, with varying spatial and spectral resolutions, have become commercially available and viable. Advanced Very High Resolution Radiometer (AVHRR) for example, is a low cost sensor available since 1978 (NOAA 2005). It has a 1 kilometer (km) spatial resolution, and cost $190 US per image, with each image covering 2400 by 6400 km's in size (USGS 2006). Spatial resolution refers to the ground area in which a pixel covers (Jensen 2005). The most recent Satellite Probatoire d'Observation de la Terre sensor (SPOT-5) was launched in 2002 and offers a 10m multispectral image covering the green to mid infrared (MIR) range of the spectrum (Spot Image 2006). A full size SPOT image is 60 by 60 km's in size, and cost approximately $1900 and $3375 for a 20m and 10m spatial resolution image respectively (Spatial Mapping 2007). IKONOS offers a 4 m spatial resolution image at $18 CAN per square km with a small 11-13 km image width. The Quickbird senor offers a multispectral image with the highest spatial resolution commercially available (2.44m), and has a standard image size is 16.5 by 16.5km. With a cost of approximately $22 per square km, it is also the costliest. The most widely used satellite

sensors are from the Landsat series. Landsat-5 TM for example, offers an image with a

30 m spatial resolution for all bands except for the thermal which is 120 m. Each image

cost approximately $500 and covers and an area of 185 by 172 km (MacDonald, *et al.*

2007).

Current available Landsat sensors include Landsat-5 and 7. Although Landsat-5

Thematic Mapper (TM) has been available since 1984, and is past its life expectancy, it

continues to record images. Its seven bands cover the blue (0.45-0.52μm) green (0.52-

0.60 μm), red (0.63-0.69 μm), Near-infrared NIR (0.76-0.90 μm), mid-infrared MIR

(1.55-1.75 μm), far-infrared FIR (2.08-2.35 μm) and thermal (10.40-12.50 μm) ranges of

the spectrum. Landsat-7 Enhanced Thematic Mapper (ETM+) was launched in 1999. It

has similar bands to Landsat-5, but its thermal band is 60m and also has a panchromatic

(black and white) band. In May 2004, the scan line corrector (SLC) failed on the

Landsat-7, resulting in dark stripes throughout the image. The next sensor to collect

Landsat like data will be the Operational Land Imager (OLI) and is scheduled to be

launched in 2011. Landsat-5 TM is the first of the two sensors compared in this thesis.

3.3 HYPERSPECTRAL IMAGERY

Hyperspectral satellite sensors are the newest addition to remote sensing

technology. The first such sensor, known as Hyperion, was launched in 2000 onboard

NASA's Earth Observation-1 (EO-1) satellite (USGS 2005). The term hyperspectral

refers to images from remote sensors that have many spectral bands, each covering

narrow sections of the electromagnetic spectrum. For example, instead of having one

blue band that recorded an average of 0.4-0.5 μm similar to multispectral imagery, a

hyperspectral image can have many bands within the blue section of the spectrum (e.g. 0.401-0.410, 0.411-0.420...0.491-0.500 μm).

There are currently only two hyperspectral satellites sensors commercially available, known as Hyperion and the Compact High Resolution Imaging Spectrometer (CHRIS). The CHRIS sensor is on the European Space Agency's Project for On-Board Autonomy (PROBA) satellite. It was launched in 2001 on a technology validation/demonstration mission, and has 63 bands with a 36m spatial resolution (European Space Agency 2005). The Hyperion sensor is the second of two sensors compared in this thesis. Its imagery is collected with two spectrometers, one collecting within the visible and nir-infrared (VNIR) range of the spectrum (bands 1-70, 356-1058nm), and the other within the short wave infrared (SWIR) range of the spectrum (bands 71-242, 852-2577nm), totaling 242 bands (Barry 2001). Hyperion has a 30m spatial resolution with images 7.5 km wide and 40-100 km long, and has a poorer quality signal-to-noise (S/N) ratio than Landsat-5 TM. The cost can range from approximately 1-4 thousand dollars US depending on scene length and tasking requirements (USGS 2007).

3.4 MULTISPECTRAL VS. HYPERSPECTRAL

The main difference between multispectral and hyperspectral imagery is the spectral resolution. Hyperspectral sensors have high spectral resolutions and collect many continuous spectral bands with narrow wavelengths (Aspinall *et al.* 2002; Smith 2001). Multispectral sensors have relatively low spectral resolutions and collect only a few spectral bands with broad wavelengths (Aspinall *et al.* 2002; Smith 2001).

Since many surface materials have diagnostic absorption features that are 10 to 20 nm wide, hyperspectral imagery has an advantage over multispectral imagery in identifying surface material (Jensen 2005). Figures 2 and 3 compare the spectral properties of jack pine with Landsat multispectral and Hyperion hyperspectral data collected in this thesis. The hyperspectral data clearly provides more detailed spectral information than the multispectral data. Hyperspectral imagery, however, has poorer quality signal to noise ratio than multispectral imagery and atmospheric correction is usually necessary (Jensen 2005).
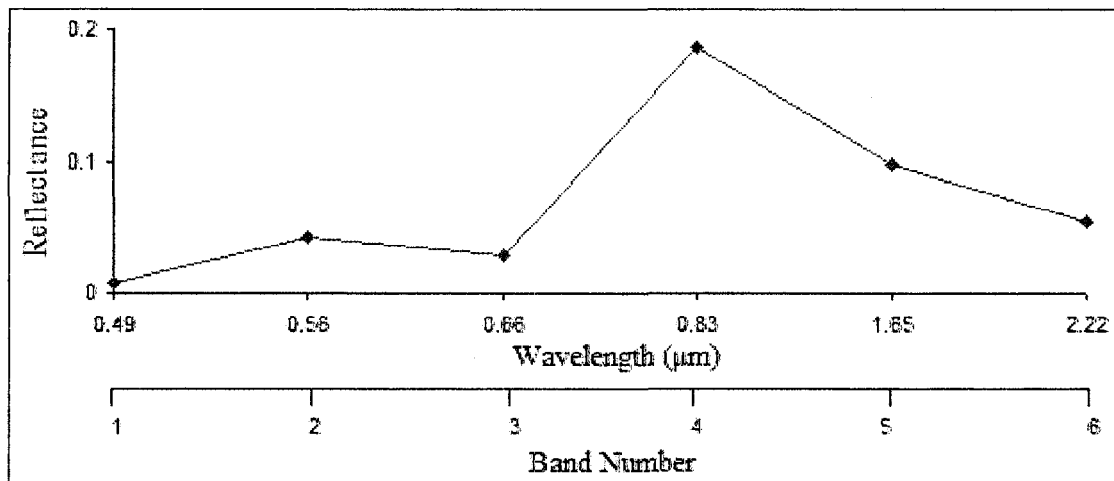
Figure 2. Spectral graph of jack pine extracted from a Landsat multispectral image.
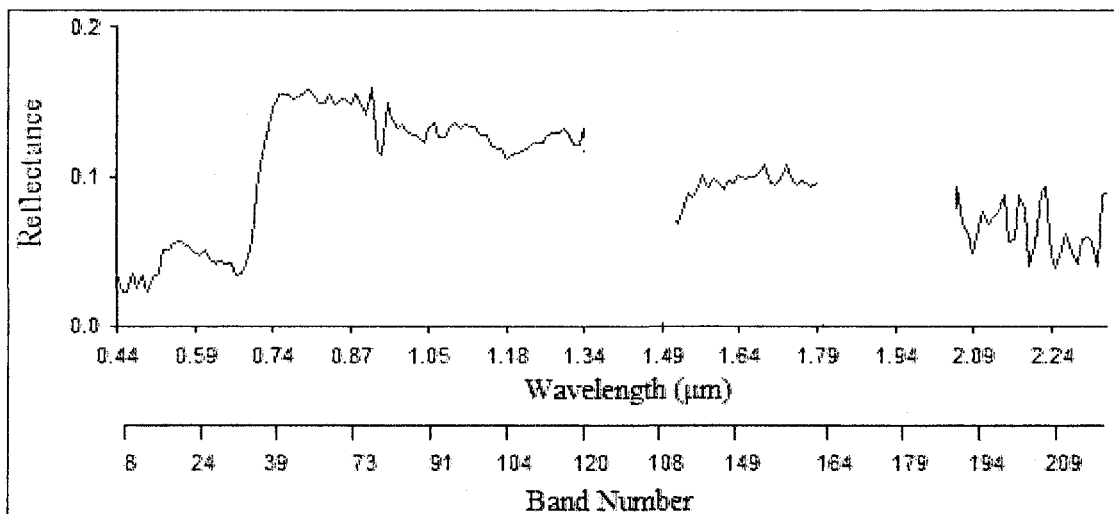
Figure 3. Spectral graph of jack pine, extracted from a Hyperion hyperspectral image.

One advantage of the high spectral resolution of hyperspectral imagery is the ability to measure canopy chemistry. Canopy chemistry can be used to identify tree species, measure old and new foliage (age), and detect stress (Goodenough *et al.* 2001; Martin *et al.* 1998). Figures 4 and 5 graphically demonstrate the ability of measuring reflectance to observe canopy chemistry such as stress, and show differences among vegetation.
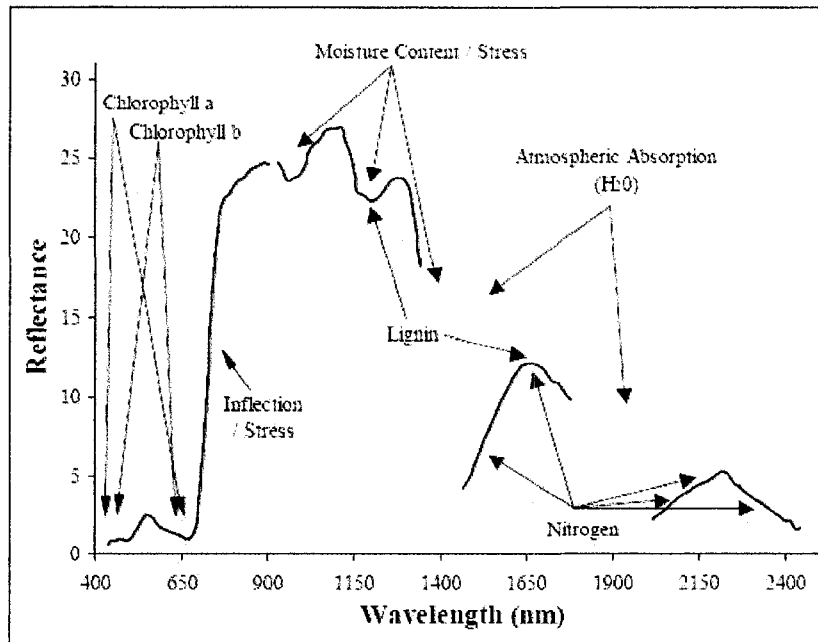
Figure 4. Vegetation chemistry measured from reflectance in the electromagnetic spectrum (Goodenough 2002).
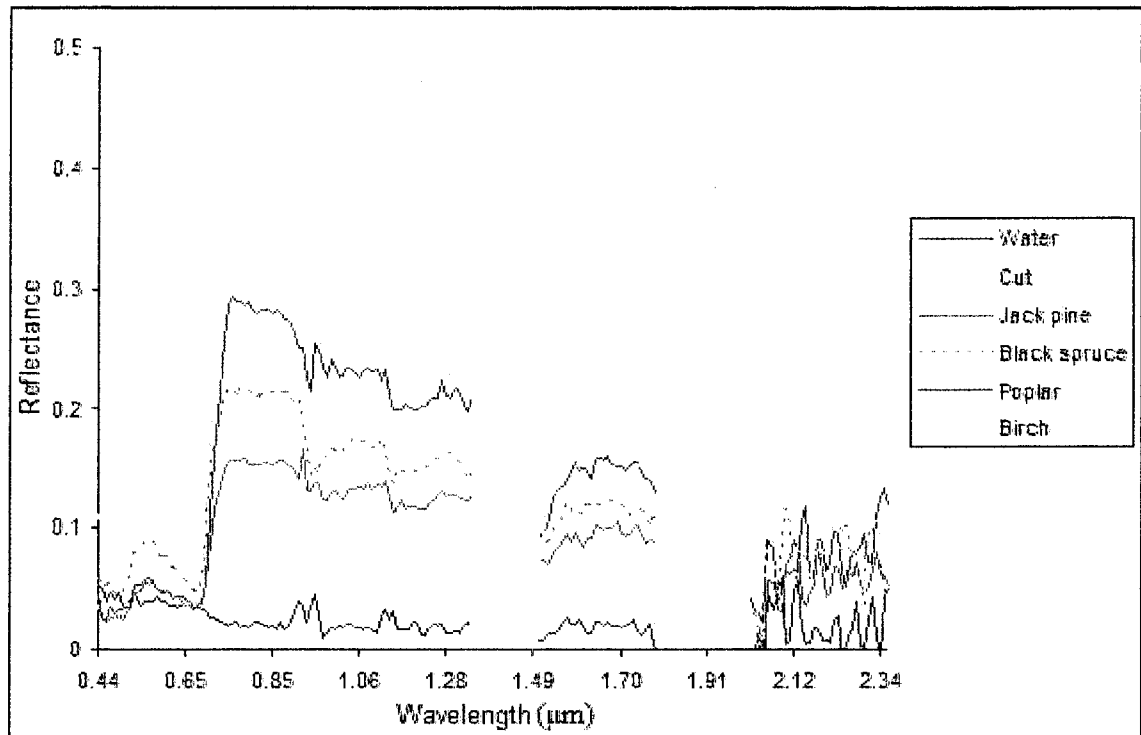
Figure 5. Spectral reflectance curves showing differences between water, clear cuts, jack pine, black spruce, poplar and white birch samples collected in this thesis.

Studies comparing multispectral and hyperspectral imagery demonstrate that hyperspectral produces higher accuracy results when classifying forest species. Goodenough *et al.* (2002) showed that classifying forests on Vancouver Island with Hyperion and Landsat satellite sensors yield overall accuracies of 92.9% and 75% respectively. Foster and Townsend (2004) demonstrated overall accuracy improvements with single date Hyperion over multi-date Landsat imagery for forest classification in the Central Appalachians. In their study, Hyperion and Landsat imagery yielded accuracies of 64.4% and 62% respectively. Thenkabail *et al.* (2004) compared Hyperion imagery to multispectral imagery (IKONOS, Advanced Land Imager, Landsat ETM+), to quantify and model biomass of tree, shrub and weed species, as well as characterizing forest land use/land cover classes (LULC) in an African rainforest. Results showed that multispectral models only explained 13-60% of

the variability in biomass, whereas Hyperion models explained 36-60% of the variability. The overall accuracy for LULC was between 42-51% for multispectral imagery, and 96% for Hyperion.

3.5 LAND COVER MAPPING

3.5.1 Forest Resource Inventory (FRI)

In Ontario, both forest companies and government estimate forest resource inventory (FRI) attributes, such as species composition, stand density, height, age, quantity, site index, and crown closure for forest management purposes. Extracting FRI data of this nature is expensive and time consuming to update and develop (Goodenough *et al.* 2002). The traditional and most utilized method for extracting FRI data uses manual interpretation of high resolution aerial photographs along with ground collected data (Treitz and Howarth 1996; Gillis and Leckie 1996).

Since September 29, 2005 the Ontario Ministry of Natural Resources has been undergoing a program to update Ontario's FRI (OMNR 2007). Digital aerial photography capturing black and white imagery at 20 cm resolution and color infrared imagery at 40 cm resolution will be used. Ground survey plots will be used to supplement aerial photographs in acquiring forest and non-forest attributes. As part of the new FRI mandate, FRI's in Ontario will be updated on a 10 year cycle (OMNR 2007).

Studies using single-date medium resolution multispectral imagery for FRI purposes have shown mixed results. Karteris (1990) showed that Landsat Thematic Mapper (TM) imagery is capable of separating conifer species with an overall

classification accuracy of 92.4% in central Michigan. Fiorella and Ripple (1993) demonstrated that Landsat TM imagery can be used to classify conifer succession stages in the central Cascade Range of Oregon conifers with an overall accuracy of 78.3%. Wordoyo and Jordan (1996), however, found Landsat TM classification accuracies not accurate enough for forest management applications in New Brunswick. In their study, the overall accuracy was 79% and 52% for species type and age class classification respectively. Only four broad forest units, such as hardwood and softwood, were used in their study. Moore and Bauer (1990) studied the use of Landsat TM imagery for classifying forest units appropriate for forest management purposes in north central Minnesota. Their study obtained overall accuracies between 63-67%. One method that could be use to increase single-date classification accuracies is to use a multi-temporal dataset. Multi-temporal refers classifications that use two or more images over a single area taken at different times of the year.

Research using multi-temporal multispectral imagery has demonstrated improved results over single-date imagery. Mickelson *et al.* (1998) demonstrated an overall accuracy of 78.9% when classifying genus level forest classification in northwestern Connecticut using Landsat TM imagery. Wolter *et al.* (1995) also showed that multi-temporal Landsat TM imagery can produce an overall species level accuracy of 80.1% in northwestern Wisconsin. One of the major drawbacks of using multi-temporal dataset, is that it is difficult to receive multiple cloud free images over an area within a single growing season. It could therefore take several years to get a complete dataset, particularly for classifications covering a large area.

Regardless of the ability for medium resolution multispectral imagery to classify forests at the FRI level, it is currently not being used in Canada. Possible reasons for this, other than classification accuracies, is its inability to be used for the collection of other FRI attributes such as stand density, height, age, quantity, site index, and crown closure. If medium resolution imagery is used, all additional attributes must still be collected in the field which would be costly. In essence, medium resolution satellite imagery is designed for acquiring cover types, not detailed information such as species classification, species composition and age level characteristics such as found in the FRI.

3.5.2 Land Cover Map of Canada

The Land Cover Map of Canada was developed by Natural Resources Canada and the Canada Centre for Remote Sensing (Natural Resources Canada 2004). It is based on satellite imagery obtained in 1995 by the Advanced Very High Resolution Radiometer (AVHRR). Its pixels, which have a 1 km spatial resolution, are classified into 31 general classes; 12 forest; 3 shrub land; 7 tundra/grasslands; 7 developing land types and 2 water classes. Forest types include 6 coniferous forests with varying densities and northern/southern locations, one broadleaf forest, 3 mixed wood forests, and 2 types of burns. The role of the Land Cover Map of Canada is to provide information for international environmental conventions on climate, desertification and biodiversity. With its large spatial resolution and general classes, the Land Cover Map of Canada is not capable of monitoring vegetation at a more detailed level such as found in the Ontario Land Cover Database (OLCD).

3.5.3 <u>Ontario Land Cover Database (OLCD)</u>

The OLCD is the most detailed provincial wide land classification in Ontario. It is produced by the OMNR using 30m spatial resolution data obtained by Landsat-5 and 7. The first edition was developed in 1995. The second and most recent edition, known as the 2000 Edition, consists of 27 broad land cover types across Ontario (Table 1). It was completed in 2004 and uses data obtained in 1999 and 2000. This thesis uses cover types similar to the OLCD. See Appendix I for a detailed description of the OLCD classes that are similar to those used in this thesis.

Table 1. Hierarchy of the OLCD 2nd edition land cover classes.

Category Level 1	Category Level 2	Category Level 3	Class Name	Class Number
Non-Vegetated	Water	Deep or Clear	Water - Deep or Clear	1
		Shallow or Sedimented	Water - Shallow or Sedimented	2
	Land	Settlement/ Infrastructure	Settlement/Infrastructure	3
		Sand/Gravel	Sand/Gravel/Mine Tailings	4
		Bedrock	Bedrock	5
		Mudflats	Mudflats	6
	Depletion	Cuts	Cuts	7
		Burns	Burns	8
Vegetated	Forest	Regenerating Depletion	Regenerating Depletion	9
		Sparse	Sparse Forest	10
		Dense	Deciduous Forest	11
			Mixed Forest	12
			Coniferous Forest	13
	Wetland	Marsh	Intertidal Marsh	15
			Supertidal Marsh	16
			Inland Marsh	17
		Swamp	Deciduous Swamp	18
			Coniferous Swamp	19
		Fen	Open Fen	20
			Treed Fen	21
		Bog	Open Bog	22
			Treed Bog	23
	Tundra	Tundra	Tundra Heath	24
	Agriculture	Pasture	Pasture	25
		Cropland	Cropland	27
Other	Other	Other	Other (Undefined)	28
			Cloud and Shadow	29

3.5.4 Research and Development

Canadian forest measuring and monitoring research with hyperspectral satellite sensors is being carried out through the Earth Observation for Sustainable Development of Forests (EOSD) initiative. EOSD programs are researching into the development large area land cover maps, including the development of change monitoring

techniques, estimating biomass, and automating processes (Natural Resources Canada 2004). The two EOSD branches that research Hyperspectral satellite sensors are the evaluation and validation of EO-1 for sustainable development (EVEOSD) branch, and the evaluation and validation of CHRIS for national forests (EVC) branch. Research areas include the Victoria and Clayoquot Sound British Columbia, Hilton Alberta, Northern Manitoba, Central Saskatchewan, and Algoma Ontario (Natural Resources Canada 2003).

Canadian projects exploring the use of new potential image classifiers, such as Definiens' eCognition object-oriented image classifier, are limited. One project that does exist involves the Canadian Space Agency, Ducks Unlimited, Environment Canada and several other organizations working on a project using eCognition in the development of a Canadian National Wetland Inventory (PCI Geomatic 2003).

3.6 SAMPLING

The most ideal method of performing error estimation when classifying an image is to use ground reference test pixels through the use of ground truth plots. Ground truth plots can be obtained either in the field using a GPS, or from remotely sensed imagery that has a higher spatial resolution than the image being classified, as such derived from aerial photography. In addition, the reliability of a ground truth plot can vary depending on its size compared to the spatial resolution of the classified image.

Congalton and Kass (1999) describe the 3x3 pixel as the most common choice for sample unit size, and acknowledge how this method takes a one pixel image

rectification error into consideration. Image rectification error, also known as geometric error, refers to distortion between an image and the GIS data it is associated with. They also recommend a minimum sample size of 50 samples per class as a general guideline for each land cover category, and a minimum of 75-100 samples per class for areas greater than 404,685 ha (one million acres) or for more than 12 classes. Stehman 2001, indicated that a land classification sample size of 100 per class ensures accuracy assessments with a standard error of 0.5 or less. Others such as Goodchild *et al.* 1994, recommend a minimum of 30 to 50 samples per class.

3.7 IMAGE CLASSIFIERS

The most common approach to extracting thematic information from remotely sensed imagery, as used for land cover classifications, is through statistical pattern recognition (Jensen 2005). This automated approach can categorize pixels based on characteristics such as spectral value, image texture, spatial size, and spatial relationship to surrounding pixels. This thesis uses two main types of statistical pattern recognitions. The first is the traditional method, also known as per-pixel analysis, where each individual pixel is classified based on its individual spectral value. The second is a newer object-oriented approach, in which pixels are first grouped (segmented) into objects, then classified based on pattern, texture, object size and spectral value and relationship to surrounding objects and pixels (Jensen 2005).

3.7.1 Traditional (Pixel-based) Classification

Traditional (pixel-based) image classifiers, are well established and commonly utilized methods in land cover mapping. These classifiers class each individual pixel

separately. Two of the most universal traditional classifier algorithms are known as supervised and unsupervised classification. Unsupervised classification is generally used when ground reference data is not available and land cover types are not well defined or known. It groups pixels based on spectral characteristics using unique statistical clustering. Supervised classification is generally used when ground reference data is available and land cover types are clearly defined. This thesis takes a supervised classification approach for its traditional classifier.

With the supervised classification algorithm, the analyst uses training sites, or pixels that intersect ground reference data grouped into homogeneous land cover types, to provide data for the algorithm. The algorithm uses spectral properties of the training pixels to calculate multivariate statistics such as mean, standard deviation, covariance matrices and correlation matrices. Based on the multivariate statistics, each individual pixel is classified into a cover type.

The supervised classification algorithm can use either parametric or non-parametric decision rules. Parametric methods assume the remotely sensed data is normally distributed, where as non-parametric does not (Jensen 2005). This thesis used the Gaussian Maximum Likelihood Classifier parametric rule, one of the most widely used supervised classification algorithms. It utilizes the mean vector and a covariance matrix to create statistical probabilities, assigning each unknown pixel to a class based on highest probability. Other decision rules such as the non-parametric Parallelepiped and the parametric Minimum Distance are disadvantaged comparatively because they can leave pixels that lie outside the decision region unclassified, where as Maximum Likelihood does not (Jensen 2005).

Although traditional classification methods are known to be effective methods in extracting land-cover data (Loveland *et al.* 1999; Huang, 2002), there are, notable limitations. These limitations include the inability to use characteristics such as texture, scale, size, relation to other classes, and shape of surrounding pixels into the classification algorithm. As a result of these limitations, the company Definiens with its' eCognition software, has developed a new rule based object-oriented image classifier (Jensen 2005).

3.7.2 Object-Oriented Classification

Definiens' eCognition is a relatively new object-oriented image classifier that takes a rule-based approach to image classification, aimed at solving some of the challenges per-pixel classifiers have encountered. Object-oriented classification essentially allows the analyst to use spectral and spatial information into the classification, an approach to image classification not yet available with traditional pixel-based classifiers (Jensen 2005).

There are two primary steps to object-oriented classification. The first is image segmentation and the second classification. Segmentation groups, or delineates, connected pixels into meaningful homogeneous objects (Definiens 2006). These homogeneous objects are based on user defined characteristics such as scale, color, shape, smoothness and compactness. A homogeneous object for example, may consist of a body of water, or a conifer stand surrounded by deciduous forest. A segmentations' scale parameter determines the average image object size. Color and shape work together when setting segmentation parameters. An increase in color criterion, which sets an object's minimum spectral standard deviation range, will

decrease the influence of the shape of an object decreases (Definiens 2006).

Smoothness and compactness parameters work together similarly. Segmentations with

high compactness values create square like objects, where as segmentations with high

smoothness value create objects less square like with smoother segmented boundaries.

Figure 6 for example, shows a segmentation with a scale parameter of 0.8, with

composition of homogeneity criterion of 0.9 color, 0.1 shape, 0.0 compactness and 1.0

smoothness. Segments (the blue lines) delineate image objects which are then classified

using a fuzzy logic based supervised nearest neighbor classifier. In this example, color

and smoothness have the most influence in the segmentation. If shape and compactness

had higher values, the segments would appear more square in shape.
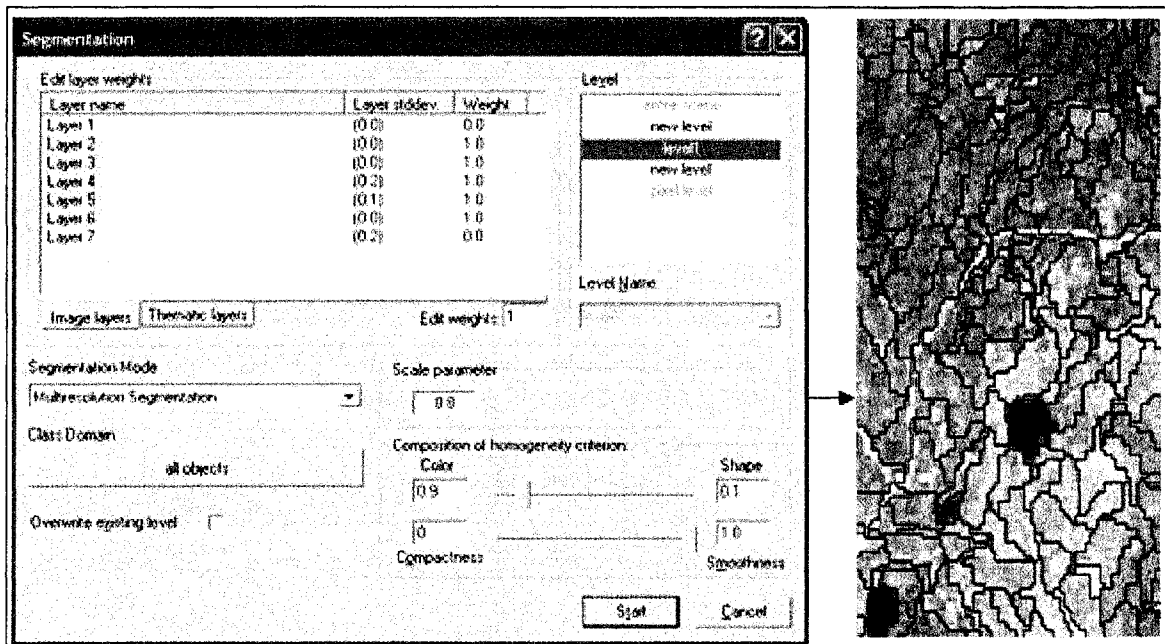
Figure 6. Example segmentation user interface (left) with segmented image (right).

The second step to object-oriented image classification, which occurs after

segmentation, is classification. Definiens' eCogntion uses a nearest neighbor classifier

algorithm. Nearest neighbor classifiers compute the euclidean distance from an

unknown pixel its neighbour training sight pixels (Jensen 2005). The unknown pixel is

assigned to the category with the nearest training sight pixel. This type of classifier can yield useful results if training data are well separated in n-dimensional space, but yield poor results if not well separated (Jensen 2005).

In addition to the nearest neighbor classifier, rules are placed on image objects (Definiens 2006). Although this rule based system is the key to the success of an image object classification, it has a steep learning curve, even for advanced remote sensing analysts. These rules are based on object levels, object hierarchy as well as object features, and are used to assist the classifier into a more meaningful classification. An image object level (Figure 7) is the collective of image objects formed by a single segmentation. Once classified, image objects can be merged by class, and re-segmented at a new lower level. Image object hierarchy refers to every image object of a lower level being linked to image objects of its super-level (Definiens 2006). For example, figure 8a shows the class hierarchy for a project showing 3 levels. The first level is the pixel-level and is shown in figure 8b. The next level is a broad level used to classify 3 super-objects (cut, forest, water). It was segmented based on the pixel level (Figure 8c), then classified. Once classified, the segments were merged together by class (Figure 8d). Figure 8e shows a new lower level created by segmenting within the super-objects. This is where image object hierarchy comes into play. At this level, cut and water classes exist within super-objects cut(super) and water(super). Conifer, deciduous and mixedwood are sub-objects which exist within super-object class forest(super). Although samples are no longer need to classify water and cut segments, they are used to further classify forest(super) into conifer, deciduous and mixedwood.
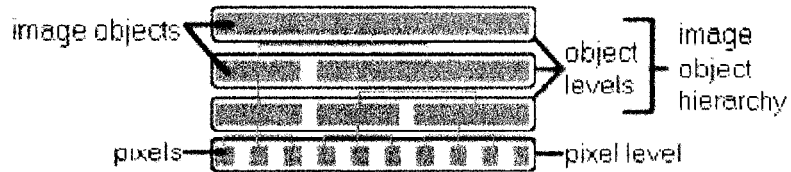
Figure 7. Image object hierarchy taken from eCognition's user guide.
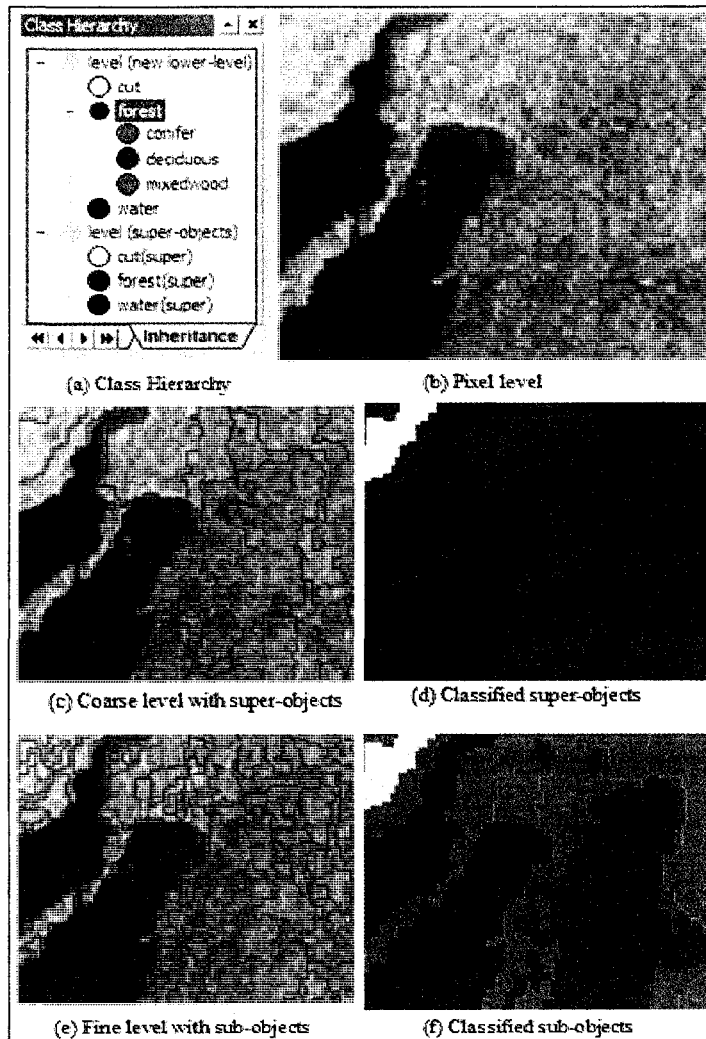
Figure 8. Example eCognition classification process.

Membership functions also play a key role object-oriented image classification.

These functions are rules applied to object features (Definiens 2006). For example, in

the boreal forest, clearcuts can look spectrally similar to and get misclassified with open

bogs. To avoid misclassifying a bog as a clearcut, exiting datasets such as wetlands

extracted from a FRI can be used to ensure that an object in a clearcut class does not

exist within the FRI's wetland boundary. To avoid a clearcut object from being misclassified into a bog, a 'relative border to' class related membership function can be applied to objects classified as bogs. If the relative border of bogs to cuts is set less than 90%, then the object remains a bog, if it is equal to or over 90% then it is not a bog. As a final example, a membership function can be used to enforce spectral thresholds for particular bands. For example, a rule can be made to ensure that a mixedwood class is only composed of objects with a mean NIR band ranging between 0.3 and 0.4 in brightness value.

Studies using object-oriented classifiers have shown improve results over single pixel classifiers. Lobo (1997) demonstrated a 22.5% improvement when using object-oriented over pixel-based classification for land cover analysis. Whiteside and Ahmad (2005), found a 9% improvement in overall accuracy when using object-oriented and per-pixel classifiers with medium resolution ASTER imagery with 10 land-cover classes in Australia. Oruc *et al.* 2004, found a 14% improvement when using object-oriented over per-pixel classifiers. Their study used Landsat ETM+ imagery with 7 land cover classes.

3.8 IMAGE REDUCTION METHODS

There are several disadvantages in applying traditional image classification methods, such as the supervised maximum likelihood classifier, to hyperspectral data. First, the increase in the number of bands vastly increases the complexity of an algorithm (Lillesand *et al.* 2004). Secondly, the maximum likelihood classifier optimally requires 10 to 100 times the number of training pixels compared to the

number of bands (Lillesand *et al.* 1994). These disadvantages have led to the development of image reduction methods. This thesis covers two of these methods, known as principal component analysis and discriminant function analysis.

3.8.1 Principal Component Analysis

Principal Component Analysis (PCA) is a widely accepted transformation technique used to reduce the dimensionality of original multispectral and hyperspectral image datasets (Jensen 2005). It compresses an image into fewer bands, each representing uncorrelated linear combinations that are easier to interpret and contain most of the information in the original dataset. Components are capable of non-correlation by creating new bands with rotated x and y axes that define the greatest variability in the data. The amount of variance in the original images accounted for by each component is represented by the eigenvalue. The percent variance explained by each PC band can be computed by multiplying the eigenvalues by 100 and dividing the sum of the eigenvalues for all PC's. The cumulative percent variance represents the amount of variance explained by several PC together. The first PC band always represents the largest percentage of variance in an image, followed by succeeding PC's in a decreasing percentage (Jensen 2005).

3.8.2 Discriminant Function Analysis

Forward stepwise discriminant function analysis is used to decrease the number of independent variables used for discrimination of groups. For the purpose of remote sensing, independent variables are the image bands, in which each bands' spectral data are used for discrimination. DFA creates a discriminant function which is based on

linear combinations of the independent variables that best separate groups (species or taxonomic classes).

Clark *et al.* (2005), achieved an 88% overall image classification accuracy when using DFA with a maximum likelihood classifier, for identifying individual tree crown classification in tropical rain forest conditions. Gong *et al.* (2000) used DFA to distinguish canopy hyperspectral *in situ* data between 6 conifer species. Using DFA on Hyperion data, Galvao *et al.* (2005), achieved an 87.5% overall accuracy in classifying five Brazilian sugarcane species. Aardt (2000) used DFA to determine spectral separability among six tree species using hyperspectral *in situ* tree crown data.

3.9 ACCURACY ASSESSMENT

There are several discrete multivariate techniques used to measure the accuracy of a classified remote sensing dataset. The fundamentals of these techniques are based on an error matrix that measures error within the classification. Some of these techniques include the overall accuracy, producer's accuracy, user's accuracy and Kappa statistics.

3.9.1 Error Matrix

The error matrix is a standard method of measuring errors with classified remotely sensed datasets. It shows the number of samples from a particular class that get misclassified into other classes. This is done through the use of a spatial relationship between pixels or polygons and ground reference data to find errors within a dataset. In the error matrix, columns represent reference (ground truth) data and rows represent classified pixels. Table 2 shows a sample error matrix used in Jensen (2005).

Table 2. Sample error matrix derived from Landsat data of Charleston, SC (Jensen 2005).

Classified Data	Reference Data					
	Residential	Commercial	Wetland	Forest	Water	Total
Residential	*70*	5	0	13	0	88
Commercial	3	*55*	0	0	0	58
Wetland	0	0	*99*	0	0	99
Forest	0	0	4	*37*	0	41
Water	0	0	0	0	*121*	121
Total	73	60	103	50	121	407

Overall Accuracy

Overall accuracy measures the image classification accuracy as a whole. It is computed by totaling the number of correctly classified samples for all classes and dividing by the total number of samples (Jensen 2005).

Example from Table 2:

$$\text{Overall Accurcy} = \frac{\text{Total correct pixels}}{\text{Total number of pixels}} = \frac{382}{407} = 93.86\%$$

3.9.3 Producer's Accuracy

Producer's accuracy measures the classification accuracy on each individual class (Jensen 2005). It indicates the probability of a reference pixel being correctly classified. Producer's accuracy is derived by dividing the total number of correct pixels in a class by the total number of pixels in that class (column total). It is also known as a measure of omission (100% - producer's accuracy).

Example from table 2.

$$\text{Producer's Accuracy} = \frac{\text{Total number correct pixels in a class}}{\text{Total pixels in that class}}$$

Residential = 70/73 = 96% (4% omission error)
Commercial = 55/60 = 92% (8% omission error)
Wetland = 99/103 = 96% (4% omission error)
Forest = 37/50 = 74% (26% omission error)
Water = 121/121 = 100% (0% omission error)

User's accuracy

User's accuracy measures the classification on individual classes as well. It

measures the reliability of a classified pixel actually being that class (Jensen 2005).

User's accuracy is derived by dividing the total number of correct pixels by the total

number of pixels classified into that class (row total). It is also known as a measure of

commission (100% - user's accuracy).

Example from table 2.

$$\text{User's Accuracy} = \frac{\text{Total number correct pixel in a class}}{\text{Row total}}$$

Residential = 70/88 = 80% (20% omission error)
Commercial = 55/58 = 95% (5% omission error)
Wetland = 99/99 = 100% (0% omission error)
Forest = 37/41 = 74% (10% omission error)
Water = 121/121 = 100% (0% omission error)

Kappa Statistics

The Kappa coefficient of agreement, denoted by K_{hat} or $\hat{K}$, is a measure of

agreement or accuracy between the classified image and reference data due to chance

(Jensen 2005). Values of K >80% represent a strong relationship between the classified

image and the reference data. Value of K < 40% represent a poor relationship. Kappa

may be calculated as follows:

$$\hat{K}_{Overall} = \frac{N\sum_{i-1}^{k}x_{ii} - \sum_{i=1}^{k}(x_{i+} \times x_{+i})}{N^2 - \sum_{i=1}^{k}(x_{i+} \times x_{+i})}$$

Where N is the total number of observations, x_{ii} is the number of observations in row i and column i, x_{i+} and x_{+i} are the margin totals for row i and column i respectively, and k is the number of rows (classes) in the matrix.

Example from table 2:

$$\hat{K}_{Residential} = \frac{N(x_{ii}) - (x_{i+} \times x_{+i})}{N(x_{i+}) - (x_{i+} \times x_{+i})} = \frac{407(70) - (88 \times 73)}{407(88) - (88 \times 73)} = 75.18\%$$

$$\hat{K}_{Overall} = \frac{N\sum_{i-1}^{k}x_{ii} - \sum_{i=1}^{k}(x_{i+} \times x_{+i})}{N^2 - \sum_{i=1}^{k}(x_{i+} \times x_{+i})} = \frac{407(382) - 36792}{407^2 - 36792} = 92.1\%$$

$$\sum_{i=1}^{k}x_{ii} = (70 + 55 + 99 + 37 + 121) = 382$$

$$\sum_{i=1}^{k}(x_{i+} \times x_{+i}) = (88 \times 73) + (58 \times 60) + (99 \times 103) + (41 \times 50) + (121 \times 121) = 36,792$$

3.10 FUTURE SENSORS

Presently, the low cost and large image size of Landsat TM multispectral imagery makes it a practical sensor for large-area land classifications. As compared to Landsat, the low availability, small image size and high cost of hyperspectral satellite imagery makes hyperspectral sensors, such as Hyperion, impractical for large-area land classification. For example, it would take approximately 25 Hyperion scenes and $25,000- $68,000 to cover an equivalent area of one Landsat scene. In addition, Hyperion's 16-day orbit cycle, acquiring leaf-on mid summer imagery of a forest the

size of several Landsat scenes, could take several years with Hyperion due to the possibility of cloud cover (USGS 2005).

In the future, however, hyperspectral imagery is expected to play a significant role in the next generation of Earth observing satellite sensors (Stuffler 2004). For example, a German team is proposing the Environmental Monitoring and Analysis Program (EnMap) sensor, as part of the next German satellite mission. The EnMap hyperspectral sensor, which is scheduled for launch in 2009, has a 30m spatial resolution, 200 continuous spectral bands, a 30km width, and a maximum swath length of 1000km (Stuffler 2004). In Canada, the Canadian Space Agency (CSA) is preparing for the launch of its own hyperspectral earth observation satellite mission (CSA 2003). The CSA is planning to launch the hyperspectral satellite sensor known as Hyperspectral Earth and Resource Observer (HERO) within the next ten years, as part of its SmallSAT program (Boyce 2004). As more hyperspectral satellites become available, and the size of hyperspectral images increase, and the price of hyperspectral imagery decreases, hyperspectral imagery could then play a financially feasible alternative role to conventional aerial photography in extracting forest inventory data.

The partial failure of Landsat 7 ETM+ in May 31 2003, provides a concern for the future of the Landsat program, and it use within this study. The problem with Landsat 7 lies in the failure of the Scan Line Corrector (SLC), which compensated for satellite movement, and is not turned off. Although Landsat 7 is still acquiring imagery with the same radiometric and geometric quality, there are lines containing no data. As a result, Landsat TM 4 and 5 have been reactivated and are currently producing imagery. They have, however, exceeded their life expectancy and it is unknown when

they will no longer produce imagery. Fortunately, the USGS and NASA are supporting the Landsat Data Continuity Mission (LDCM), in which a new Landsat sensor called the Operational Land Imager (OLI) will be produced. The OLI is scheduled for launch in 2009 (NASA 2007).

With the prospect of future commercial hyperspectral satellites capable of capturing larger images at a lower cost and producing improved accuracies, there is a potential for hyperspectral imagery to become a feasible alternative for large-area land classifications. Research, however, must first demonstrate the potential improvements hyperspectral imagery could have over multispectral imagery. There is therefore a need to better understand the potential use and benefits of hyperspectral imagery in large-area land classification applications. Presently, this are no research studies using satellite based hyperspectral imagery with focus taxonomic groups and species found in the upland areas of the boreal forest of northwestern Ontario.

METHODOLOGY

4.1 STUDY AREA

The study area is located in the south central section of the Dog River-Matawin

Forest Management Unit, 150 km west of Thunder Bay, Ontario (Figure 9). The size of

the study area is approximately 7.5 by 42 km, and is encompassed within the Boreal

Forest Region (Rowe 1972). Common tree species include black spruce *Picea mariana*

(Mill.) B.S.P., jackpine *Pinus banksiana*, white birch *Betula papyrifera*, trembling

aspen *Populus tremuloides* and balsam fir *Abies balsamea*. Common wetlands consist

of marsh, fen and bog. Criteria used in choosing the study area was based on the

location of an existing Hyperion image, cloud cover in remotely sensed imagery, road

access, and existing wetland ground truth plots.
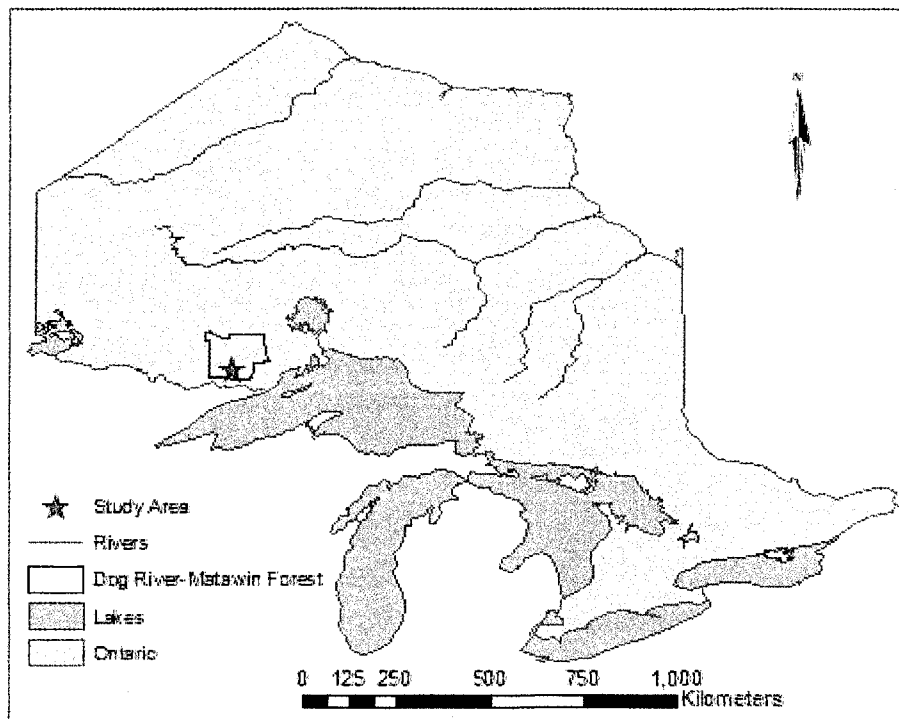
Figure 9. Geographic location of the Dog River Matawin Forest Management Unit and
the study area used within.

The study area was subset into two overlapping areas (Figure 10). Study area 1 is 7.5 by 42 km and is the larger of the two. Its northern most limit extends to a gravel pit. This pit was used to collect *in situ* spectral reflectance measurements for atmospheric correction, and its southern limit extends to the southern most section study area 2. Study area 2 is 7.5 by 30km and was used for collecting ground truth plots and analysis.
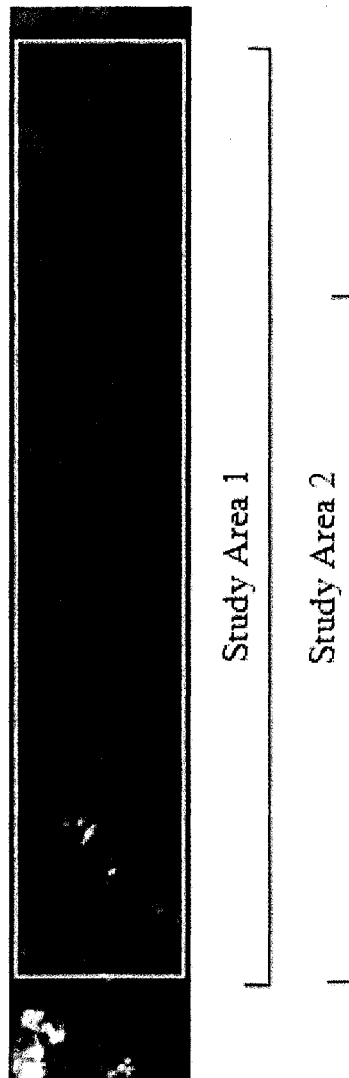
Figure 10. Hyperion image showing boundaries of the two study areas used.

4.2 RADIOMETRIC CORRECTION

4.2.1 Hyperion Abnormal Pixel Correction

Hyperion images are processed from level 0 (raw) to level 1a before distribution. Level 1a processing includes radiometric correction, smear correction, echo correction, background removal, bad pixel repair, and image quality checking (Han 2002). After visually inspecting individual bands, however, it became apparent that abnormal pixels (dark vertical stripes) are still present.

Abnormal pixels in Hyperion level 1a mainly appear in columns as continuous and intermittent dark stripes (Han 2002). There are four classes of abnormal pixels (Table 3). Class 1 abnormal pixels occur continuously throughout an entire column and consistently have atypical DN (digital number) values such -32768 or 0 (Figure 11). Class 2 abnormal pixels occur continuously throughout a column and have pixels with DN values lower than their immediate left and right neighbors (Figure 11). Class 3 abnormal pixels occur intermittently throughout a column and have atypical DN values, appearing as dark dots. Class 4 abnormal pixels, the most common, occur intermittently throughout a column, are not constant in value, and have DN values lower than their immediate left and right neighbors (Han 2002) (Figure 12). The difficulty in visually detecting, as well as the intermittent nature of class 3 and 4 abnormal pixels makes the use of standard remote sensing software functions that replace entire bad columns with the average of neighboring pixel values an impractical and incorrect solution to fixing Hyperion's abnormal pixels. These abnormal pixels, however, must be corrected prior to further analysis (Han 2002).

Table 3. Abnormal pixel classes in level 1a Hyperion imagery.

Class Type	Description
Class 1	Continuous with atypical DN values
Class 2	Continuous with constant DN values
Class 3	Intermittent with atypical DN values
Class 4	Intermittent with lower DN values
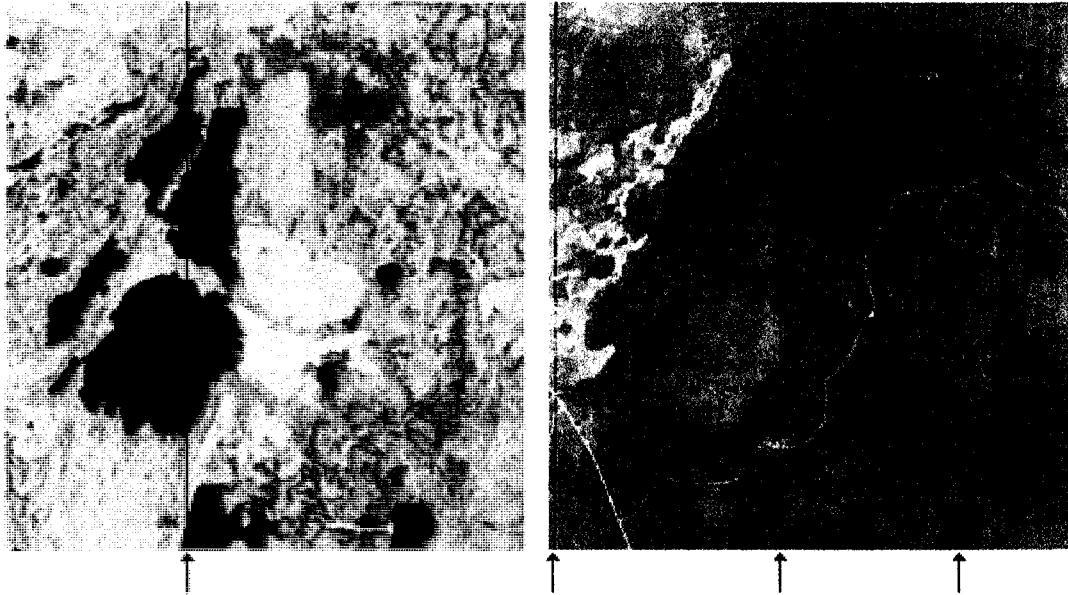
Figure 11. Band 94 (left) showing class 1 abnormal pixels and band 11 (right) showing class 2 abnormal pixels.

Figure 12. Band 57 showing class 4 abnormal pixels.

There are multiple possible causes for the occurrence of abnormal pixels in Hyperion imagery. Hyperion's pushbroom imager uses separate detectors for each column within an image (Han 2002). Dark vertical strips could occur from improper detector calibration. Atypical abnormal pixels could be created during the SWIR smear and echo correction, in which the correction algorithm does not account for negative numbers. This could have been corrected by setting negative values to zero after the smear correction and before the echo correction (Han 2002).

Abnormal pixels can be corrected by replacing their DN values with the average DN value of their immediate left and right neighbors (Han 2002). This method can be used because all four classes commonly run in vertical strips (in columns) and have DN values less than their left and right neighbors. These similarities can be used to create an automated correction process using customized computer programming software. Han (2002), created an Interactive Data Language (IDL) program to automate the abnormal pixel correction process, using a three-dimensional array. In his program, each pixel's DN value was compared to its left and right neighbor, and labeled as abnormal if its value is less than both neighbors. The program then counts the total number of abnormal pixels and total number pixels in each column. If the number of abnormal pixels in a column is greater than a threshold of 50% of the total number of pixels in a column, and if the number of consecutive abnormal pixels exceeds a user-defined-threshold-value (longest vertical ground feature, usually five pixels), then the abnormal pixel DN values are replaced with the average of their immediate left and right neighbors (Han 2002).

I used Visual Basic programming with a series of scripts in collaboration with

ERDAS Imagine, ESRI's ArcObjects and Microsoft Excel Objects to correct abnormal

pixels based on the parameters described in Han (2002). ERDAS modeler was first

used to separate the Hyperion image into individual bands. See Appendix II to view an

example model. Each band was named after the band number. For example, the first

band was name 'band1' and the second band was named 'band2'. Each band name

thereafter was utilized in a dynamic naming system throughout the series of scripts to

follow. Using a dynamic naming system through scripting avoided user input errors

which could have easily occurred with the large number of bands which were required

to be processed.

The separated images were then converted from raster to ASCII format through

customized script in ArcMap using VBA with ArcObjects (Chang 2005). See

Appendix III to view the script's code. The user adds all images into ArcMap (See

Appendix IV for illustration), and then runs the script. The script uses a folder browser

dialog box to allow the user to pick a folder to save the ASCII files (ESRI Forums

2006). It then loops through each image layer and exports an ASCII file for each

image, saving each file with same name as its image layer.

ASCII files, representing individual bands, were dynamically imported into

Excel format using a customized script run in Excel. See Appendix IV for illustration

and Appendix V for programming code. This script opens a file browser dialog box

which allows the user to select an ASCII file to import (Anonymous 2006, Peason

2005). A browse folder dialog box is then used to select an output folder in which the

new Excel document is to be saved. The script then imports the ASCII file using a

space delimiter and deletes the first six rows that contain header information. The name of the new Excel document is then saved based on the name of the ASCII file (Anonymous 2006, Peason 2005).

The correction of abnormal pixels was accomplished through a script written with VBA using Excel Objects (Peason 2005). See Appendix VI to view the script's code. The script loops through each column and counts the number of pixels with DN values less than their immediate left and right neighbors. If the total number of abnormal pixels in a column exceeds a threshold of fifty percent of the total number of pixels in the column, then the program loops through that column again. During the column's second pass, the program counts the number of consecutive abnormal pixels. If the number of consecutive abnormal pixels exceeds a threshold of five pixels, the DN value of those abnormal pixels are replaced with the average of its immediate left and right neighbor DN values. The script then saves the Excel document. See Appendix IV for an illustration of a correct image in Excel.

Corrected abnormal pixel Excel documents were exported back into ASCII format, through a script written with VBA using Excel Objects (Anonymous 2006, Peason 2005). See Appendix VII to view the script's code. The script then uses a space delimiter to separate Excel cell values in the ASCII file. The new ASCII file is dynamically saved using the name of the Excel document. See Appendix VIII to view the script's code. Header information was then copied from the original ASCII document when exported from image format to ASCII, and pasted into the new ASCII file with corrected abnormal pixels.

ASCII files with the corrected abnormal pixels were converted back to image format using ESRI's ASCII to Raster tool. ERDAS modeler was used to combine each corrected band back into a single image composed of 242 bands. The model utilized the Stacklayers function to combine the images, and utilized the data type option to bring the image data type to its original signed 16-bit format. See Appendix IX for an example model. Once abnormal pixel were no longer present the image was ready to be converted from raw DN values to radiance.

4.2.2 Convert to Radiance

Absolute spectral radiance, which is the most precise radiometric measurement in remote sensing, was used as a common scale for Landsat and Hyperion pixel values prior to atmospheric correction. Spectral radiance units used are measured in watts per square meter per steradian per micrometer $[W/(m^2 \cdot sr \cdot \mu m)]$. Hyperion level 1b raw DN values were converted to absolute radiance using parameters described in Barry (2001). Landsat TM5 raw DN values (Level 0 (L0)) were converted to spectral radiance (Level 1 (L1)) using the radiometric calibration procedure described in Chander and Markham (2003).

Converting Hyperion DN values to radiance requires dividing the VNIR bands (1-70) by 40 and the SWIR bands (71-242) by 80. The procedure used included the separation of the VNIR from the SWIR bands, and the use of ERDAS modeler to divide the VNIR bands by 40 and SWIR bands by 80. Appendix X shows the model used in this processing step. The image was converted from signed 16-bit to 32-bit floating single data during processing.

Converting Landsat L0 DN values (Qcal) to radiance (Lλ) requires knowledge of original calibration rescaling factors used on a scene by scene basis. This information, such as the gain (Grescale) and biases (Brescale), which are band-specific rescaling factors, can be found in the header files provided with the imagery. This is due to changes in the instrument because of aging (Chander and Markham 2003). The equation used in this conversion is Lλ = Grescale X Qcal + Brescale,, where:

> Lλ = spectral radiance at the sensor's aperture in $W/(m^2 \cdot sr \cdot \mu m)$
> Grescale = (LMAXλ – LMINλ / Qcal max) x Qcal + LMINλ
> Qcal = quantized calibrated pixel value in DNs
> Qcalmin = maximum quantized calibrated pixel value (DN = 0)
> Qcalmax = maximum quantized calibrated pixel value (DN = 255)
> LMINλ = spectral radiance that is scaled to Qcalmin in $W/(m^2 \cdot sr \cdot \mu m)$
> LMAXλ = spectal radiance that is scaled to Qcalmax in $W/(m^2 \cdot sr \cdot \mu m)$

Calculations used on each band is summarized in table 4. Once converted to radiance, the images are ready for atmospheric correction. See Appendix XI to view the model used to convert raw level 0 Landsat DN values to absolute radiance.

Table 4. Equations used to convert Landsat TM5 bands from L0 DN values to L1 spectral radiance.

Band	Equation
1	0.762824 * Qcal + (-1.52)
2	1.442510 * Qcal + (-2.84)
3	1.039880 * Qcal + (-1.17)
4	0.872558 * Qcal + (-1.51)
5	0.119882 * Qcal + (-0.37)
7	0.065294 * Qcal + (-0.15)

4.3 ATMOPHERIC CORRECTION

Empirical Line Calibration (ELC) within ERDAS's Spectral Analysis Workstation was used to atmospherically correct the Landsat and Hyperion images,

which were previously radiometrically corrected. *In situ* data was collected on July 22/2004 (2-3pm) with an Analytical Spectral Devices (ASD) FieldSpec Pro spectroradiometer, which has a 0.35-2.50 μm spectral range, a 0.001 μm band width, and a 10 nm spatial resolution. Objects used for *in situ* data collection include a gravel pit located in the northern most section of study area 1, as well as a deep water sample from a lake within the study area. The *in situ* data was collected by Jason Freeburn.

4.4 BAD BAND REMOVAL

In this thesis, the term bad band with Hyperion imagery refers to bands that are non-calibrated, have extreme values due to water absorption, spectral overlap, or poor image quality. Hyperion imagery is collected with 242 bands, of which 198 are calibrated. See Appendix XII for average wavelength value for each band for the original 242 band image. Non-calibrated bands include bands 1-7 (355-426nm), 58-76 (852-1058nm) and 225-242 (2405-1577nm). These bands were removed before classification because their Level 0 DN values were equal to zero and do not represent surface reflectance values. Band 77 (912nm) was removed because it has spectral overlap with band 56 (915nm). Bands 8 (427nm) and 221-224 (2365-2395nm) were removed because visual inspection showed poor image quality. Water absorption bands 120-143 (1346-1578nm) and 165-186 (1800-2012nm) removed as well. Table 5 provides a summary of bad bands and the reason for each bands removal. In total 87 bands were considered bad bands and removed prior to classification, resulting in an image with 155 useful bands. Figure 13 shows a graph of a deciduous tree sample with all 242 bands depicting the bad bands. The 155 band Hyperion image was used for

further processing and interpretation to follow. See Appendix XIII for wavelength

information on each band for the 155 band Hyperion image.

Table 5. Summary table showing which bands were removed prior to classification and
the reason why they were removed.

Band	Reason for Band Removal
1-7, 58-76, 225-242	Not calibrated
8, 221-224	Poor image quality
77	Spectral overlap
120-134, 165-186	Water absorption/Extreme values
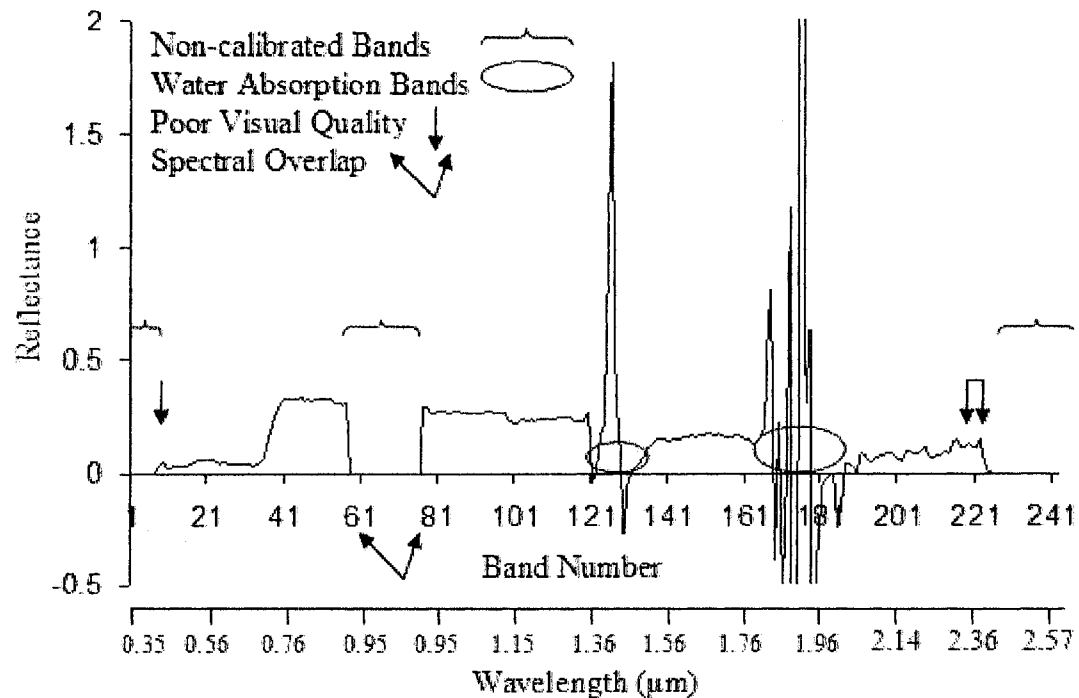
Figure 13. Illustrates reflectance and location of bad bands using a deciduous tree
sample with all 242 bands.

4.5 GEOMETRIC CORRECTION

The 2004 Hyperion image was geometrically corrected to a 2002 Landsat TM

image with a 25m spatial resolution, which was previously geometrically corrected

using an Ontario Base Map (OBM) drainage layer. Image to image rectification was

thereafter used to geometrically correct the 2004 Landsat image the geometrically

correct Hyperion image. A RMS less than one pixel was accomplished for both

geometric corrections. Nearest Neighbor with a 30m spatial resolution was used for re-

sampling purposes. The projected coordinate system used was North American Datum

1983 Universal Transverse Mercator Zone 15 North.

4.6 CLOUD REMOVAL

Clouds and cloud shadows were removed from both images. Areas identified as

cloud were converted to vector format and removed from the FRI. This avoided the

collection of samples in clouded areas. This process involved creating and combining

areas of interests around clouds in both images. DN values within areas of interested

were changed to abnormally high brightness values using ERDAS Fill tool's max

option. This allowed clouded areas to be easily separated from the rest of the image

using an unsupervised classification. Once classified, clouds were recoded to a value of

one and the rest of the image to a value of zero. ESRI's Raster to Polygon tool was

used to convert the image to vector format and used to cut out clouds from the FRI.

Because clouds were different in each image, clouds and cloud shadows were

permanently removed from both images and not used in the classification analysis.

4.7 SAMPLE DESIGN

4.7.1 Field Sample Units

The Dog River-Matawin forest resource inventory (FRI) was used as a base to

collect samples. The FRI is a set of polygons containing data such as age, forest unit

type, and species composition. This FRI consists of 11 units for mature forest, including

balsam fir, white birch, mixed conifer 1, mixed conifer 2, mixed hardwood, other

conifer, jack pine, poplar, red/white pine, spruce lowland and spruce upland. In

addition to these units, clear cuts 5 years old or younger were found within the study

area, and the OBM lakes layer was used to sample water. Details on units used to

collect samples are summarized in Table 6. Once collected, samples were aggregated

into appropriate classes for analysis. Visual comparison of imagery with the FRI

indicated that the FRI needed to be updated to account for recent harvested areas prior

to ground truthing. A combination of Landsat and SPOT 5m panchromatic imagery

was used to update the FRI using ESRI's digitizing tools.

Table 6. Sample units used for collecting field data.

Sample Unit	Description	Parameters
BF1	Balsam Fir	Bf >= 60%
BW1	White Birch	Bw >= 70%
MC1	Mixed Conifer 1	Sb + Sw + Bf + Pj + Pr + Pw + Ce + La >= 50% AND Po <= 20% AND Po + Bw <= 30%
MC2	Mixed Conifer 2	Sb + Sw + Bf + Pj + Pr + Pw + Ce + La >= 60%, OR Sb + Sw + Bf + Pj + Pr + Pw + Ce + La >= 50% AND WG in Sb, Sw, Pj, Bf, Ce, La, Pr, Pw, OC
MH1	Mixed Hardwood	Po + Bw + OH >= 50%
OC1	Other Conifer	Ce + La >= 60%
PJ1	Jack Pine	Pj >= 60% AND Po <=20%
PO1	Poplar	Po >= 70%
PRW	Red/White Pine	Pr + Pw >= 30%
SPL	Spruce Lowland	Ecosite in 34, 35, 36 OR Ecosite = 37 AND Sb >= 70%
SPU	Spruce Upland	WG = Sb OR Sw, AND Sb + Sw >= 70% AND Po + Bw <= 20%
CUT	Clear Cut	Age <=5
WATER	Lake	OBM Lakes layer

4.7.2 Sample Plot Design

A systematic point sample design, developed by the Minnesota Department of

Natural Resources (DNR) as an ArcView extension, was used to generate random

upland ground truth plots. This extension creates a random point shapefile of

systematically placed points within a selected polygon using user defined parameters.

Sample points were based on forest units provided by the FRI. Parameters within the

design required points to be located within a minimum of 60m from the edge of FRI

boundaries, and 60m between points. Plots inaccessible due to natural objects such as

rivers were removed. If the number of sample points within a forest unit contained in

excess of 500 points, then number of points within that forest unit was reduced to 500,

using ArcView's select features randomly extension. Table 7 summarizes the number

of potential ground truth sample points available for each sample type after point

reductions described above.

Table 7. Summary of the number of potential sample plots after removal of inaccessible
plots and plots exceeding the 500 maximum points parameter.

Forest Unit Type	Number of Potential Plots
BF1	23
BW1	137
MC1	500
MC2	500
MH1	500
OC1	12
OH1	61
PJ1	500
PO	407
PR	141
SPL	500
SPU	160
Clearcut	200
Water	100
Total	3741

4.7.3 Sample Collection

Ground truth plots were 3 by 3 pixels (90x90m) in size (Figure 14.). Sample plot spatial locations were recorded using a Garmin Map 76 GPS in the center of each plot. The goal for the minimum number of samples collected per sample type was 30-50. A sample was accepted if the forest unit was uniform within a 45m radius of the center of each plot. A sample was rejected if the forest unit varied within a plot. The focus of each plot was based on species composition that would be seen from an aerial perspective. Effort was made to collect points in a wide variety of stands, ages and species composition, while taking access and time into consideration. While ground truthing, sample plots were allowed to be moved up to one half pixel (15m) if it was necessary to meet the criteria for an acceptable plot.

SPL	SPL	SPL
SPL	GPS Point ● SPL	SPL
SPL	SPL	SPL

90m
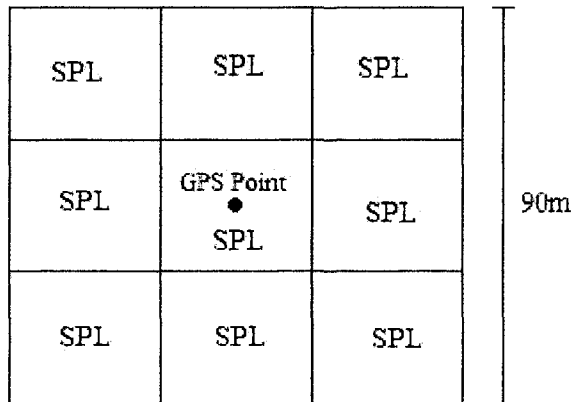
Figure 14. A 3x3 pixel (90x90m) homogeneous sample area of black spruce lowland with a GPS point taken in the centre.

The OBM lakes layer was used to generate water plots based on a systematic point sample design. Parameters within the design required points to be located within a minimum of 60m from the edge of water boundaries, and 60m in distance between points. One hundred samples were randomly selected from this grid using an ArcView extension, and used in the analysis (Table 7). Water samples were not visited in the

field, but were visually inspected using Landsat, Hyperion and Spot panchromatic imagery for confirmation.

Wetland ground truth plots were collected prior to the start of this thesis, and were provided by Jason Freeburn. These sample plots were collected using a 3 by 3 cell plot size with a GPS coordinate taken in the center of each plot. A random sample design was not used for wetland plots using FRI, as used with upland plots, because the FRI was not designed for monitoring spatial wetland data boundaries and classes. Instead, the location of ground plots was determined in the field. The Terrestrial and Wetland Ecosites of Northwestern Ontario (NWST) Field Guide was used with to collect ecosite types. Table 8 summarizes the ecosite types found in the study area. Appendix XIV provides further description for each ecosite. These ecosites were generalized into marsh, fen and bog for the initial classification purposes, and then further generalized into one class (wetland) for the final accuracy assessment. This generalization of wetlands was done for two reasons; the first was due to the focus of this study being on upland habitat; and the second was to not impose upon Jason Freeburn's similar concurrent remote sensing study focusing on wetlands in which the wetland samples use in this thesis were taken from.

Table 8. NWST wetland ecosite's found within study area.

Ecosite	Name
34	Treed Bog
39	Open Bog
40	Treed Fen
41	Open Poor Fen
42	Open Moderately Rich Fen
45	Shore Fen
46	Meadow Marsh
47	Sheltered Marsh
48	Exposed Marsh

4.7.4 Sample Aggregation

A total of 556 upland ground truth plots were collected in the field. All upland

classes had more than 30 samples except for BF1, PR, and OC1, which were excluded

from further analysis. These latter three classes either had samples rejected in the field

or did not have enough samples to start with. Although there were 50 jack pine samples

collected, the majority had a species composition of 60-70% jack pine. With the lack of

jack pine samples representing a species composition of 80-100% jack pine, 100

samples were randomly selected from FRI stands with a species composition equal to or

greater than 80% jack pine. In addition to upland plots, 100 water samples extracted

from the OMB lakes layer and 140 existing wetland plots were used. Sample types

used in further analysis include BW, MC1, MC2, MH1, OH1, PJ, PO, SPL, SPU, Cut,

Marsh, Fen, Bog, and Water, totaling 893 samples (Table 9). After field sampling,

samples were generalized for analysis into 11 classes consisting of water, marsh, fen,

bog, black spruce, jack pine, mixedwood, dense deciduous, sparse deciduous, and cuts.

Training and testing sites were extracted from these samples, using 50% for training and 50% for testing.

Table 9. Number of samples collected per class.

Class	Number of Samples	Class	Number of Samples
Water	100	Jack Pine	150
Marsh	27	Mixedwood	120
Fen	33	Dense Deciduous	132
Bog	80	Sparse Deciduous	48
Black Spruce	125	Cut	78

4.8 CLASSIFICATION (PIXEL-BASED)

4.8.1 Introduction

Two levels of classification were used in the analysis (Figure 15). Level 1 was used as a preliminary step and produce six general classes consisting of water, wetland, conifer, mixedwood, deciduous and cuts. This level was used to separate water, wetland, and upland, as well as create general upland classes. In level 2, pixels classified as conifer and deciduous from level 1, were separated and further classified into spruce, jack pine, dense deciduous and sparse forest. The final classified image consisted of 8 classes, including water, wetland, black spruce, jack pine, mixedwood, dense deciduous, sparse deciduous and clear cuts.

CLASSIFICATION LEVEL 1	CLASSIFICATION LEVEL 2
Water	Water
Marsh	Wetland (Marsh, Fen, Bog)
Fen	
Bog	
Conifer	Black Spruce
	Jack Pine
Mixedwood	Mixedwood
Deciduous	Dense Deciduous
	Sparse Deciduous
Cut	Cut

Figure 15. Classes used in level 1 and 2 supervised classifications.

Level 1 classification was used to generate six general classes ranging from water to upland (Table 10). Although I focused on upland habitat classification, the presence and possible spectral similarities between water, upland and wetland classes cannot be ignored. Due to spectral differences, marsh, fen, and bog classes were initially used during the level 1 supervised classification. Once classified, their pixels were aggregated into one class called wetland for the accuracy assessment.

Table 10. Classes used in first classification level.

Class	Class Name	Description
1	Water	OBM lakes
2	Wetland (Marsh)	Shadow, Sheltered, Exposed
3	Wetland (Fen)	Treed, Open Poor, Open Moderately Rich, Shore
4	Wetland (Bog)	Treed, Open
5	Conifer	Sb + Pj+ Bf+ Ce+ La+ Pr+ Sw + Pw >= 80% and Age > 5
6	Mixedwood	Sb + Pj+ Bf+ Ce+ La+ Pr+ Sw + Pw < 80% and Po + Bw + Ah + Mh + Ms < 80% and Age > 5
7	Deciduous	Po + Bw + Ah + Mh + Ms >= 80% and Age > 5
8	Cut	Age <= 5

The level 2 classification produced the final classes for the analysis. Using masking techniques, conifer was further classified into black spruce and jack pine, deciduous into dense and sparse forest. As well, marsh, fen, and bog were aggregated into a single class called wetland. This produced a final classification consisting of 8 classes: Water, Wetland, black spruce, jack pine, mixedwood, dense deciduous, sparse deciduous, and cuts (Table 11).

Table 11. Classes used in the level 2 (final) classification.

Class	Class Name	Description
1	Water	OBM lakes
2	Wetland	Marsh, Fen, Bog
3	Black Spruce (Sb)	Sb + Pj+ Bf+ Ce+ La+ Pr+ Sw + Pw > 80% and Sb >= Pj and Age > 5
4	Jack Pine (Pj)	Sb + Pj+ Bf+ Ce+ La+ Pr+ Sw + Pw > 80% and Pj > Sb and Age > 5
5	Mixedwood (Mxwd)	Sb + Pj+ Bf+ Ce+ La+ Pr+ Sw + Pw < 80% and Po + Bw + Ah + Mh + Ms < 80% and Age > 5
6	Dense Deciduous	Po + Bw + Ah + Mh + Ms >= 80%, Age > 5 and Canopy Closure > 50%
7	Sparse Deciduous	Po + Bw + Ah + Mh + Ms > 80%, Age > 5 and Canopy closure < 50%
8	Cut	Age <= 5

4.8.2 Feature Selection (Level 1)

For the Hyperion image, a stepwise discriminant function analysis was used to select the best combination of bands to be used in a supervised classifier with the classes in level 1. Using spectral values of samples from the eight classes, the DFA produced 37 possible steps (band combinations) that could be used for band selection. Step 9, a 9 band combination, produced the most desirable results and was therefore chosen for analysis. These bands include bands 7, 26, 28, 31, 40, 82, 86, 89 and 120.

For the Landsat image, all bands, except the thermal band, were used for band selection. A stepwise discriminant function analysis was not used to select Landsat bands because of the limited number of bands. The second reason a discriminant function analysis was not used on the Landsat imagery, was because initial classification trials, which are not reported in this thesis, showed best results with using the six band combination as opposed to any other combination of bands.

4.8.3 Classifying Spruce and Pine

The Hyperion and Landsat images were clipped to the level 1 conifer class defined by each image, then further classified into black spruce and jack pine. Black spruce was defined with a species composition of black spruce greater or equal to jack pine, and jack pine was defined with a species composition of jack pine greater than black spruce. Hyperion used a stepwise discriminant function analysis to select the best combination of bands to classify spruce and pine with a supervised classifier. Step 9, a 9 band combination, produced the most desirable results and was therefore chosen for analysis. Bands used include bands 14, 68, 60, 13, 25, 32, 17, 138, 152. Landsat used a six band combination to run in a supervised classifier. Accuracy assessment was not documented until the pixels in the new classes were added back into a full 8 class final image.

4.8.4 Classifying Dense and Sparse Deciduous

The Hyperion and Landsat images were clipped to the level 1 deciduous class defined by each image, and then further classified into dense and sparse deciduous forest. Dense deciduous was defined as having a canopy closer >50% and sparse forest was defined as having a canopy closure of <50%. Hyperion used a stepwise

discriminant function analysis to select the best combination of bands to classify dense and sparse deciduous with a supervised classifier. Step 8, an eight band combination, produced the most desirable results and was therefore chosen for analysis. Bands used include bands 77, 64, 23, 130, 99, 115, 104 and 138. Landsat used a six band combination to run in a supervised classifier. Accuracy assessment was not documented until the pixels in the new classes were added back into a full 8 class final image.

4.8.5 Principal Component Analysis (PCA)

4.8.5.1 *Landsat Level 1*

Principal component bands 1 through 3 were chosen for the Landsat supervised classification. The first PCs account for 97.31% of the variance in the original six band dataset (Table 12). The second PC accounts for 2.33% of the remaining variance. Cumulatively, these first two PC account for (explain) 99.65% of the variability in the original image. The third component accounts for another 0.24%, bringing the total to 99.89%. The remainder components cumulatively represent 0.11% of the variability in the original image. The first PC is most positively correlated with Landsat's NIR band (Table 13). The second PC is most negatively correlated with Landsat's MIR and FIR bands. The third PC is most negatively correlated with Landsat's green band. Visual inspection of the PC bands shows good image quality in PC 1 through 3, and poor image quality in PCs 4 through 6 (Appendix XV).

Table 12. Eigenvalues from TM PCA.

	PC1	PC2	PC3	PC4	PC5	PC6	Total
Eigenvalues	0.0364	0.0009	0.0001	0.0000	0.0000	0.0000	0.0374
% Variance	97.31	2.33	0.24	0.04	0.04	0.03	100
Cumulative	97.31	99.65	99.89	99.94	99.97	100	

Table 13. Eigen matrix from TM PCA.

Band	PC 1	PC 2	PC 3	PC 4	PC 5	PC 6
1	0.054	-0.194	-0.319	0.793	0.448	0.167
2	0.135	-0.283	-0.676	-0.522	0.162	0.382
3	0.090	-0.339	-0.420	0.089	-0.329	-0.764
4	0.871	0.464	-0.099	0.072	-0.103	0.004
5	0.415	-0.540	0.469	-0.203	0.484	-0.201
6	0.197	-0.510	0.190	0.209	-0.648	0.448

4.8.5.2 *Landsat Level 2*

Principal components 1-3 were used for the level 2 classification as well. Several preliminary steps were taken after level 1 classification and before the final level 2 accuracy assessment. First, level 1 conifer pixels masked and further classified into black spruce and jack pine. Secondly, classified level 1 deciduous pixels were masked and further classified into dense and sparse forest. Thirdly, marsh, fen and bog were aggregated into one wetland class. Finally, pixels classified as water, mixed wood and cut from level 1, were combined with wetland, black spruce, jack pine, dense deciduous, and sparse deciduous classified pixels from level 2 to produce a final image consisting of 8 classes (Table 11). This image was used in a final accuracy assessment.

4.8.5.3 *Hyperion Level 1*

Principal component bands 1 through 4 were chosen for the Hyperion supervised classification. The first PC accounts for 95.94% of the variance in the

original dataset (Table 12). The second PC accounts for 2.87% of the remaining variance. Cumulatively, these first two PCs account for (explain) 98.81% of the variability in the original image. The third component accounts for another 0.36% and the fourth component accounts for 0.10%, bringing the total to 99.28%. The remaining components cumulatively represent 0.72% of the variability in the original image. The first PC is most positive correlated with Hyperion NIR section (bands 32-48) of the VNIR bands (Appendix XVI). The second PC is most positively correlated with Hyperion SWIR bands (122-137). The third and fourth PC's are most positively correlated with Hyperion's red green and blue VNIR bands (1-23). Visual inspection of the PC bands shows good image quality in PC 1 through 4, and a poor decreasing image quality in the remaining PC's (Appendix XVII).

Table 14. Eigenvalues from Hyperion PCA.

	PC1	PC2	PC3	PC4	PC5	PC6	...	PC155	Total
Eigenvalues	0.941	0.028	0.004	0.001	0.001	0.001	...	0.000	0.981
% Variance	95.94	2.87	0.36	0.10	0.09	0.07	...	0.00	
Cumulative	95.94	98.81	99.18	99.28	99.36	99.43	...	100	

4.8.5.4 *Hyperion Level 2*

Principal components 1-4 were used for the level 2 classification as well. Several preliminary steps were taken after level 1 classification and before the final level 2 accuracy assessment. First, level 1 conifer pixels masked and further classified into black spruce and jack pine. Secondly, classified level 1 deciduous pixels were masked and further classified into dense and sparse forest. Thirdly, marsh, fen and bog were aggregated into one wetland class. Finally, pixels classified as water, mixed wood and cut from level 1, were combined with wetland, black spruce, jack pine, dense

deciduous, and sparse deciduous classified pixels from level 2 to produce a final image consisting of 8 classes (Table 10). This image was used in a final accuracy assessment.

4.8.6 Final Classification

Pixels classified as water, wetland, mixedwood and cut from level 1, were combined with spruce, pine, dense deciduous, and sparse classified pixels from level 2 to produce a final image with 8 classes (Table 10 above). This process was done separately for Landsat and Hyperion, producing two final images with pixel values from 1 to 8 which were used for final accuracy assessment.

4.9 OBJECT-ORIENTED IMAGE ANALYSIS

4.9.1 Introduction

Definiens' eCognition v5.0 software was used for the object-oriented image classification. In general, individual pixels were segmented into objects and classified based on a nearest neighbor classifier, each class having a unique set of rules. Segmentation was avoided in pixels where clouds are present in the image by assigning a global no data value to an image with pixels values of zero where clouds exist and values of one for pixels to be analyzed. Bands 1-6 were used to classify with Landsat and a discriminant function analysis was used to select bands to classify with Hyperion. The same training and testing samples used in the pixel-based analysis were used for the object-oriented analysis.

4.9.2 Landsat

Three object levels were used to classify the Landsat image using bands 1 to 6. The first level (level 3) is the coarsest, and was used to generate two classes; cut and no

cut. Child classes of no-cut included water, marsh, fen, bog, conifer, mixedwood and deciduous (Figure 16a). The only concern at this level is to not confuse between cuts and no-cuts. Misclassification among no-cut child classes such as conifer and mixedwood or deciduous and mixedwood, is not a concern because these classes are merged after level 3 is classified.

Level 3 multiresolution segmentation was based on the pixel level. Parameters used in the segmentation were bands 2-6 having a weight of 1, a scale of 1.8, and a color composition of homogeneity of one (Figure 17). This segmentation created large image objects (Figure 16b). Once classified (Figure 16c), image objects classified as no-cut were merged into one single no-cut class (Figure 16d). Image objects classified as cuts were merged with objects within their own class and remained as cuts for the rest of the analysis.

Figure 16. Level 3 hierarchy (a), segmentation (b), classification (c) and final cut and no-cut objects (d).

Figure 17. Segmentation interface showing parameters used in level 3.

The second level (level 2) is less coarse than the previous, and was used to further classify no-cuts from level 3, into general classes consisting of water, marsh, fen, bog, conifer, mixedwood and deciduous. See Figure 18 for class hierarchy. In this hierarchy, bog, fen and marsh are child classes of the parent class wetland. A child contains the same class properties as a parent class (wetland), and a parent class will hold all the objects of its children. Essentially, the wetland class was used to aggregate marsh, fen and bog into a single class for the final classification at the next level.

Level 2 segmentation was based on super-objects from level 3. Objects created in this segmentation were smaller than objects in the previous level (Figure 19). Parameters used in the segmentation were bands 2-6 having a weight of 1, a scale of 0.2, and composition of homogeneity was 0.9 for color, 0.1 for shape, 0.1 for compactness and 0.9 for smoothness. Segmentation parameters were based on best initial classification using nearest neighbor classifier and inheritance rules. Cuts did not require the nearest neighbor classifier because its final objects were generated in the previous level. Feature-related and class-related rules were not used for the initial classification in determining segmentation parameters, but were used afterwards to improve the classification. Inheritance rules used are shown in table 15. An example of how these rules work can be described with level 3 no-cut and level 2 water. If one inheritance rule for level 2 water is that the existence of super-object no-cut from level 3 is equal to 1, the only level 2 objects that can be classified as water, must be located or contained within the same spatial area as no-cut from level 3.
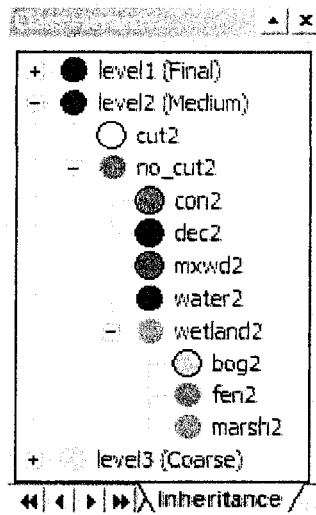
Figure 18. Class hierarchy used in level 2.
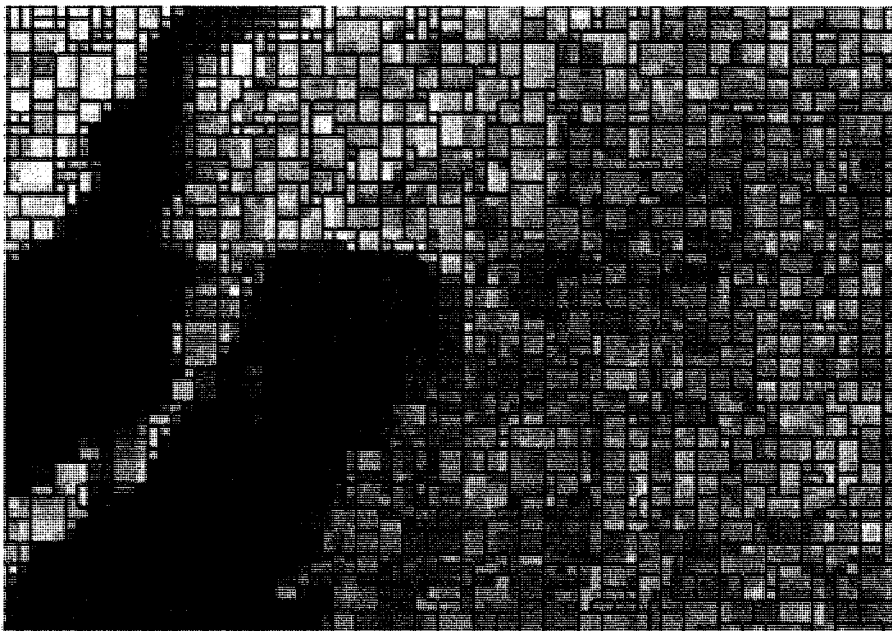
Figure 19. Level 2 segmentation.

Table 15. Inheritance rules used at level 2.

Class	Inheritance Rules
Water	Existence of super-objects level 3 no-cut = 1
Marsh	Existence of super-objects level 3 no-cut = 1
Fen	Existence of super-objects level 3 no-cut = 1
Bog	Existence of super-objects level 3 no-cut = 1
Conifer	Existence of super-objects level 3 no-cut = 1
Mixedwood	Existence of super-objects level 3 no-cut = 1
Deciduous	Existence of super-objects level 3 no-cut = 1
Cut	Existence of super-objects level 3 cut = 1

Once the initial Level 2 classification was generated, a set of feature-related and class-related rules were developed to improve the classification. Feature-related rules were created using membership functions. These membership functions were simply spectral thresholds applied to classes, and were based on the average spectral value of all pixels contained in an object. For example, figure 20 shows the mean spectral values for all mixedwood sample objects. A smaller than membership function was applied to band 3 with a left border of 0.04 and a right border of 0.05. This means that the probability of an object being classified as mixedwood is good if its band 3 mean spectral value is less than 0.04. As the mean of band 3 increases from 0.04 to 0.05, its potential of being classified as mixedwood decreases. Objects with mean band 3 values greater than 0.05 cannot be classified as mixedwood. A smaller than membership function was used on conifer mean band 6, deciduous mean band 5, mixedwood mean band 3 and mixedwood mean band 4. Details on left and right border values used are shown in figure 21. A greater than membership function was used on bog mean band 4 and fen mean bands 4, 5 and 6. Details on left and right border values used are shown in figure 22.
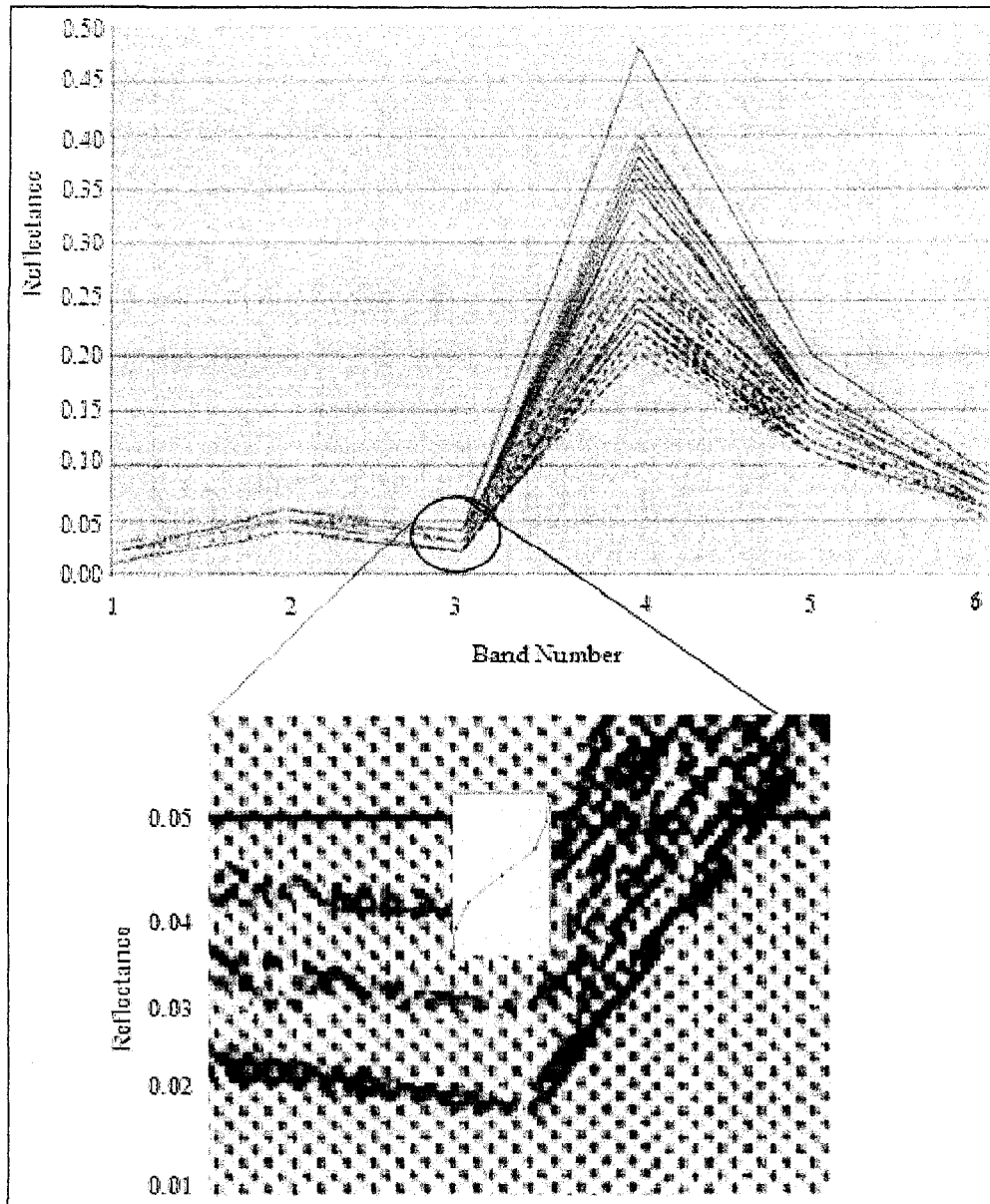
Figure 20. Landsat spectral graph of mixedwood samples illustration a membership function being applied to band 3.
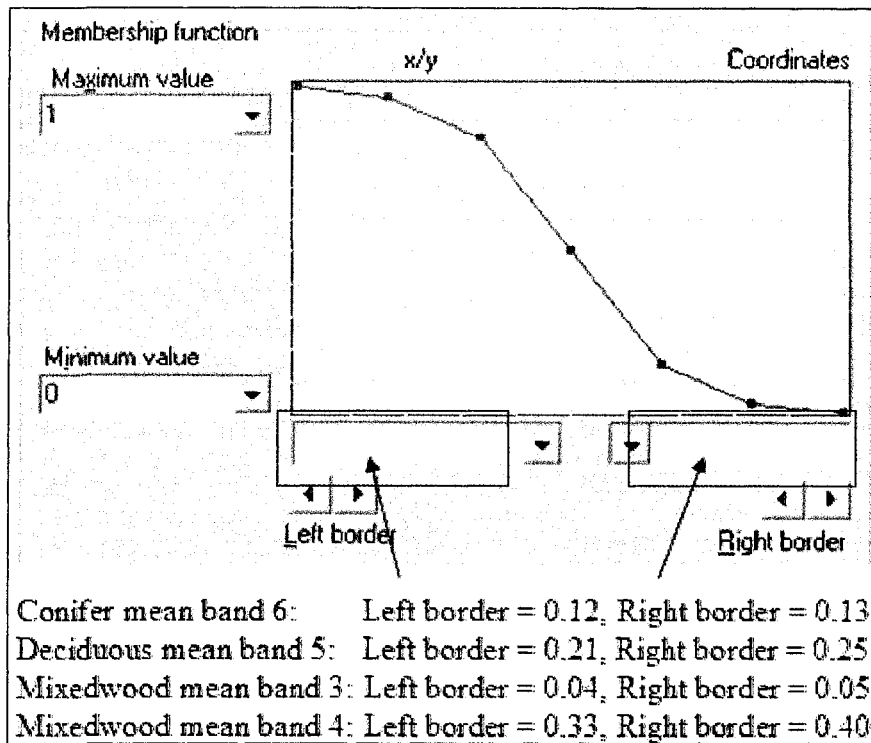
Figure 21. Smaller than member function curve used for class-related features.

Figure 22. Greater than member function curve used for class-related features.

Membership functions were also used to created class-related rules. The 'relative border to' membership function was applied to several classes. This function refers to the ratio of shared border between neighboring classes. For example, figure 23 shows a classified image consisting of water in blue, fen in purple, and land in green. If the relative border of a water object to marsh is equal to 1, then that water object is completely surrounded by fen. If the relative border of a water object to marsh is equal to 0 then there is no fen touching that water object border. In this study, a relative border to marsh was applied to classified water objects, a relative border to water was applied to classified marsh objects, and a relative border deciduous was applied to classified fen objects. A smaller than membership function curve was used for all three rules. Details on left and right border values used are shown in figure 24. The 'loop until nothing changes' option was applied to the classifier when the relative border to function was used. Once classified, segments for individual classes were merged prior to segmenting the next level.

Figure 23. Illustration showing the relative border of water objects to marsh.

Relative border of water to marsh: Left border = 0.5, Right border = 1
Relative border of marsh to water: Left border = 0.7, Right border = 0.8
Relative border of fen to deciduous: Left border = 0.6, Right border = 1
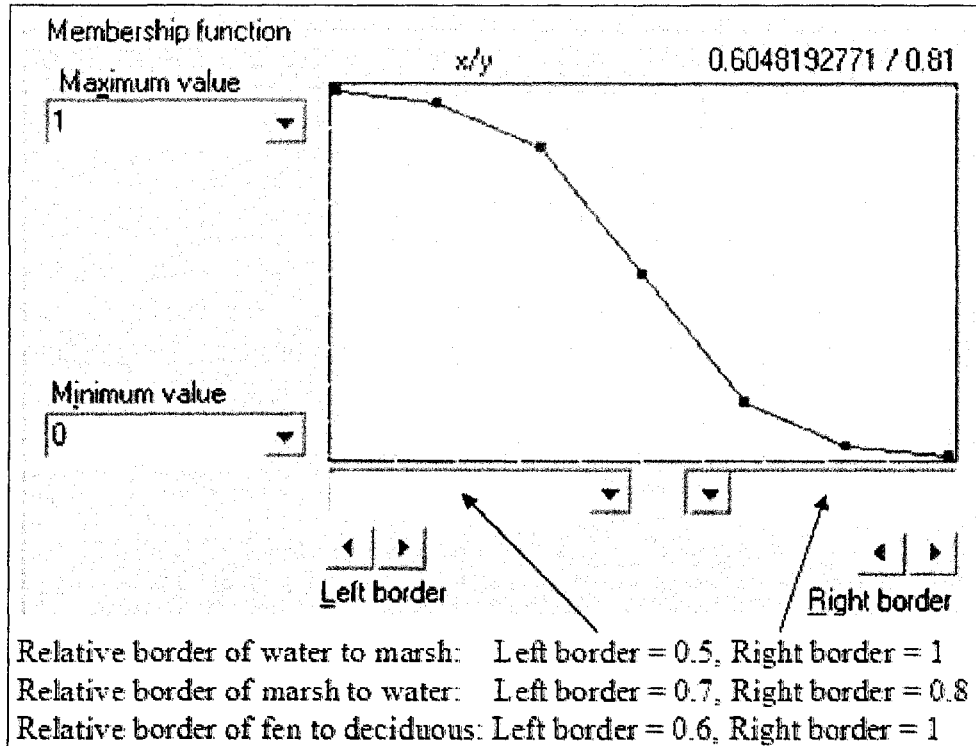
Figure 24. Smaller than relative border to membership function curve applied to water, marsh and fen.

The third level (level 1) contained the final classes in which the accuracy assessment was based on. It was used to further classify conifer into black spruce and jack pine, as well as deciduous into dense and sparse deciduous. It was also used to illustrate some addition capabilities of object-oriented image classification. The class hierarchy consist of water, wetland (aggregated marsh, fen and bog), black spruce, jack pine, mixedwood, dense deciduous, sparse deciduous, cuts (Figure 25). Once these eight classes were classified, their segments were merged by class. After the merge, water was further classified into 4 child classes based on size and a new class called island was also produced.
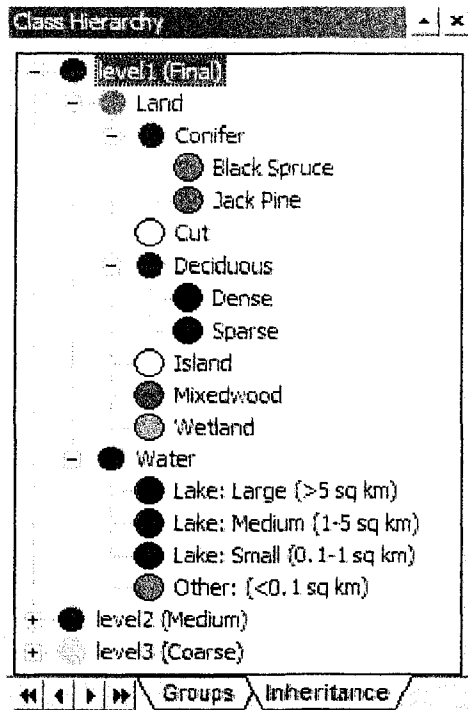
Figure 25. Class hierarchy used in level 1.

The final segmentation (level 1) was based on super-objects from level 2.

Parameters used in this segmentation were bands 2-6 having a weight of 1, a scale of 2,

and the composition of homogeneity was 0.9 for color, 0.1 for shape, 0.1 for

compactness and 0.9 for smoothness. Objects created in this segmentation were larger

than the previous level (Figure 26). Segmentation parameters were based on best initial

classification of spruce, pine, dense deciduous and sparse deciduous, using a nearest

neighbor classifier with inheritance rules. Details on inheritance rules are shown in table

16.
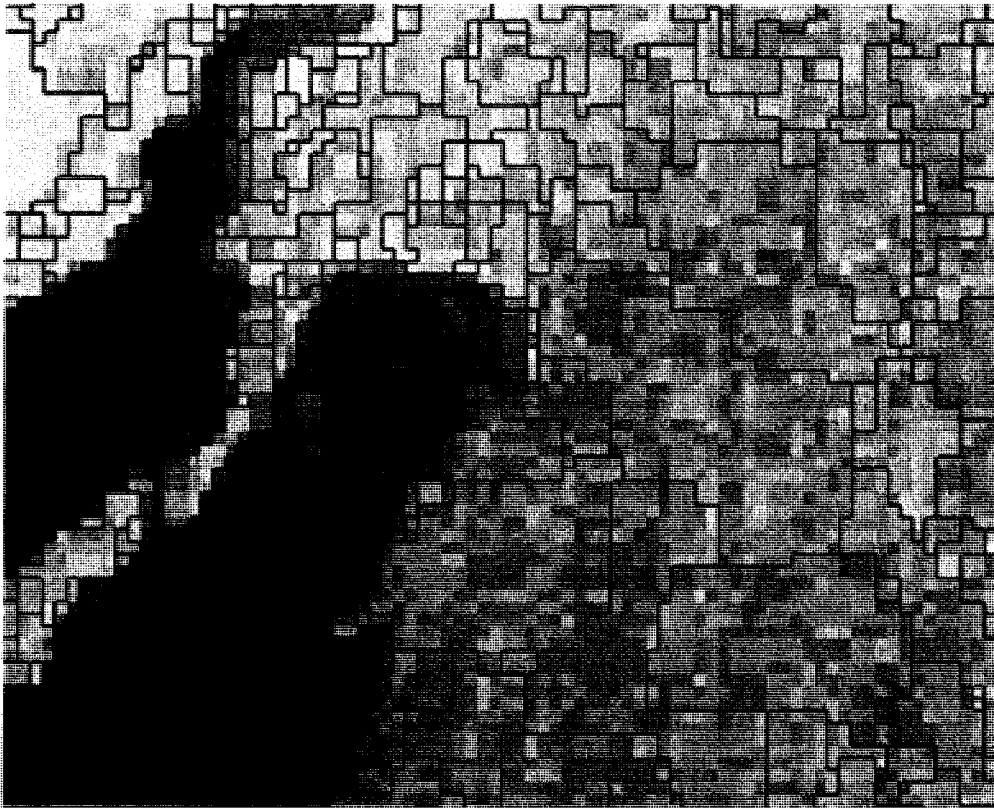
Figure 26. Level 1 segmentation used to classify conifer into spruce and pine as well as deciduous into sparse and dense.

Table 16. Inheritance rules used at level 1.

Class	Inheritance Rules
Water	Existence of super-objects level 2 water = 1
Wetland	Existence of super-objects level 2 wetland = 1
Black Spruce	Existence of super-objects level 2 conifer = 1
Jack Pine	Existence of super-objects level 2 conifer = 1
Mixedwood	Existence of super-objects level 2 mixedwood = 1
Dense Deciduous	Existence of super-objects level 2 deciduous = 1
Sparse Deciduous	Existence of super-objects level 2 deciduous = 1
Cut	Existence of super-objects level 2 cut = 1

Once the initial Level 1 classification was generated, a set of feature-related and class-related rules were developed to classify islands and further classify water into four child classes based on area. These child water classes are shown in table 17. The large lake class was defined by applying an area threshold greater or equal to 5 square

kilometers (Figure 27). The medium lake class was defined by using a membership

function constraining the area of the class between 1 and 5 square kilometers (Figure

28). The small lake class was defined by using a membership function with the same

curve as the medium size lake but limiting the area to between 0.1 and 1 square

kilometers. The fourth child water class consisted of all other objects classified as

water. A threshold was applied to this class, limiting the area to less than 0.1 square

kilometers. Finally, a class based algorithm called 'find enclosed by class' was used to

classify islands. This algorithm found black spruce, jack pine, dense deciduous, sparse

deciduous, mixedwood and cut objects that were completely contained within water,

and classified them as island. For example, figure 29 shows some spruce, pine,

mixedwood and dense deciduous objects that were enclosed by water and reclassified

into islands.

Table 17. Child classes of parent class water.

Class Name
Lake: Large (>5 sq km)
Lake: Medium (1-5 sq km)
Lake: Small (0.1-1 sq km)
Other: (<0.1 sq km)
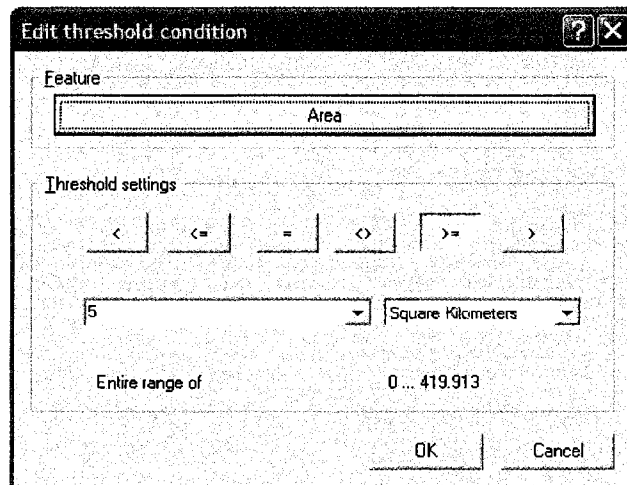
Figure 27. Threshold used to classify large lakes with an area greater than 5 km².
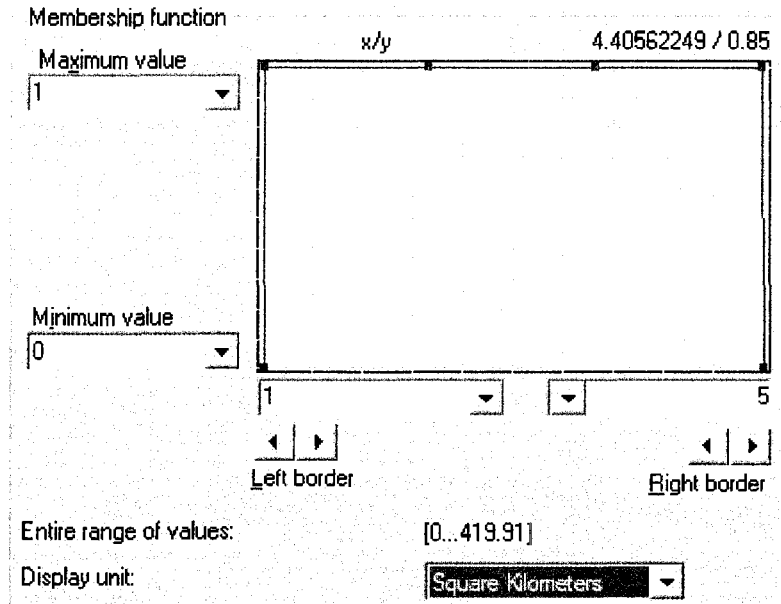
Figure 28. Membership function used to classify medium lakes between 1 and 5 km².

Figure 29. Illustration showing the change of spruce, pine, mixedwood and dense
deciduous classes enclosed by water being classified into island (yellow).

4.9.3 <u>Hyperion</u>

Four object levels were used to classify the Hyperion image. The same bands

selected from the pixel-based discriminant function analysis were used for object-

oriented classification. The first level (level 4) was the coarsest, and was used to

generate two classes; cut and no-cut. Child classes of no-cut included water, marsh,

fen, bog, conifer, mixedwood and deciduous. See figure 30a for class hierarchy. The

only concern at this level was to not confuse between cuts and no-cuts.

Misclassification among child classes of no-cut, such as conifer with mixedwood or

deciduous with mixedwood, was not a concern because theses class objects were

merged after level 4 was classified.

Level 4 multiresolution segmentation was based on the pixel level. Parameters

used in this segmentation were bands 7, 8, 11, 12, 13, 14, 17, 23, 25, 26, 27, 28, 31, 32,

33, 34, 40, 44, 47, 57, 58, 60, 64, 67, 68, 73, 77, 79, 80, 82, 74, 86, 89, 90, 92, 96, 99,

104, 110, 111, 113, 114, 115, 120, 130, 137, 138, 139, 152, and 154 having a weight

equal to 1. These bands are DFA bands in which SPSS declared as variables used in

each DFA used in the pixel-based analysis. Other parameters include a scale of 1.2 and

a color composition of homogeneity of 1.0 (Figure 31). This segmentation produced

large objects (Figure 30b). Once classified (Figure 30c), image object classified as no-

cut were merged into one single no-cut class (Figure 30d). Image objects classified as

cuts were merged with objects within their own class and remained as cuts for the rest
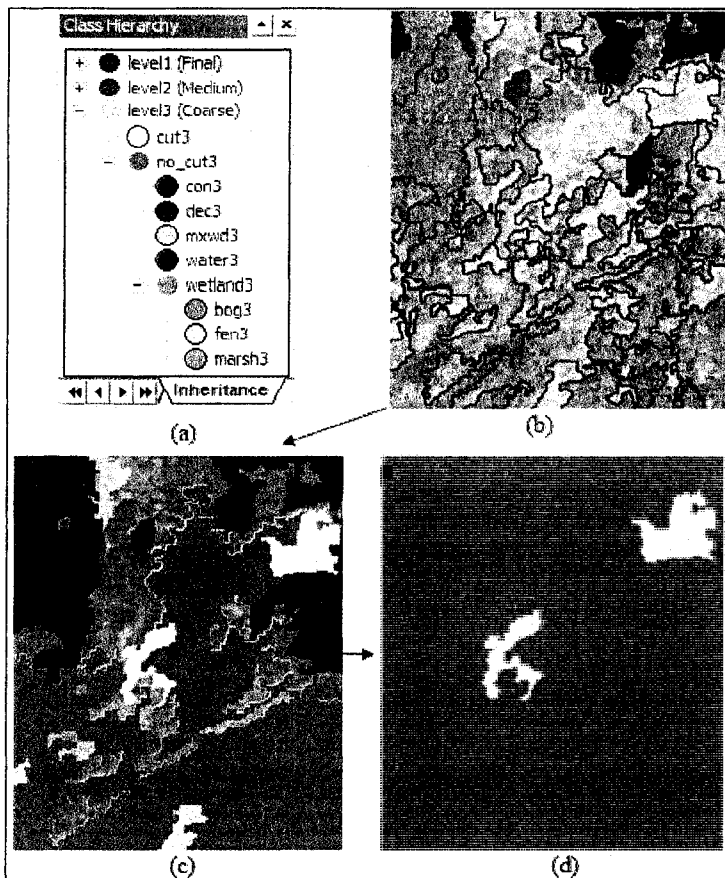
of the analysis.
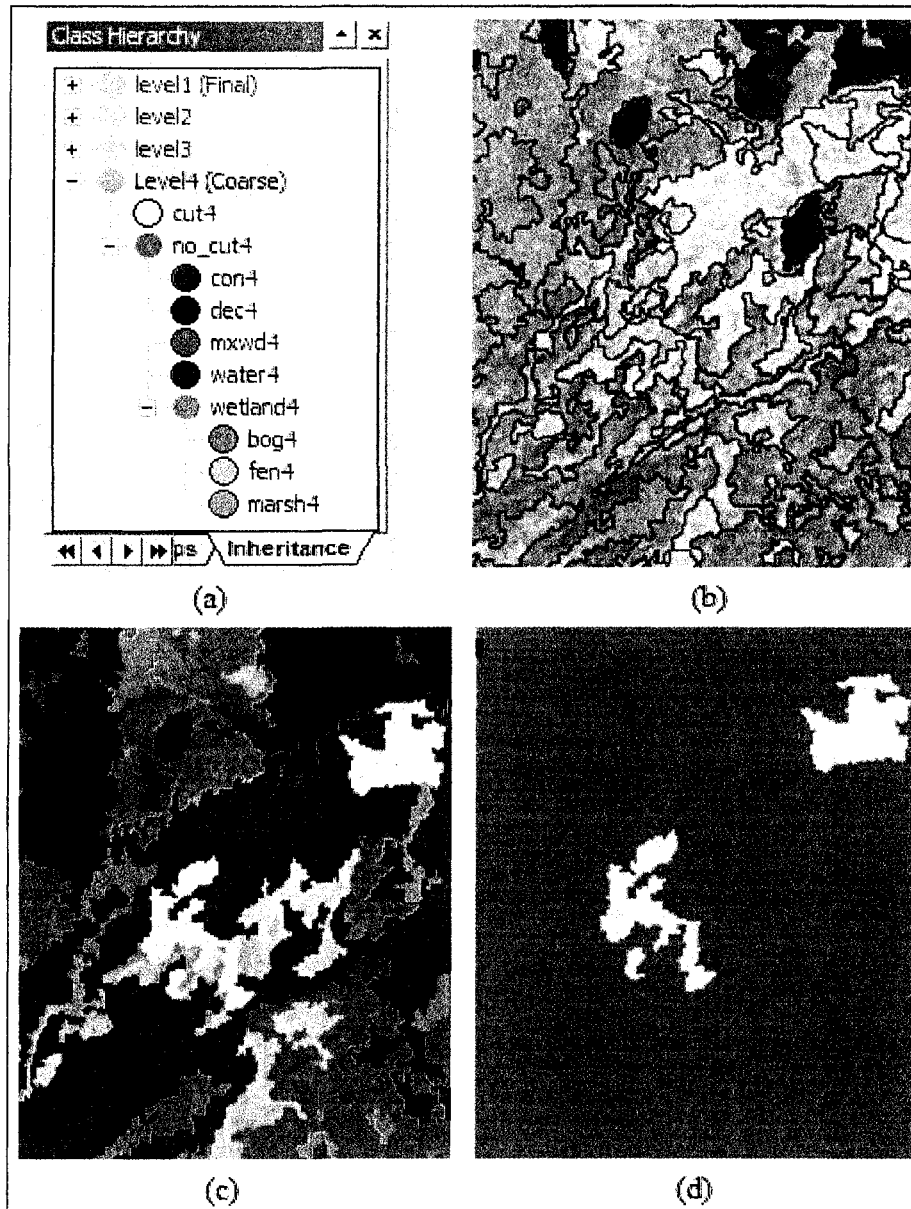
Figure 30. Hyperion Level 4 hierarchy (a), segmentation (b), classification (c) and final cut and no-cut objects (d).
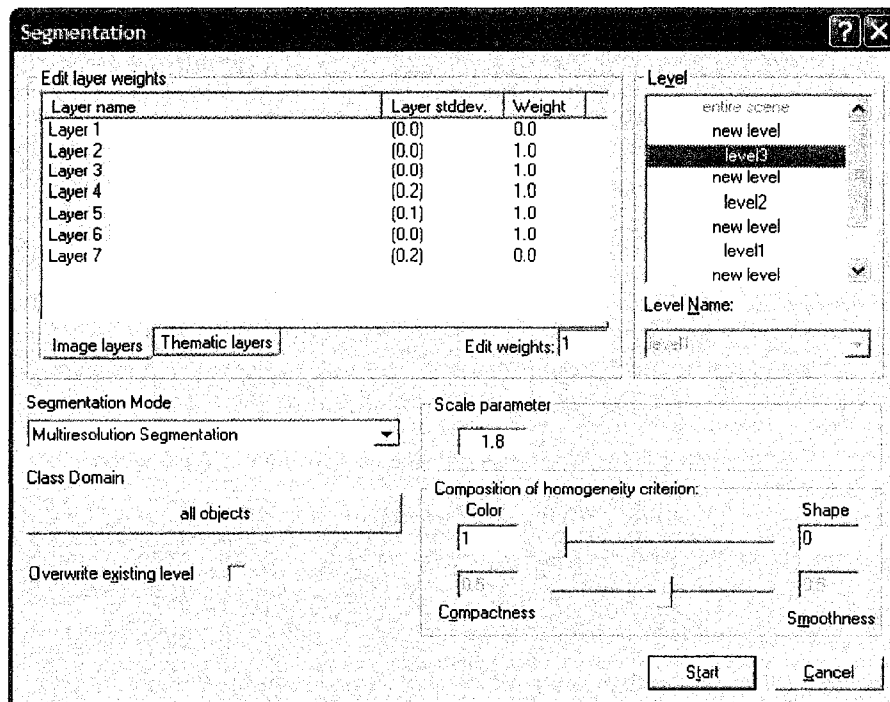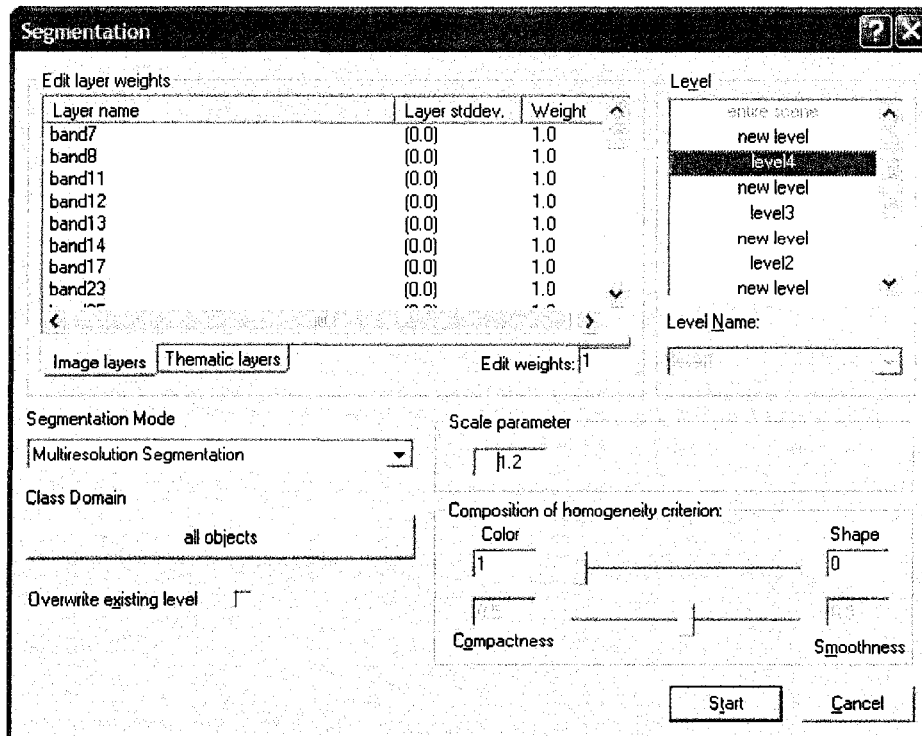
Figure 31. Segmentation interface showing parameters used in level 4.

The third level (level 3) is less coarse than the previous, and was used to further

classify super-object no-cuts from level 4, into general classes consisting of water,

marsh, fen, bog conifer, mixedwood and deciduous. See Figure 32 for class hierarchy.

In this hierarchy, bog, fen and marsh are child classes of the parent class wetland.

Essentially, the wetland class was used to aggregate marsh, fen and bog into a single

class for the final classification level to follow.

Level 3 segmentation was based on super-objects from level 4. Objects created

in this segmentation were smaller than in the previous level (Figure 33). Parameters

used in the segmentation were bands 11, 33, 44, 86 having a weight equal to 1, a scale

of 0.2, and composition of homogeneity was 0.9 for color, 0.1 for shape, 0.1 for

compactness and 0.9 for smoothness. Bands selected for segmentation were based

standardized canonical DFA coefficients (from level 1 pixel-based DFA) while

attempting to select bands dispersed across the electromagnetic spectrum.
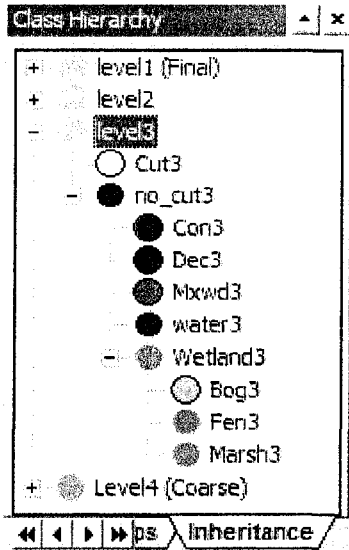
Figure 32. Hyperion's level 3 class hierarchy.
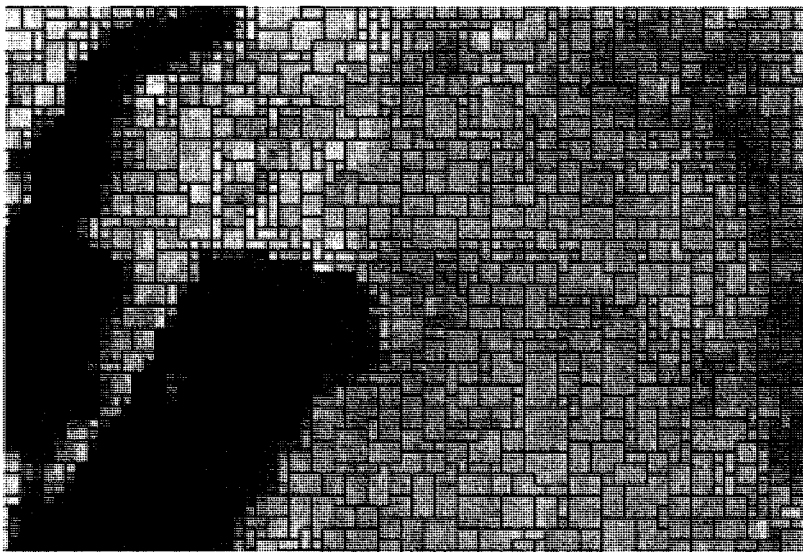
Figure 33. Hyperion's level 3 segmentation.

Segmentation parameters were based on best initial classification using a nearest

neighbor classifier and inheritance rules. Bands selected for the nearest neighbor

classification were based on the level 1 pixel-based DFA. Step 13, which consisted of

bands 7, 14, 26, 28, 31, 40, 57, 82, 86, 89, 92, 114, 120 provided to optimal initial

classification. Cuts did not require the nearest neighbor classifier because its final

objects were generated in the previous level. Feature-related and class-related rules

were not used for the initial classification in determining segmentation parameters, but were used afterwards to improve the classification. Inheritance rules used are shown in table 18.

Table 18. Inheritance rules used at level 3.

Class	Inheritance Rules
Water	Existence of super objects level 4 no-cut = 1
Marsh	Existence of super objects level 4 no-cut = 1
Fen	Existence of super objects level 4 no-cut = 1
Bog	Existence of super objects level 4 no-cut = 1
Conifer	Existence of super objects level 4 no-cut = 1
Mixedwood	Existence of super objects level 4 no-cut = 1
Deciduous	Existence of super objects level 4 no-cut = 1
Cut	Existence of super objects level 4 cut = 1

Once the initial Level 3 classification was generated, a set of feature-related and class-related rules were developed to improve the classification. A smaller than membership function was used on deciduous mean band 8, deciduous mean band 13, mixedwood mean band 34, bog mean band 7, fen mean band 7, and marsh mean bands 7 and 44. Details on left and right border values used are shown in figure 34. A greater than membership function was used on bog mean bands 34 and 44, as well as fen mean bands 13, 34, and 89. Details on left and right border values used are shown in figure 35.

Deciduous mean band 8:   Left border = 0.038, Right border = 0.046
Deciduous mean band 13:   Left border = 0.085, Right border = 0.095
Mixedwood mean band 34: Left border = 0.270, Right border = 0.330
Bog mean band 7:   Left border = 0.105, Right border = 0.115
Fen mean band 7:   Left border = 0.080, Right border = 0.090
Marsh mean band 7:   Left border = 0.330, Right border = 0.400
Marsh mean band 44:   Left border = 0.256, Right border = 0.266

Figure 34. Smaller than member function curve used for class-related features.

Bog mean layer 34: Left border = 0.170, Right border = 0.210
Bog mean band 44: Left border = 0.185, Right border = 0.198
Fen mean band 13: Left border = 0.070, Right border = 0.080
Fen mean band 34: Left border = 0.190, Right border = 0.200
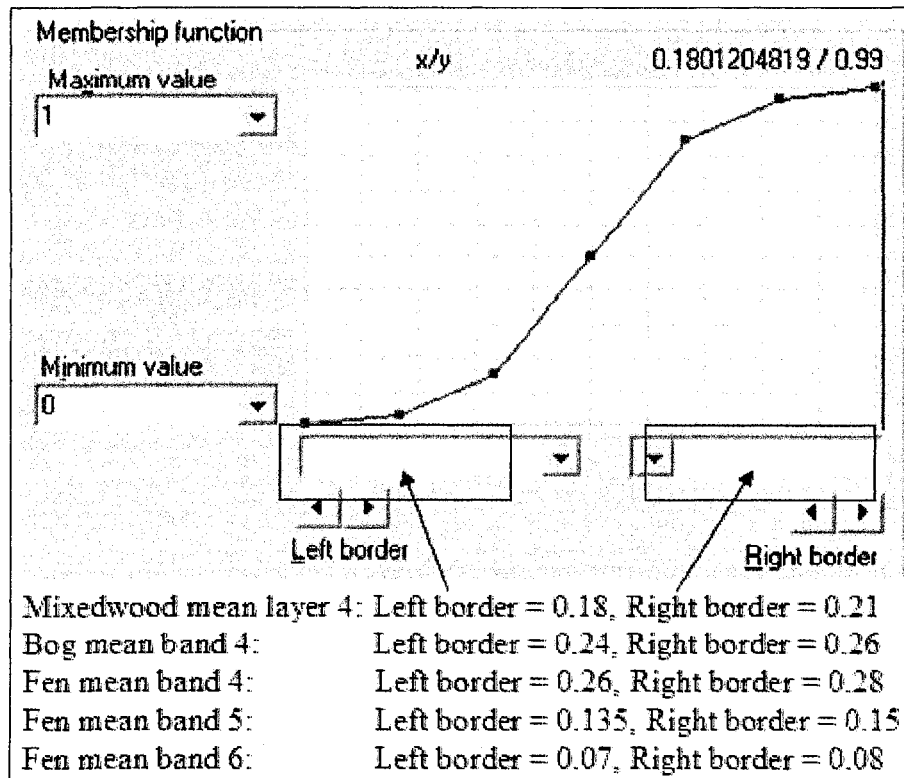Fen mean band 89: Left border = 0.150, Right border = 0.160
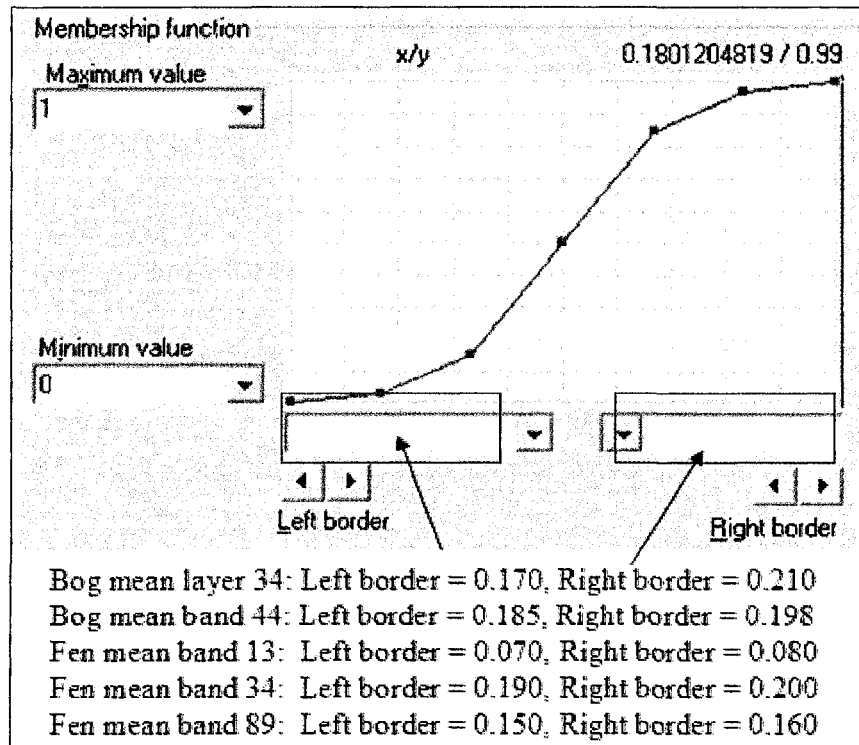
Figure 35. Greater than member function curve used for class-related features.

Membership functions were also used to created class-related rules. A 'relative border to' marsh membership function was applied to classified water objects, a 'relative border to' water was applied to classified marsh objects, and a 'relative border to' deciduous classes was applied to classified fen objects. All three rules had a smaller than membership function curve. Details on left and right border values used are shown in figure 36. The 'loop until nothing changes' option was applied to the classifier when the relative border to function was used. Once classified, segments for individual classes were merged prior to segmenting the next level.
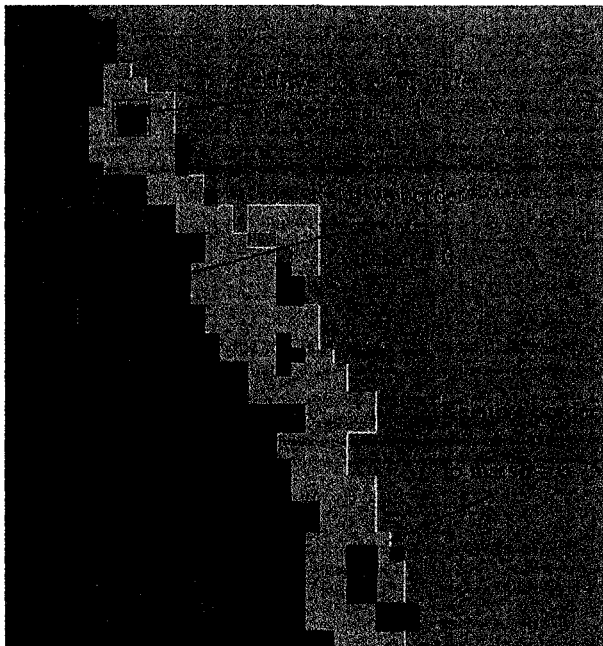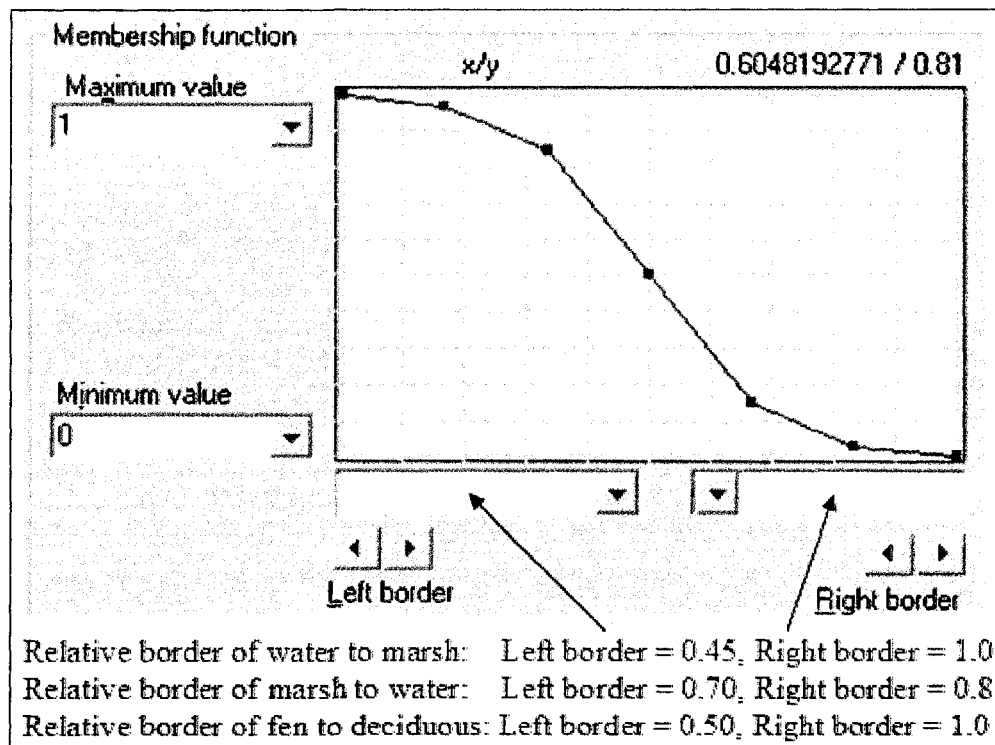

Figure 36. Smaller than relative border to membership function curve applied to water, marsh and fen showing left and right border values.

The third level (level 2) was used to further classify deciduous into dense and sparse deciduous. Level 2 segmentation was based on super-objects from level 3. See Figure 37 for class hierarchy. In this hierarchy, bog, fen and marsh are aggregated into a single class called wetland. Objects created in this segmentation were smaller than

level 4 and larger than the previous level 3 (Figure 38). Parameters used in the segmentation were bands 11, 33, 44, 86 having a weight equal to 1, a scale of 2, and composition of homogeneity was 0.9 for color, 0.1 for shape, 0.1 for compactness and 0.9 for smoothness. Segmentation parameters were based on best initial classification using a nearest neighbor classifier and inheritance rules. Bands selected for the nearest neighbor classified were based on the level 1 pixel-based DFA.

For the classification parameters, step 8 from the pixel-based DFA which discriminated dense from sparse deciduous was found to be the optimum band combination. These bands consisted of bands 23, 64, 77, 99, 104, 115, 130, and 138. Cut, wetland, conifer, water and mixedwood did not require the nearest neighbor classifier because their final objects were generated in the previous level. Inheritance rules used are shown in table 19. Feature related and class related rules were not applied to dense and sparse deciduous classes. Once classified, segments for individual classes were merged prior to segmenting the next level.
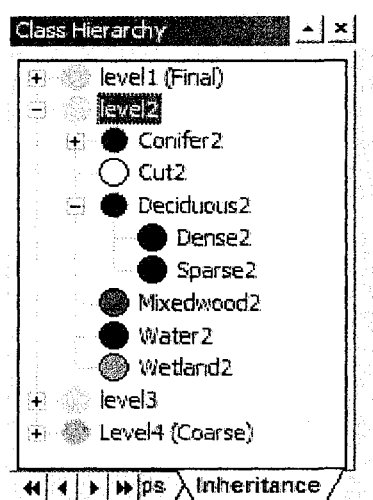
Figure 37. Hyperion's level 2 class hierarchy.
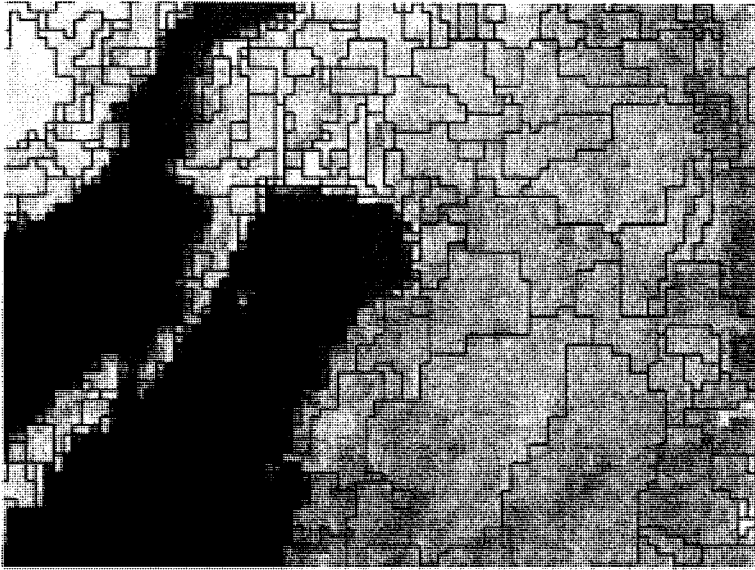
Figure 38. Level 2 segmentation used to classify deciduous into dense and sparse deciduous.

Table 19. Inheritance rules used at level 1.

Class	Inheritance Rules
Water	Existence of super-objects level 2 water = 1
Wetland	Existence of super -objects level 2 wetland = 1
Black Spruce	Existence of super-objects level 2 conifer = 1
Jack Pine	Existence of super-objects level 2 conifer = 1
Mixedwood	Existence of super-objects level 2 mixedwood = 1
Dense Deciduous	Existence of super-objects level 2 deciduous = 1
Sparse Deciduous	Existence of super-objects level 2 deciduous = 1
Cut	Existence of super-objects level 2 cut = 1

The fourth level (level 1) contained final classes in which the accuracy assessment was based on. It was used to further classify conifer into black spruce and jack pine, as well as illustrate some additional capabilities of using an object-oriented classification approach. See Figure 39 for class hierarchy. The class hierarchy consist of water, wetland (aggregated marsh, fen and bog), black spruce, jack pine, mixedwood, dense deciduous, sparse deciduous, cuts. Once these eight classes were classified, their segments were merged by class. After the merge, water was further classified into four child classes based on size and a new class call island was also produced.

Level 1 segmentation was based on super-objects from level 2. Objects created in this segmentation were the same size as level 3 (Figure 40). Parameters used in the segmentation were bands 11, 33, 44, 86 having a weight equal to 1.0, a scale of 0.2, and composition of homogeneity was 0.9 for color, 0.1 for shape, 0.1 for compactness and 0.9 for smoothness. Segmentation parameters were based on best initial classification using a nearest neighbor classifier and inheritance rules. Bands selected for the nearest neighbor classified were based on the level 2 pixel-based DFA, discriminating spruce and pine.

For the classification parameters, step 11 from the pixel-based DFA which discriminated pine from spruce was found to be the optimum band combination. These bands consisted of bands 14, 17, 25, 32, 47, 58, 60, 68, 138, 152, and 154. Cut, wetland, conifer, water, mixedwood, sparse deciduous and dense deciduous did not require the nearest neighbor classifier because their final objects were generated in the previous levels. Inheritance rules used are shown in table 20. Once classified, segments for individual classes were merged prior to classifying islands and further classifying water into four child classes.
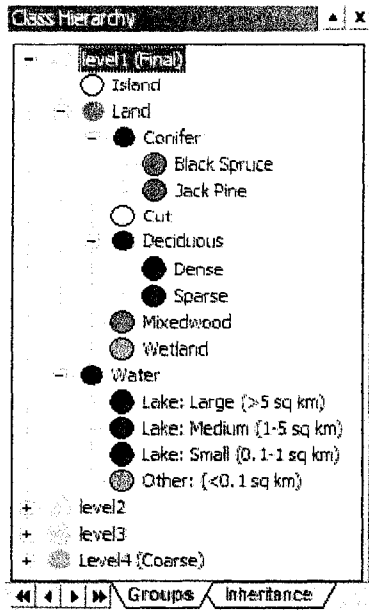
Figure 39. Hyperion's level 1 class hierarchy
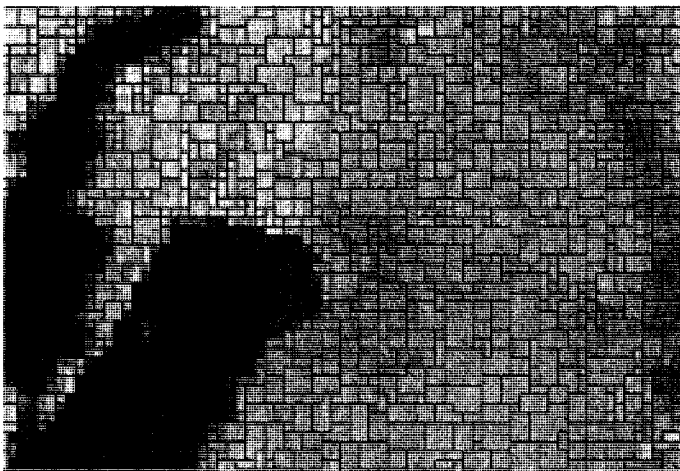
Figure 40. Level 1 segmentation used to classify conifer into black spruce and jack pine.

Table 20. Inheritance rules used at level 1.

Class	Inheritance Rules
Water	Existence of super objects level 2 water = 1
Wetland	Existence of super objects level 2 wetland = 1
Black Spruce	Existence of super objects level 2 conifer = 1
Jack Pine	Existence of super objects level 2 conifer = 1
Mixedwood	Existence of super objects level 2 mixedwood = 1
Dense Deciduous	Existence of super objects level 2 deciduous = 1
Sparse Deciduous	Existence of super objects level 2 deciduous = 1
Cut	Existence of super objects level 2 cut = 1

Once the initial Level 1 classification was generated, a set of feature-related and class-related rules were developed to classify islands, spruce, pine and further classify water into four child class which based on area. A smaller than membership function was applied to the spectral value of jack pine (Figure 41). A larger than membership function was applied to the spectral value of both jack pine and black spruce (Figure 42).

Child water classes are shown in table 16 above. The large lake class was defined by applying an area threshold greater or equal to 5 square kilometers (Figure 27). The medium lake class was defined by using a membership function constraining the area of the class between 1 and 5 square kilometers (Figure 28). The small lake class was defined by using a membership function with the same curve as the medium size lake but limiting the area to between 0.1 and 1 square kilometers. The fourth child water class consisted of all other objects classified as water. A threshold was applied to this class, limiting the area to less than 0.1 square kilometers. Finally, a class based algorithm called 'find enclosed by class' was used to classify islands. This algorithm found black spruce, jack pine, dense deciduous, sparse deciduous, mixedwood and cut objects that were completely contained within water, and classified them as island.

Figure 41. Smaller than member function curve applied to band 25 for jack pine.

Black Spruce mean band 13: Left border = 0.056, Right border = 0.068
Jack Pine mean band 114: Left border = 0.080, Right border = 0.110
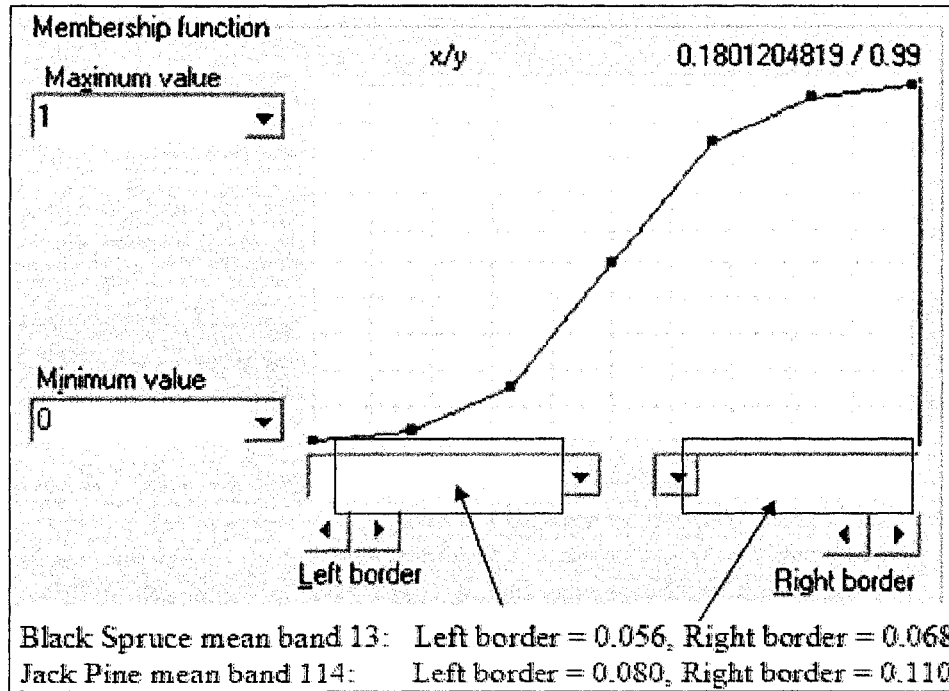
Figure 42. Greater than member function curve applied to class-related features for spruce and pine.

CHAPTER 5
RESULTS

5.1 RADIOMETRIC CORRECTION

5.1.1 Hyperion Abnormal Pixel Correction

Visual comparison between level 1a and level 1b Hyperion bands clearly

indicated that the abnormal pixel correction process was successful. Figure 43 shows

the obvious dark continuous class one abnormal pixel strip no longer present in the

corrected image. Figure 44 shows that less obvious class 2 abnormal pixels are no

longer present in the corrected image either. Figure 45 shows an improvement in the

common but difficult to see class 4 intermittent abnormal pixels.
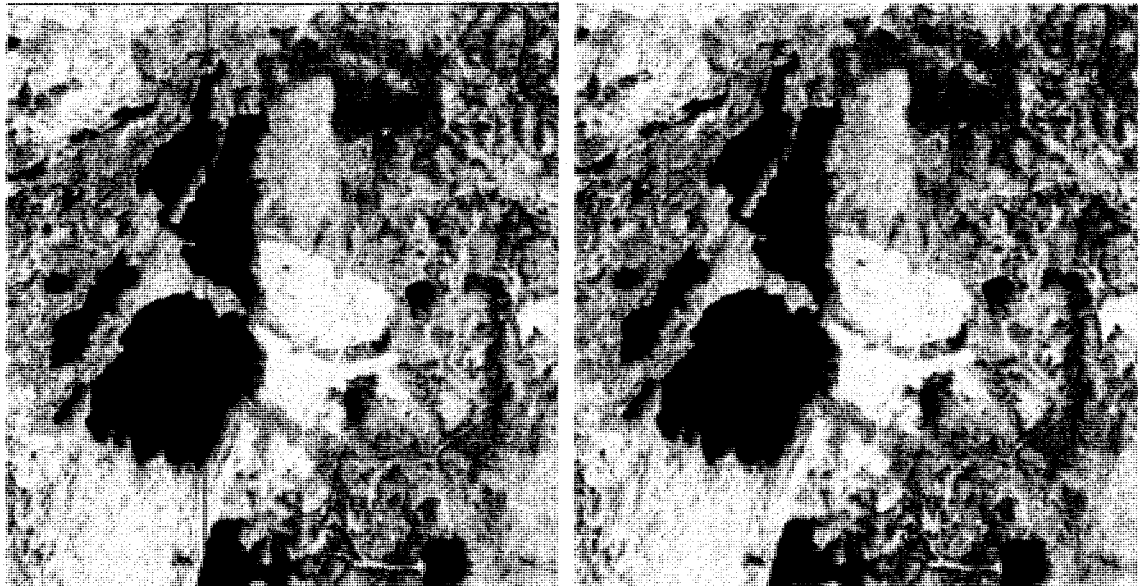
Figure 43. Band 94 level 1a (left) and level 1b (right) Hyperion imagery, showing
Class 1 abnormal pixel correction.
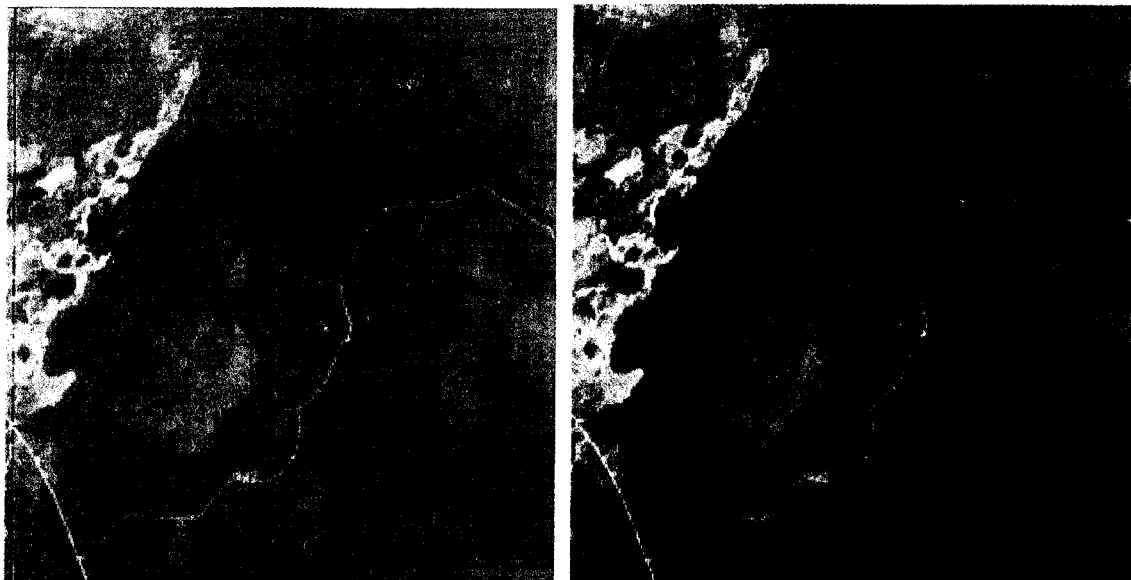
Figure 44. Band 11 level 1a (left) and level 1b (right) Hyperion imagery, showing Class 2 abnormal pixel correction.
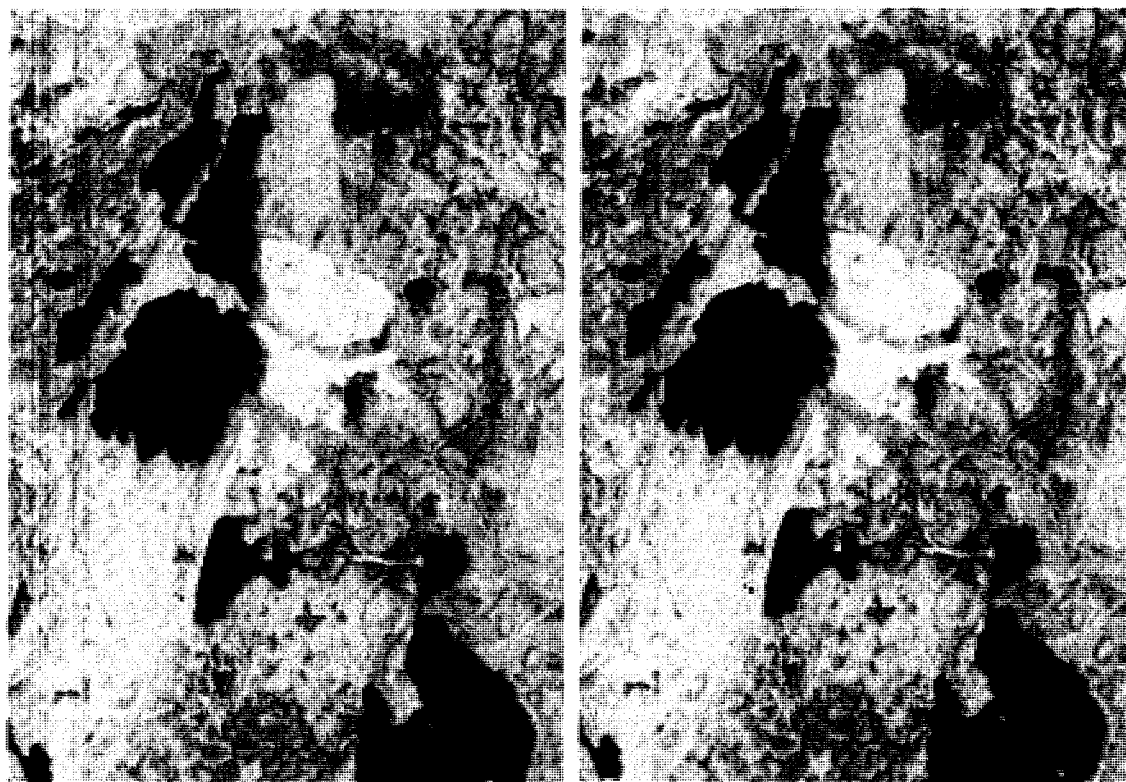
Figure 45. Band 57 level 1a (left) and level 1b (right) Hyperion imagery, showing class 4 abnormal pixel correction.

5.1.2 <u>Convert to Radiance</u>

The conversion of raw Hyperion DN values to spectral radiance changed the

reflectance scale (Figures 46 and 47). A greater decrease in SWIR bands DN values

than in the VNIR bands were also observed. The conversion of Landsat L0 to L1

radiance showed greatest changes with the decrease in the blue, and MIR and FIR

(Figure 48 and 49). Both Hyperion and Landsat graphs resemble radiometrically

corrected datasets of vegetation as found in literature such as Jensen 2005.
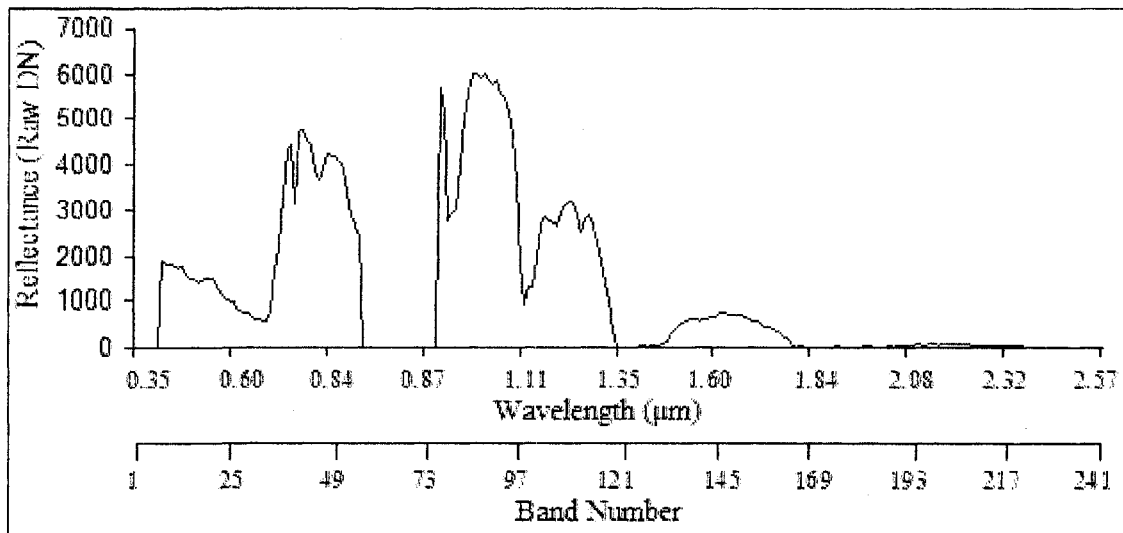
Figure 46. Deciduous vegetation from an un-radiometrically corrected Hyperion image.
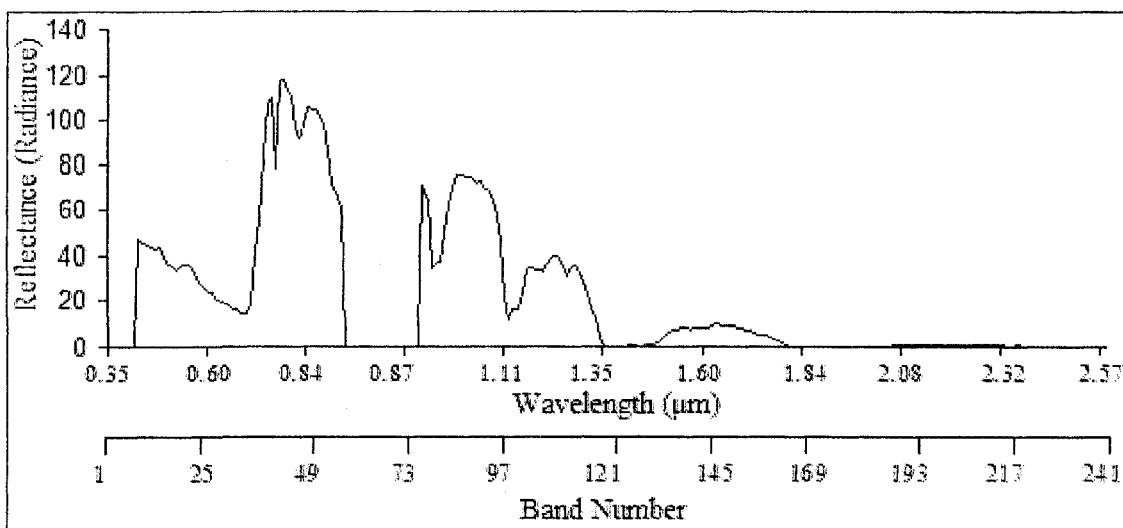
Figure 47. Deciduous vegetation from a radiometrically correct Hyperion image.
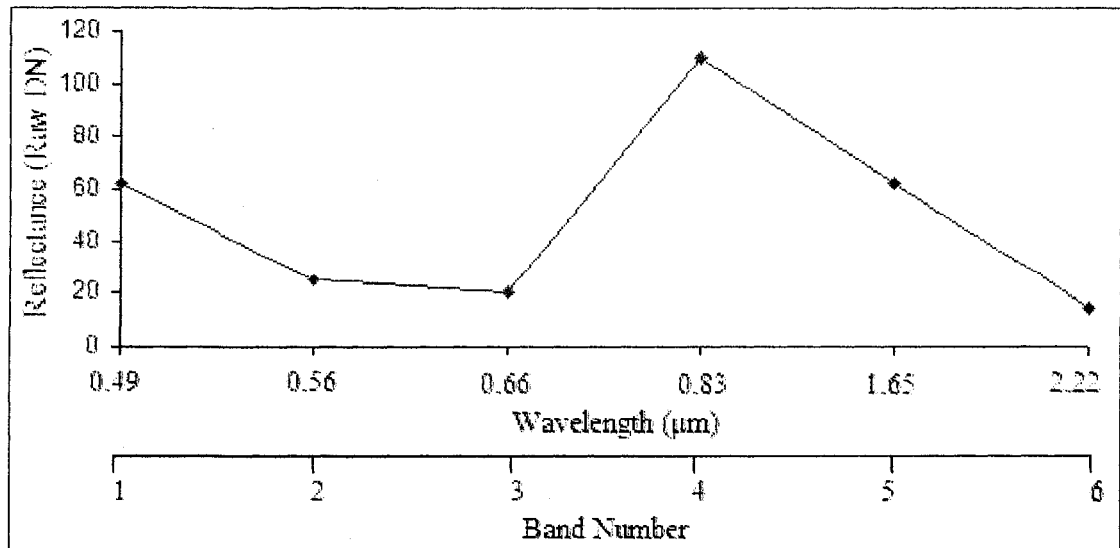
Figure 48. Deciduous vegetation from an un-radiometrically corrected Landsat image.
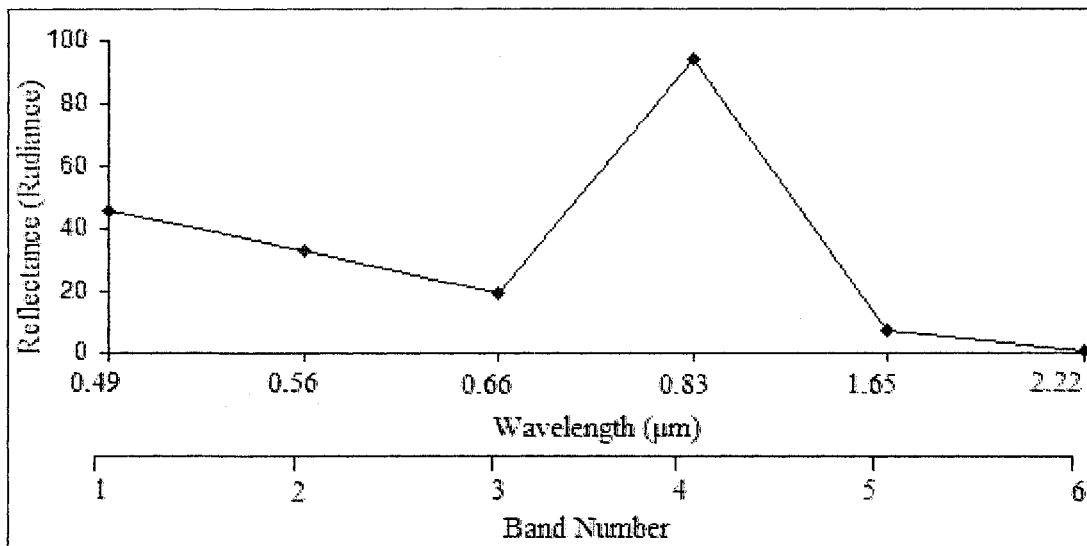
Figure 49. Deciduous vegetation from radiometrically corrected Landsat image.

5.2 ATMOSPHERIC CORRECTION & BAD BAND REMOVAL

The visual inspection of vegetation graphs demonstrated that atmospheric

correction resulted in graphs similar to atmospherically corrected datasets illustrated in

remote sensing text books such as Jensen (2005). Atmospherically correcting with

Landsat was straightforward, and the output image was ready for geometric correction

(Figure 50). Hyperion, however, was problematic, and the presence of bad bands within the Hyperion dataset was evident and needed to be removed.

During the atmospheric correction process of the Hyperion image, the spectral analysis workstation required non-calibrated bands (1-7, 58-76, 225-242) to first be removed, resulting in an image with 198 bands. Figure 51 shows a graph of a deciduous sample from the atmospheric correct image with non-calibrated bands removed. Of the 198 bands, however, there still remained bad bands that contain extreme values. These bands were the water absorption bands and bands that show poor visually image quality. Figure 52 shows a graph of a deciduous sample that is atmospherically corrected and has all bad bands removed. With the completion of the atmospheric correction and the removal of all bad bands, the new Hyperion image consisted of 155 good bands, and was ready for geometric correction. See appendix XIII for new wavelengths of each new band number.
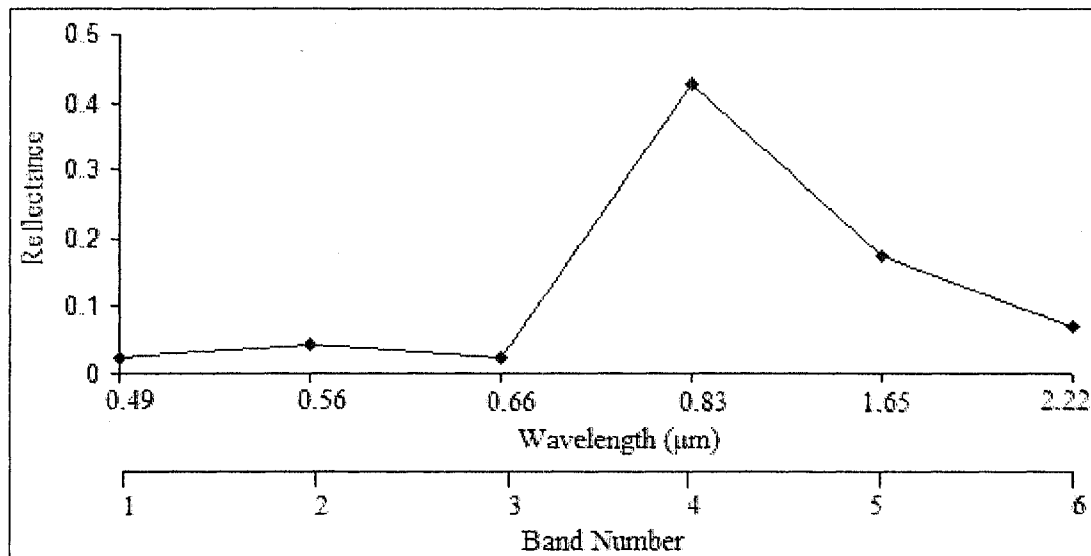
Figure 50. Atmospheric corrected Landsat graph of deciduous vegetation.
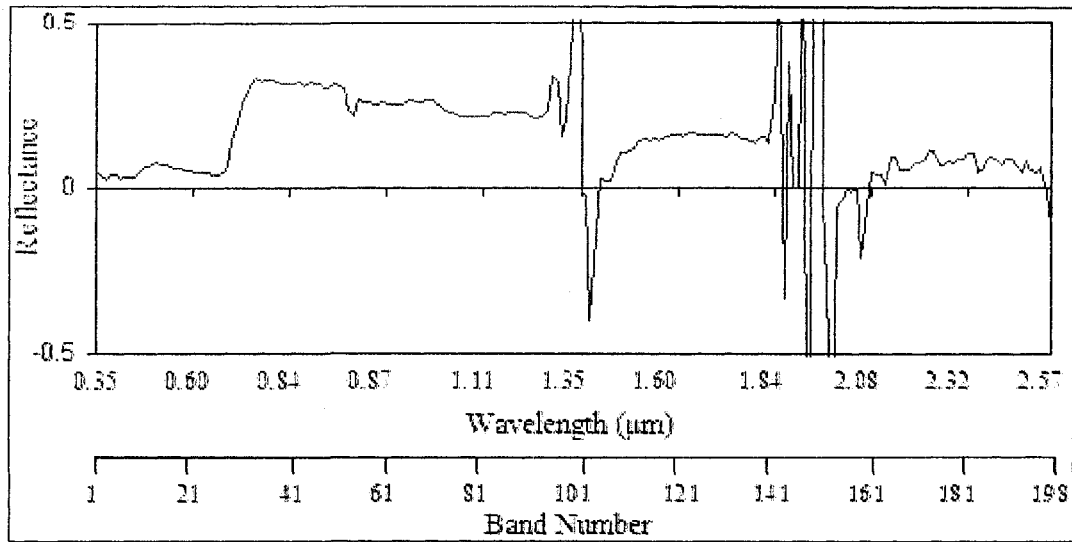
Figure 51. Atmospheric corrected Hyperion (198 bands) graph of deciduous vegetation, still showing water absorption bands with extreme values.
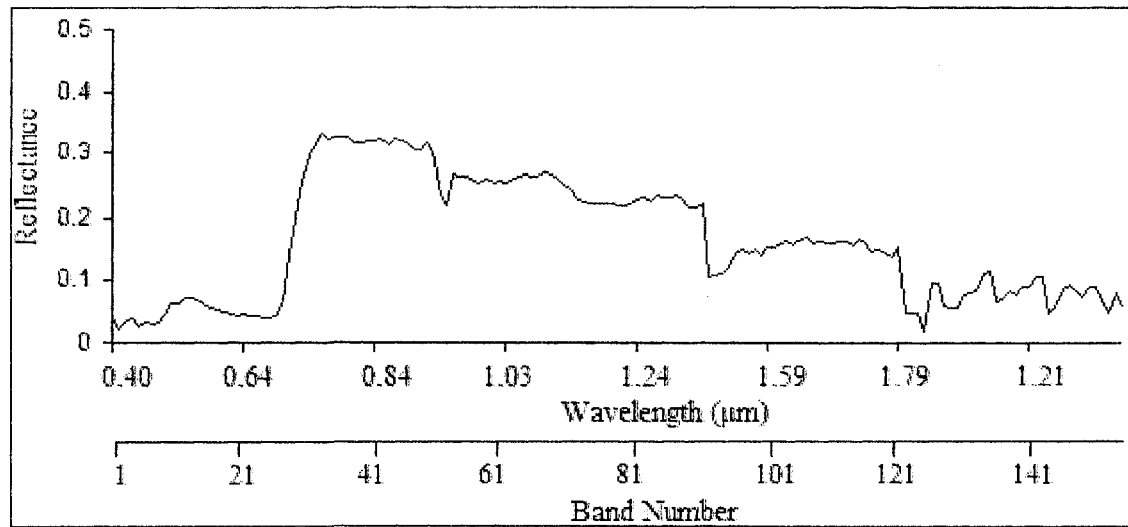
Figure 52. Atmospheric corrected Hyperion (155 bands) graph of deciduous vegetation with all bad bands removed.

5.3 IMAGE ANALYSIS (PIXEL-BASED)

5.3.1 <u>Discriminant Function Analysis (Level 1)</u>

Stepwise discriminant function analysis (DFA) was used as a feature (band) selection method for Hyperion. Hyperion imagery has high correlations (> 0.90) between bands (predictor variables) when wavelengths are close to one another. Appendix XVIII shows a pooled within-groups correlation matrix showing average correlations for the first 19 bands. Bands 5 through 19 showed a high correlation with one or more other bands. In addition, some bands selected in the stepwise DFA showed high correlations as well (Appendix XIX). Although datasets with high correlated predictor variables is a violation of one of the assumptions in stepwise DFA, it is unavoidable with the nature of hyperspectral imagery and DFA was used with this violation.

Discriminant scores represent individual case (sample) values that result from applying a discriminant function formula. Overall, the discriminant function analysis worked well. Figure 53 uses discriminant functions 1 and 2 to show how well the functions separate each group. Discriminant function 1 separates water and cuts well from all other classes, except for some overlap with marsh. It does not however, separate deciduous, mixedwood, conifer, fen and bog well from one another. Although function 2 shows some overlap between mixedwood with deciduous and conifer, it does separate deciduous from conifer, marsh, bog and fen well. Both functions show some overlap with marsh, fen and bog. All group means are well separated except for mixed wood and fen, and conifer and bog.

Canonical Discriminant Functions
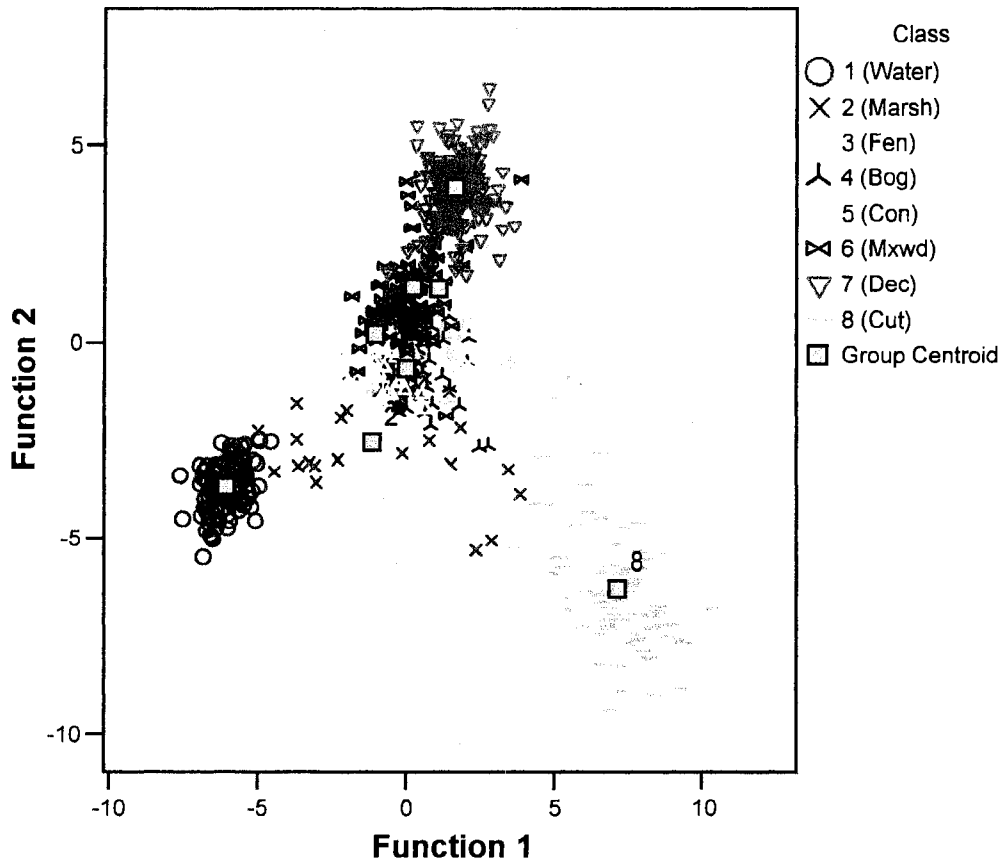
Figure 53. Scatter plot of canonical discriminant function scores for functions 1 and 2.

Wilks' Lambda measures unexplained variability in the data, and shows how

well each function separates cases into groups (Appendix XX), with smaller values

indicating better separation. The null hypothesis of the Wilks' Lambda test is that

group means are equal. Group function scores differed significantly for all functions

(p< 0.001). The null hypothesis was rejected, and therefore all test of functions separate

the groups. Functions 1-7 (< 0.1%), 2-7 (0.4%), and 3-7 (3.8%) showed low

unexplained variability in the model. Functions 4-7 showed moderate unexplained

variability in the model (20.8%). Functions 5-7 (52.9%), 6-7 (70.9%) and 7 (86.7%) showed higher unexplained variability in the model.

Canonical correlation indicates how much relationship there is between the discriminant scores on that axis and the group structure. The square of the canonical correlation is the percent of total variability in scores explained by differences among groups. In general, a higher the canonical correlation represents greater separation in scores amoung groups. Functions 1-4 hold the highest amount of variability in the discriminant scores based on group structure (Appendix XX). Ninety point six percent (0.952^2) of the variability in the discriminant scores of function 1 is based on group structure, which is high. Sixty point seven percent (0.779^2) of the variability in the discriminant scores of function 4 is based on group structure. Twenty-five point four percent (0.504^2) of the variability in the discriminant scores of function 5 is based on group structure, which is low.

Standardized canonical discriminant function coefficients compare the importance each band (independent variable) has on individual functions. Coefficients with large positive or negative values correspond to variables with greater discriminating ability. Appendix XXI lists the coefficients for functions 1-4. Discriminant function 1 is most correlated with transition band 32 between red and NIR, as well as NIR band 44. Function 2 is most correlated with transition bands 28 and 31 between visible red and NIR, as well as SWIR bands 84 and 86. Function 3 is most correlated with SWIR bands 84 and 86, and function 4 is most correlated with NIR bands 31 and 34.

5.3.2 Discriminant Function Analysis (Level 2)

5.3.2.1 Black Spruce and Jack Pine

Stepwise discriminant function analysis (DFA) was used as a feature (band) selection method, for separating groups (spruce and pine). The boxplot in Figure 54 was used as a graphical way of comparing the separation of groups (spruce and pine) defined by a factor variable (scores from function 1). Overall, it shows good separation between groups. The box represents the interquartile range, which is derived by the upper and lower quartiles, and represents 50% of the data (Wikipedia 2007). The lower quartile (1st quartile) cuts off the lower 25% of the scores and the upper quartile (3rd quartile) cuts off the highest 25% of the scores. This results in a box stretching from the lower 25th percentile to the upper 75th percentile. The non-overlapping the interquartile ranges in this case indicates the groups are well separated. The horizontal line within a box represents the median. The medians in this case are well separated indicating good separation between groups. The whiskers, which are lines attached to the boxes, represent the minimum and maximum score values, except for outliers. They extend a maximum of 1.5 times the 1st and 3rd quartile value. The non-overlapping of the whiskers when comparing the two groups indicated good separation. The overlapping of some outliers from pine with the whiskers of spruce, indicates a small amount of misclassification when separating the two groups. Outliers are extreme cases with data values that fall outside the extent of the whiskers (Wikipedia 2007).
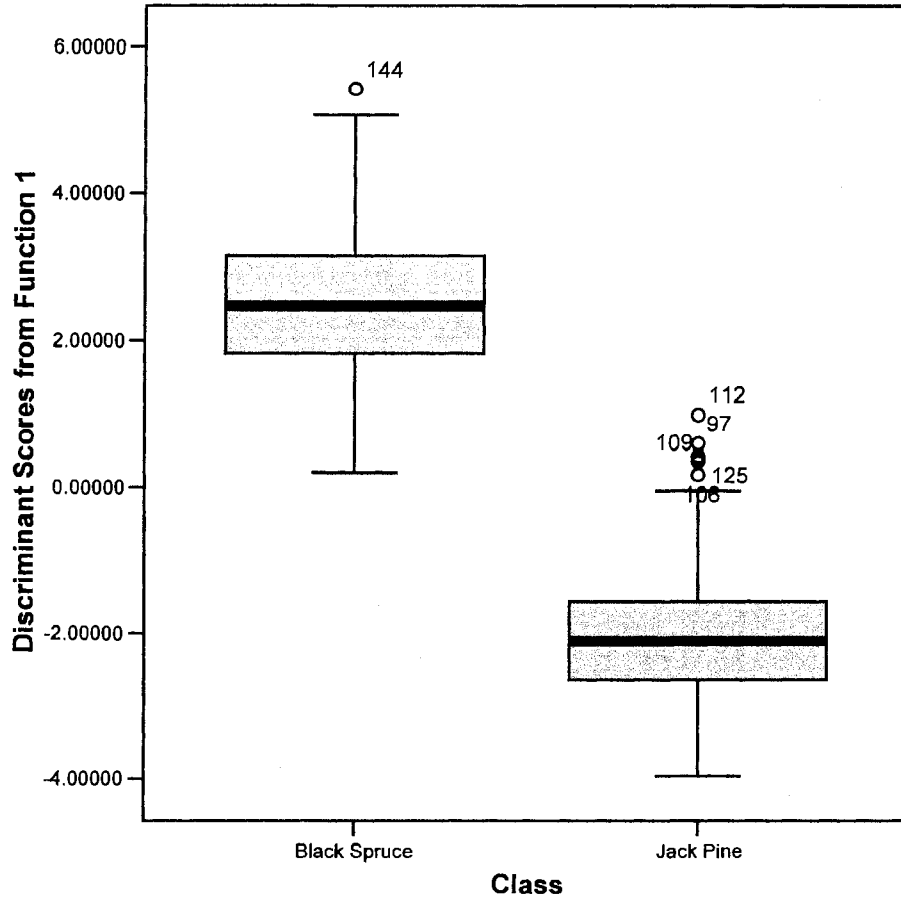
Figure 54. Box plot of spruce and pine function 1 discriminant scores.

Wilks' Lambda for Function 1 showed a low 16.5% of unexplained variability

of the data in the model, indicating good separation of cases into groups (Appendix

XXII). Test of function 1 was significant (p<0.001), meaning function 1 significantly

separates the groups. Canonical correlation indicated that 83.54% (0.914^2) of the

variability in the discriminant scores of function 1 is based on group structure

(Appendix XXII). Standardized canonical discriminant function coefficients indicate

that function 1 is most correlated with NIR bands 40 and 41 and SWIR band 59

(Appendix XXII).

5.3.2.2 Dense and Sparse Deciduous

The discriminant function analysis produced one function to separate the dense

and sparse deciduous forest for the Hyperion image. The box plot in Figure 55

compares the discriminant scores for function 1 for dense and sparse deciduous. The

non-overlapping of the interquartile ranges and associated whiskers indicates good

separation between classes. There is however, one overlapping outlier which indicates

that the separation of groups is not complete.
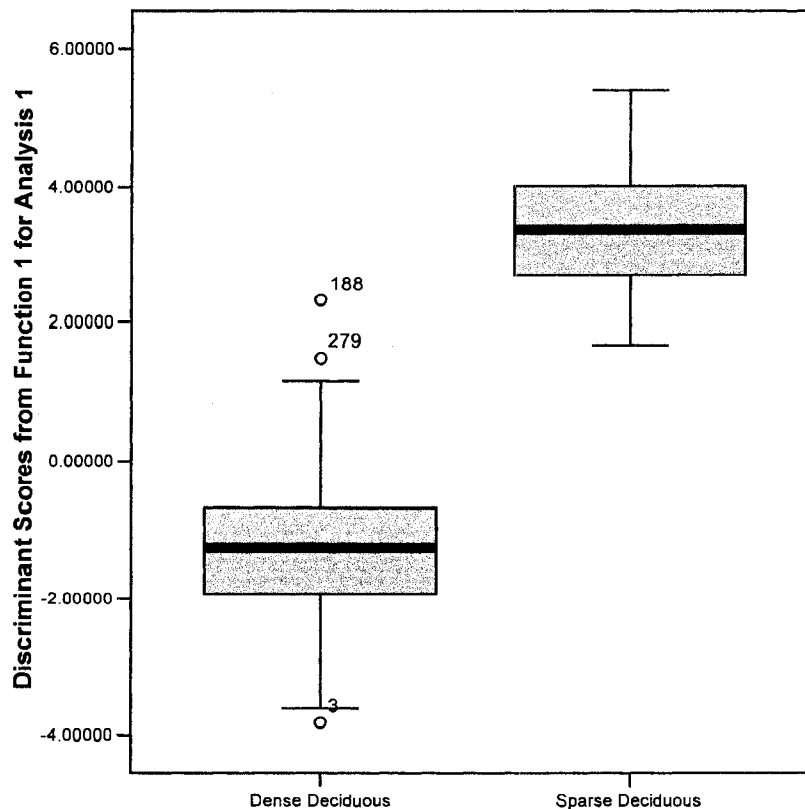
Figure 55. Boxplot of function 1 discriminant scores for dense and sparse deciduous.

Wilks' Lambda for Function 1 showed a low 19.2% of unexplained variability

of the data in the model, indicating good separation of cases into groups (Appendix

XXIII). Group scores differed significantly in function 1 (p<0.001), meaning function 1

significantly separates the groups (Appendix XXIII). Canonical correlation indicated

that 80.8% (0.899²) of the variability in the discriminant scores of function 1 is based on

group structure (Appendix XXIII). Standardized canonical discriminant function

coefficients indicate that function 1 is most correlated with NIR band 77 (Appendix

XXIII).

5.3.3 Error Matrices (Feature Selection)

Error matrices used for the final classification comparing Landsat (standard 6

bands) and Hyperion (DFA) are shown in tables 21 and 22. Both sensors misclassified

wetlands with water, spruce and sparse deciduous. In addition Landsat also

misclassified wetlands with cuts, whereas Hyperion did not. Spruce got misclassified

with jack pine and mixedwood only once with both sensors. Hyperion misclassified

jack pine with spruce less often than Landsat. Both sensors misclassified mixedwood

with spruce, jack pine, and dense deciduous. Landsat misclassified sparse deciduous

with dense deciduous whereas Hyperion perfectly classified sparse deciduous.

Hyperion also perfectly classified cuts where as Landsat misclassified cuts with

wetlands. See appendices XXIV and XXV for an illustration of the classified images.

Table 21. Error matrix for Landsat final supervised classification using band selection.

Classified	Reference Data	Row

Data	Water	Wetland	Black Spruce	Jack Pine	Mixed-wood	Dense Dec.	Sparse Dec.	Cut	Total
Water	48	2	0	0	0	0	0	0	50
Wetland	2	59	15	0	3	0	0	2	81
Black Spruce	0	5	46	12	17	0	0	0	80
Jack Pine	0	0	1	59	4	0	0	0	64
Mixed-wood	0	0	1	4	30	6	0	0	41
Dense Dec.	0	0	0	0	6	59	6	0	71
Sparse Dec.	0	3	0	0	0	0	19	0	22
Cut	0	2	0	0	0	0	0	37	39
Column Total	50	71	63	75	60	65	25	39	448

Table 22. Error matrix for Hyperion final supervised classification using band selection.

Classified Data	Reference Data								Row Total
	Water	Wetland	Black Spruce	Jack Pine	Mixed-wood	Dense Dec.	Sparse Dec.	Cut	
Water	48	0	0	0	0	0	0	0	48
Wetland	2	64	12	0	0	0	0	0	78
Black Spruce	0	5	49	5	12	0	0	0	71
Jack Pine	0	0	1	66	2	0	0	0	69
Mixed-wood	0	0	1	4	39	2	0	0	46
Dense Dec.	0	0	0	0	7	63	0	0	70
Sparse Dec.	0	2	0	0	0	0	25	0	27
Cut	0	0	0	0	0	0	0	39	39
Column Total	50	71	63	75	60	65	25	39	448

5.3.4 Accuracy Assessment (Feature Selection)

Accuracy assessment comparing Landsat and Hyperion showed that Hyperion is capable of distinguishing among classes better than Landsat. Overall classification accuracy's were 79.69% and 87.72% for Landsat and Hyperion respectively (Table 23). Hyperion Producer's accuracy was consistently equal to or higher than Landsat in all classes. The most notable difference was with sparse deciduous were Hyperion had a 100.00% and Landsat had a 76.00% producer's accuracy. User's accuracy and Kappa statistics were consistently higher with Hyperion in all classes. Overall Kappa statistic was 76.50% and 85.81% for Landsat and Hyperion respectively.

Table 23. Accuracy assessment comparing Landsat and Hyperion from band selection supervised classification.

Class	Producers Accuracy (%)		Users Accuracy (%)		Kappa Statistics (%)	
	Landsat	Hyperion	Landsat	Hyperion	Landsat	Hyperion
Water	96.00	96.00	96.00	100.00	95.50	100.00
Wetland	83.10	90.14	72.84	82.05	67.72	78.67
Black Spruce	73.02	77.78	57.50	69.01	50.55	63.94
Jack Pine	78.67	88.00	92.19	95.65	90.62	94.78
Mixedwood	50.00	65.00	73.17	84.78	69.02	82.43
Dense Dec.	90.77	96.92	83.10	90.00	80.23	88.30
Sparse Dec.	76.00	100.00	86.36	92.59	85.56	92.15
Cut	94.87	100.00	94.87	100.00	94.38	100.00
Overall Classification Accuracy (%)	79.69	87.72			76.50	85.81

5.3.5 **Principal Component Analysis (PCA)**

5.3.5.1 *Error Matrices (PCA)*

Error matrix for Landsat and Hyperion's final classes produced with a maximum likelihood supervised classifier using PC bands are shown in tables 24 and 25. Both sensors misclassified water with wetlands. Landsat misclassified wetland with spruce and sparse deciduous, whereas Hyperion misclassified wetland with water, spruce, pine

and mixedwood. Both sensors misclassified spruce with wetland, pine, and mixedwood, as well as misclassified pine with spruce and mixedwood. Landsat and Hyperion misclassified mixedwood with wetland, spruce, pine and dense deciduous. In addition Landsat also misclassified mixedwood with sparse deciduous. Although both sensors misclassified dense deciduous with sparse and mixedwood, Landsat also misclassified mixedwood with wetland. Hyperion perfectly classified sparse deciduous, whereas Landsat misclassified sparse with dense deciduous and wetland. Hyperion perfectly classified cuts, whereas Landsat misclassified cuts with wetland.

Table 24. Error matrix for Landsat final supervised classification using PC's 1-3.

Classified Data	Reference Data								Row Total
	Water	Wetland	Black Spruce	Jack Pine	Mixed-wood	Dense Dec.	Sparse Dec.	Cut	
Water	*46*	0	0	0	0	0	0	0	46
Wetland	4	*68*	26	0	2	4	1	2	107
Black Spruce	0	2	*31*	15	9	0	0	0	57
Jack Pine	0	0	3	*52*	6	0	0	0	61
Mixed-Wood	0	0	3	8	*40*	9	0	0	60
Dense Dec.	0	0	0	0	2	*45*	2	0	49
Sparse Dec.	0	1	0	0	1	7	*22*	0	31
Cut	0	0	0	0	0	0	0	*37*	37
Column Total	50	71	63	75	60	65	25	39	448

Table 25. Error matrix for Hyperion final supervised classification using PC's 1-4.

Classified Data	Reference Data								Row Total
	Water	Wetland	Black	Jack	Mixed-	Dense	Sparse	Cut	

		Spruce	Pine	wood	Dec.	Dec.		
Water	*44*	1	0	0	0	0	0	0	45
Wetland	6	*67*	36	0	5	0	0	0	114
Black Spruce	0	1	*21*	1	1	0	0	0	24
Jack Pine	0	1	2	*67*	17	0	0	0	87
Mixed-wood	0	1	4	7	*34*	7	0	0	53
Dense Dec.	0	0	0	0	3	*53*	0	0	56
Sparse Dec.	0	0	0	0	0	5	*25*	0	30
Cut	0	0	0	0	0	0	0	*39*	39
Column Total	50	71	63	75	60	65	25	39	448

5.3.5.2 *Accuracy Assessment (PCA)*

Accuracy assessment comparing PC bands with Landsat and Hyperion showed that Hyperion is generally capable of distinguishing among classes better than Landsat. Overall classification accuracy's were 76.12% and 78.13% for Landsat and Hyperion respectively (Table 26). Overall Kappa Statistic's were 72.39% and 74.66% for Landsat and Hyperion respectively. Producer's, user's and Kappa statisitics showed that both sensors could distinguish cuts and water well, but had difficulties classifying the remainder classes. For example, although Landsat's producer's accuracy for wetland was 95.77%, its Kappa statistic was 56.69%. This indicates that although the probability of a reference pixel being correctly is high, the reliability of a pixel actually being in that class is low.

Table 26. Accuracy assessment comparing TM and Hyperion supervised classification using PC's.

Class	Producers Accuracy (%)	Users Accuracy (%)	Kappa Statistics (%)

	Landsat	Hyperion	Landsat	Hyperion	Landsat	Hyperion
Water	92.00	88.00	100.00	97.78	100.00	97.50
Wetland	95.77	94.39	63.55	58.77	56.69	51.01
Black Spruce	49.21	33.33	54.39	87.50	46.92	85.45
Jack Pine	69.33	89.33	85.25	77.01	82.28	72.39
Mixedwood	66.67	56.67	66.67	64.15	61.51	58.61
Dense Dec.	69.23	81.54	91.84	94.64	90.45	93.73
Sparse Dec.	88.00	100.00	70.97	83.33	69.25	82.35
Cut	94.87	100.00	100.00	100.00	100.00	100.00
Overall Classification Accuracy (%)	76.12	78.13			72.39	74.66

5.3.6 Comparing Feature Selection to PCA

Feature selection, through the use of DFA with Hyperion and selecting the standard six bands from Landsat, proved to be more efficient than PCA. Landsat's overall classification accuracy was 76.12% and 79.69% for PCA and feature selection respectively (Table 27). Hyperion's overall classification accuracy was 78.13% and 87.72% for PCA and feature selection respectively. Feature selection was therefore determined to be the optimum method for reducing the dimensionality of the imagery and was therefore chosen to be used in further object-oriented image analysis.

Table 27. Overall classification accuracy comparing feature selection to PCA methods of Landsat and Hyperion imagery.

	Landsat		Hyperion	
	Feature Selection	PCA	Feature Selection	PCA
Overall Classification Accuracy (%)	79.69	76.12	87.72	78.13

5.4 IMAGE ANALYSIS (OBJECT-ORIENTED)

5.4.1 Error Matrices

Error matrices for the final classification of Landsat and Hyperion using an object-oriented approach are shown in tables 28 and 29. Landsat misclassified wetland with water, spruce and pine. Hyperion misclassified wetland with water, spruce, and mixed-wood. Both sensors misclassified spruce with wetland, pine and mixedwood. Both sensors also misclassified jack pine with spruce, and mixedwood. Both sensors misclassified mixedwood with spruce, pine and dense deciduous. In addition, Hyperion also misclassified mixedwood with wetland. Although both sensors misclassified dense deciduous with mixedwood, Landsat also misclassified dense deciduous with wetland. Both sensors classified sparse deciduous and cuts perfectly. See Appendices XXVI and XXVII for an illustration of the object-oriented classified images.

Table 28. Error matrix from Landsat object-oriented image analysis.

Classified Data	Reference Data								Row Total
	Water	Wetland	Black Spruce	Jack Pine	Mixed-wood	Dense Dec.	Sparse Dec.	Cut	
Water	49	2	0	0	0	0	0	0	51
Wetland	1	60	13	0	0	2	0	0	76
Black Spruce	0	7	45	3	7	0	0	0	62
Jack Pine	0	2	1	65	7	0	0	0	75
Mixed-wood	0	0	4	7	36	1	0	0	48
Dense Dec.	0	0	0	0	10	62	0	0	72
Sparse Dec.	0	0	0	0	0	0	25	0	25
Cut	0	0	0	0	0	0	0	39	39
Column Total	50	71	63	75	60	65	25	39	448

Table 29. Error matrix from Hyperion object-oriented image analysis.

Classified Data	Reference Data								Row Total
	Water	Wetland	Black Spruce	Jack Pine	Mixed-wood	Dense Dec.	Sparse Dec.	Cut	
Water	49	1	0	0	0	0	0	0	50

Wetland	1	*58*	7	0	1	0	0	0	67
Black Spruce	0	11	*52*	2	8	0	0	0	73
Jack Pine	0	0	1	*68*	5	0	0	0	74
Mixed-wood	0	1	3	5	*39*	2	0	0	50
Dense Dec.	0	0	0	0	7	*63*	0	0	70
Sparse Dec.	0	0	0	0	0	0	*25*	0	25
Cut	0	0	0	0	0	0	0	*39*	39
Column Total	50	71	63	75	60	65	25	39	448

5.4.2 Accuracy Assessment

Accuracy assessment comparing pixel-based to object-oriented approaches for Landsat are shown in Table 30. Landsat's overall classification accuracy was higher with object-oriented (85.04%) than with pixel-based (79.69%). Producer's accuracy for object-oriented was higher than pixel-based for all classes except spruce. The most notable differences were a 10% increase in mixedwood, and sparse deciduous and cuts changing to 100% accuracy, with a 26% increase in sparse deciduous. Contrary to producer's accuracy, user's accuracy showed a 15.08% increase in spruce with object-oriented over pixel based, and decrease in pine. User's accuracy showed an increase in all other classes. Kappa statistics showed that object-oriented increased all classes except for jack pine and black spruce. Overall Kappa statistic was 76.50% and 82.70% for pixel-based and object-oriented respectively.

Table 30. Accuracy assessment for Landsat comparing pixel-based to object-oriented image classification.

Class	Producers Accuracy (%)		Users Accuracy (%)		Kappa Statistics (%)	
	Pixel-	Object-	Pixel-	Object-	Pixel-	Object-

Class	Producers Accuracy (%)		Users Accuracy (%)		Kappa Statistics (%)	
	Pixel-Based	Object-Oriented	Pixel-Based	Object-Oriented	Pixel-Based	Object-Oriented
Water	96.00	98.00	96.00	96.08	95.50	97.74
Wetland	83.10	84.50	72.84	78.95	67.72	81.34
Black Spruce	73.02	71.43	57.50	72.58	50.55	66.84
Jack Pine	78.67	86.67	92.19	86.67	90.62	83.99
Mixedwood	50.00	60.00	73.17	75.00	69.02	55.20
Dense Dec.	90.77	95.38	83.10	86.11	80.23	94.50
Sparse Dec.	76.00	100.00	86.36	100.00	85.56	100.00
Cut	94.87	100.00	94.87	100.00	94.38	100.00
Overall Classification Accuracy (%)	79.69	85.04			76.50	82.70

Accuracy assessment comparing pixel-based to object-oriented approaches for Hyperion are shown in Table 31. Hyperion's overall classification accuracy was identical with object-oriented (87.72%) and pixel-based (87.72%). Producer's accuracy showed a small increase in water, spruce, and pine with object-oriented, a decrease in wetland, and remained the same for mixedwood, dense deciduous, sparse deciduous and cuts. User's and Kappa statistics showed similar small fluctuations in class accuracies. The overall Kappa Statistic was 85.81% and 85.80% for pixel-based and object-oriented respectively.

Table 31. Accuracy assessment for Hyperion comparing pixel-based to object-oriented image classification

	Based	Oriented	Based	Oriented	Based	Oriented
Water	96.00	98.00	100.00	98.00	100.00	97.75
Wetland	90.14	81.69	82.05	86.57	78.67	78.47
Black Spruce	77.78	82.54	69.01	71.23	63.94	79.14
Jack Pine	88.00	90.67	95.65	91.89	94.78	88.82
Mixedwood	65.00	65.00	84.78	78.00	82.43	60.60
Dense Dec.	96.92	96.92	90.00	90.00	88.30	96.35
Sparse Dec.	100.00	100.00	92.59	100.00	92.15	100.00
Cut	100.00	100.00	100.00	100.00	100.00	100.00
Overall Classification Accuracy (%)	87.72	87.72			85.81	85.80

5.5 HYPERSPECTRAL WAVELENGTHS

Hyperion has many highly correlated bands, of which only a select few were actually used in the analysis. Since the large number of bands in hyperspectral imagery can be overwhelming, as well as increase the amount required image preparation, processing time, and analysis time, it may be desirable to select only a few bands for future sensors. It was therefore one of the objectives in this thesis to document the wavelengths that were most correlated to the discriminant functions and the bands used for classification. These bands and their wavelengths are illustrated in figure 56 and listed in table 32.
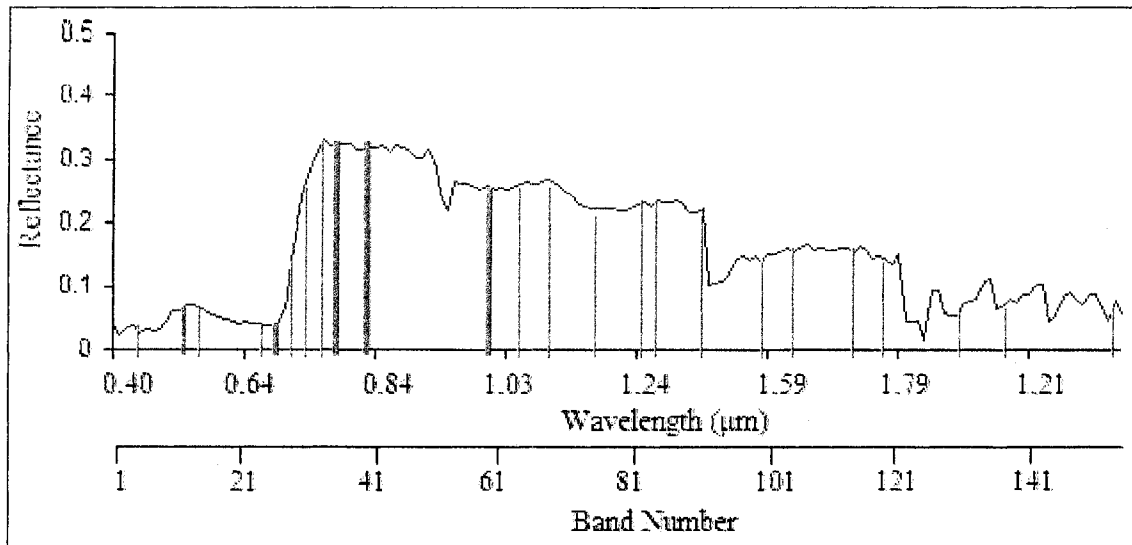
Figure 56. Graph of Hyperion bands and their wavelengths contributing to the classification.

Table 32. Wavelengths of bands contributing to the classification.

Band Number	Average Wavelength (μm)	Band Number	Average Wavelength (μm)	Band Number	Average Wavelength (μm)
7	0.498	34	0.773	86	1.286
13	0.559	40	0.834	89	1.316
14	0.569	41	0.844	99	1.568
17	0.600	59	1.013	104	1.619
23	0.661	60	1.023	115	1.730
25	0.681	64	1.064	120	1.780
26	0.691	68	1.104	130	2.103
28	0.712	77	1.195	138	2.184
31	0.742	82	1.245	152	2.325
32	0.752	84	1.266		

DISCUSSION

6.1 INTRODUCTION

This discussion covers the hyperspectral wavelengths that contributed to the classification, reasons for choosing the classes used in this study, the optimal method in reducing image dimensionality, as well as some factors effecting classification and classification error. The advantages and disadvantages of using multispectral and hyperspectral imagery, as well as using pixel-based and object-oriented classifiers, are also covered. Finally, it discusses the OLCD and how it could possibly be improved, as well as makes recommendations for future research and development.

6.2 CLASSES USED

The classes used in this analysis were similar to those used in the OLCD. There are, however, some differences. First, the 1995 OLCD edition broke up conifer into spruce and pine. In the 2000 edition the OLCD used a single conifer class. I separated spruce and pine for several reasons. The first was to increase the number of classes, the second to push the limits of the imagery, and the third to better explain misclassification among classes. The other class difference between the OLCD and this thesis is the wetlands. The OLCD breaks bogs into open and treed bog, and fen into open and treed fen. I did not break these classes apart because of the small number of samples available.

6.3 ECOLOGICAL FACTORS

Classification error occurs when samples from different classes have similar spectral properties. In general, the classes that became misclassified with each other were similar for Landsat and Hyperion when using both pixel-based and object-oriented classifiers. Spatial relationships between samples and classes were used to determine some of the reasons for classification errors. Some of these reasons for misclassification can be traced to ecosystem, species composition, sample design and age.

6.3.1 Age and Ecosystem

Age and ecosystem or ecosite type can be used to explain some of the misclassification among classes. Since a single cover class can have numerous ecosites, it makes sense that some samples within a class will have an ecosite approaching similar properties to the next cover class. In addition, young vegetation can be spectrally different then older vegetation.

Misclassification between water and wetland was partially due to sample design and ecosystem type. Sample design is described later on in this chapter. The type of wetland being misclassified with water was Exposed Marsh (ES48). Exposed marsh is an emergent mineral substrate with greater than 25% of its plants emergent and occurs along shores. It is a transition ecosystem between wetland and water.

Wetland and black spruce were commonly misclassified with one another. When looking at misclassified spruce samples, it was mainly young spruce as well as the samples with FEC types V37 that were misclassified into wetland, and treed bog samples misclassified into spruce. Spruce samples included V17-20, V31, and V33-37,

which ranged from upland black spruce to poor wetland black spruce. The type of bogs included treed bogs (ES34) and open bogs (ES39). When comparing low land black spruce V37 to treed bog ES34, they were nearly identical. The description in NWST states that treed bog (ES34) has the same characteristics as V37. One solution to this problem would be to consider V37 samples as treed bog in the future. Age also played a role in misclassification between spruce and wetland. This was expected because a younger spruce stand has a greater soil exposure than a mature spruce stand, giving the younger similar spectral properties to a treed bog.

Age also played a role in Landsat's misclassification between wetland and cuts when using the pixel-based approach. Although the physical properties of wetlands and cuts are drastically different, this was expected because wetlands and cuts can look similar spectrally (Figure 57). The age of cuts ranged between 1-5 years old. The two misclassified cut samples were four years old, and were misclassified into marsh. The misclassification of older cuts into wetlands was expected because preliminary analysis used an age class less than 10 years or younger to represent cuts, which was the same as the Ontario Land Cover. The preliminary analysis, however, showed a higher amount of misclassification between cuts and wetlands when using cuts older than five years. This indicates that the optimal threshold for classifying cuts could be between five and ten years of age.

It is difficult to determine reasons why dense and sparse deciduous separated from each other so well. Although there was some spectral overlap between dense and sparse deciduous, sparse samples generally had higher infrared values than dense deciduous. One possible reason for this is that the sparse deciduous samples had a thick

mountain maple, alder and beaked hazel understory which would have been well exposed to the satellite sensor. In addition, the ecosites also differed, with sparse deciduous consisting of V2 (black ash hardwood and mixedwood) and V3.1 (maple – yellow birch - hardwood - mixedwood), whereas dense deciduous consisted of V4 (white birch hardwood and mixedwood), V5 (aspen hardwood), V6 (aspen- birch-balsam fir—mountain maple), V7 (aspen – balsam fir), V8 (aspen – white birch – mountain maple), V9 (aspen - mixedwood) and V10 (aspen – spruce – jack pine).
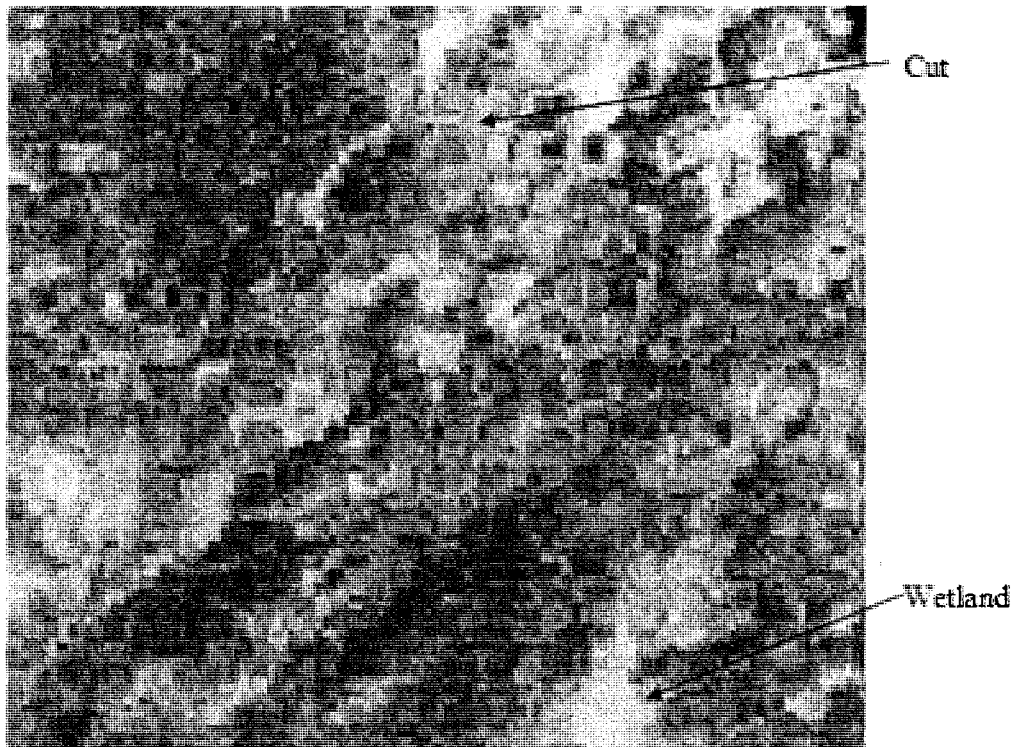
Figure 57. Landsat image showing spectral similarities between cuts and wetlands.

6.3.2 Species Composition

Species composition can be used to explain classification errors among upland classes such as spruce, pine, mixedwood, and dense deciduous. When taking species composition into consideration, a spruce sample could have a species composition similar to a jack pine sample. For example, spruce is defined having more than 80%

conifer, with spruce being greater or equal to jack pine. Jack pine is defined as having more than 80% conifer with jack pine greater than spruce. It is therefore possible to have a jack pine species composition of 60% jack pine and 40% black spruce, as well as a black spruce composition of 50% jack pine and 50% black spruce. Chances are that these samples are spectrally similar to one another, and as differences in species composition between jack pine and black spruce increase, the spectral differences between the two will increase as well. This logic can also be applied to classification errors between jack pine and mixedwood as well as mixedwood and dense deciduous.

6.3.3 Sample Design

The sample design played a role in the misclassification between wetland and water. As mentioned above, the type of wetland that got misclassified with water was exposed marsh (ES48). The reason the sample design played a role in this misclassification was because the water samples were not collected in the field, they were extracted using a systematic random point design the OBM Lakes layer. The exposed marsh samples, however, were collected in the field and were located inside the OBM lakes boundary. Essentially, some random water samples were located near the edge of lakes where they could be considered as exposed marsh.

6.3.4 Number of Samples

One source of error in this analysis is the small number of samples used per class. According to sources such as Congalton and Green (1999) and as Goodchild *et al.* (1994), this study needed a minimum of 30-75 samples per class. Classes that did not meet the minimum number of samples include sparse deciduous, marsh, and fen. The reason for the wetlands not having enough samples was because they were supplied

by another concurrent study and by the time they were received it was too late in the season to collect more samples. The reason sparse deciduous did not have enough samples was because I did not take the 50% training and 50% testing into account when setting up the sample design. Training refers to the sample plots used to drive the classifier and testing refers to the samples used to assess the accuracy of the classification.

It is possible that the low number of samples affected the classification of the hyperspectral imagery by limiting the number of bands that could be used in the classification. For example, when determining the optimum band combination for Hyperion, the classification accuracy would increase as the number of bands increase. This would occur until a certain point where the accuracy of the classes with lowest number of samples dropped dramatically, indicating that a greater number of bands require a greater number of samples. If there were more samples used in the analysis, Hyperion's accuracy may have been increased, and there may have been a greater difference between the multispectral and hyperspectral imagery. An increase in the number of samples however, can greatly increase a project's budget costs, as well as extended the time in which it takes to complete a project.

6.4 REDUCING IMAGE DIMENSIONALITY

Reducing the dimensionality of a dataset can save processing time, hardware space and simplify an analysis. With hyperspectral imagery, this reduction is mandatory because present classifiers cannot deal such large numbers of bands. Feature selection and PCA were applied to Landsat and Hyperion to determine the optimum

method of reducing the dimensionality of the imagery. Feature selection proved to be the optimum method over PCA for both sensors. This was shown through the overall classification accuracy, producer's error, user's error and Kappa statistics.

There was no expectation in classification accuracy when comparing feature selection to PCA for Landsat. With Hyperion, however, feature selection was expected to be the optimum method over PCA. This was because of the Hyperion's low signal to noise ratio and high correlation between bands. One alternative to using PCA is to use a Minimum Noise Fraction (MNF). MNF is a form of principal components designed for hyperspectral datasets that contain low signal to noise ratio's. Although MNF was not included in the analysis, it was included in classification trials. The MNF bands produced, however, were poor in quality with various brightness gradients across the MNF bands. The quality was simply too poor to be used in an analysis. The reason for the poor MNF bands was due to the 'smile' effect. The 'smile' effect refers to an across-track shift in wavelength from the center wavelength, caused by change in dispersion angle with field position (Goodenough *et al.* 2003). The only approach found in literature that can correct the brightness gradient without causing false spectra is through moving linear fitting and interpolation (Goodenough *et al.* 2003). This method, however, requires many *in situ* data sample locations across an image, in which data was not available for this study, and is not practical for large area land classifications. Hopefully, future space borne hyperspectral satellites will not have this 'smile' effect.

The use of a stepwise DFA with SPSS for Hyperion feature selection worked well. One challenge when using a DFA on imagery is extracting sample pixel values. This was a challenge because ERDAS and eCognition do not have a DFA tool built into

their software. In this study, a script was written in ArcMap that looks at the spatial relationship between a sample and its intersecting pixel, and writes the pixel values to the shapefile database. This process was tedious and would be even more difficult and time consuming for an analyst without programming knowledge, particularly if there was a large number of samples were manual pixel value extraction is not an option. With ERDAS, it would be optimal to have a DFA tool build into the signature editor. Ecognition has a similar tool to a DFA called 'Feature Space Optimization'. This tool picks optimum features to use in the classification at different dimensions. Initial trials with this tool did not work as well as the DFA, most likely due to the high correlation between bands. It is therefore also recommended that eCognition develop a DFA tool within their software.

Although the DFA worked well, finding the optimum DFA step or band combination was time consuming. In this thesis, steps 6 through 20 were tested for each classification. It can take 24 hours to use ERDAS's signature editor, run a supervised classification, recode the classified image and run the accuracy assessment to find the optimal step. This time can accumulate into weeks or months of time when considering an analyst is still developing the optimum classes to use in his or her analysis, as well as considering the properties of each class such as the species composition and ecosystem types.

6.5 MULTISPECTRAL VS. HYPERSPECTRAL

6.5.1 <u>Cost</u>

The high cost of Hyperion's hyperspectral imagery makes it, at the present time, impractical for large area classifications such as the OLCD. In addition, Hyperion's image size is a fraction of Landsat's. The rational behind the comparison of multispectral to hyperspectral is that if hyperspectral shows improvements over multispectral, then there is a need for further development of hyperspectral imagery. With this development, in the future, hyperspectral imagery may one day be as cheap and come with image sizes as large as Landsat's. Only then will hyperspectral imagery become practical for large area land classifications such as the OLCD.

6.5.2 <u>Preprocessing</u>

Preprocessing of Landsat multispectral imagery is simple and straight forward, whereas Hyperion's hyperspectral imagery is difficult. There are few publications dealing with Hyperion, making it difficult to find resources to follow. In addition, software such as ERDAS and eCogntion, have an insufficient number of tools to deal with hyperspectral imagery. Although there was no tool to fix the abnormal pixels, for the purpose of this thesis, it will be assumed that images from future hyperspectral sensors will have abnormal pixels corrected upon purchase.

The requirement for atmospheric correction using *in situ* data with hyperspectral imagery is a concern. This requirement makes rationalizing hyperspectral imagery's applicability for large area land classifications a challenge. For example, even if Hyperion's imagery was the same cost and size as Landsat's, it would still require atmospheric correction. In order for each Hyperion image to be atmospherically

corrected, *in situ* data would have to be collected for atmospheric correction, which can be difficult and costly to obtain. Landsat's multispectral sensor does not require atmospheric correction with *in situ* data and is therefore much simpler to use.

6.5.3 Accuracy

The main advantage hyperspectral imagery has over multispectral imagery is its greater ability to distinguish among classes. Accuracy assessment using both pixel-based and object-oriented showed that hyperspectral imagery can distinguish between classes better than multispectral imagery. There is also potential for hyperspectral imagery to show an even greater ability to distinguish between classes then multispectral as the number of classes increase.

6.6 PIXEL-BASED VS. OBJECT-ORIENTED

This study showed that when using Landsat's multispectral imagery, an object-oriented classifier can provided better separation among classes than the pixel-based classifier. This indicates that there is room to improve current pixel-based classifications. Once an analyst has experience with eCognition, it can be just as fast, if not faster than using a traditional pixel-based classifier. Ecognition's object-oriented classifier could therefore be a practical alternate for large area classifications, such as the OLCD, at the present time.

As mentioned in Chapter 1, the OLCD 2000 edition updated all of Ontario except for southern Ontario. Some of the classes in the OLCD, known to have a low level of confidence, include settlement/infrastructure, agriculture, and pasture

(Spectralanalysis 1999). This low level of confidence could be a reason why southern Ontario was not updated in the 2000 edition. Although these low confidence level classes were not included in this study, the ability of feature based rules such as size, area, shape, and texture being incorporated into object-oriented classification, may help improve the confidence level of study classes. More research needs to be done using Landsat and eCognition with classes found in southern Ontario.

Hyperion's overall classification was identical when comparing pixel-based and object-oriented classifiers. Based on the results from Landsat, this was not expected. One possible reason for this was that there was not much room for improvement because the pixel-based classification accuracy assessment was already high. For example, two of the eight classes (sparse deciduous and cut) already had a producer's accuracy of 100% with the pixel-based classifier. Of the remaining six class, three of them (water, wetland and dense deciduous) had accuracies over 90%. This resulted in only three classes with accuracies less than 90%.

One disadvantage of using eCognition is its high cost. ECognition is expensive and is only designed for analysis, which means image processing software such as ERDAS is still required. The main advantage eCogntion is its ability to develop rules which can lead to a more meaningful classification than pixel-based. Having rules and steps clearly shown within eCognition's processing tree and embedded into each class, could make it easier for classifications to be updated, particularly if different analysts are used. Also, eCognition has superior masking abilities over pixel-based software. With eCognition, masking takes place within the project through the use of different levels. With pixel-based software, separate masking images and models must be

created which it time consuming and can become confusing. Finally, pixel-based classifications can look noisy, having a 'salt and pepper' effect. Object-oriented classifications do not have this 'salt and pepper' effect to the degree as pixel-based classifications.

6.7 RECOMMENDATIONS

6.7.1 Software Improvements

It is recommended that ERDAS and eCognition both build a DFA tool within their software. In addition, eCognition has a steep learning curve, even for advanced remote sensing analysts. It is therefore recommended that eCognition provides more examples in their user guide and provides a better explanation on how the program works.

6.7.2 Ontario Land Cover

The OLCD was developed using a pixel-based classifier. With the results of this study showing that an object-oriented approach can distinguish among classes better than a traditional pixel-based classifier, it is recommended that the MNR explores the use of an object-oriented classifier for the OLCD.

6.7.3 Future Research

It is recommended that more research is needed in developing hyperspectral sensors with larger images. This will help hyperspectral imagery become more applicable for large area land classifications. If *in situ* data is required for the atmospheric correction of hyperspectral imagery, research may be needed in developing a method for standardizing *in situ* data across Ontario. One possible solution is to

investigate the set up of permanent *in situ* stations across Ontario. Another solution is to improve space-based calibration instruments to eliminate the need for *in situ* data for hyperspectral atmospheric correction.

ECognition has the ability to easily incorporate hydrological models as well as other source data, such as from an FRI, into a classification. Although not recorded in this study, I did explore the use of slope into the object-oriented classification. Slope did not appear to be useful in improving classification accuracy, possibly due to the coarse spacing between available elevation points. For example, the current FRI digital terrain model (DTM) is 30m around lakes and streams and 100m everywhere else. Fortunately, the Ontario MNR is creating a new FRI with a new DTM, hopefully more detailed than the existing DTM. With an improved FRI, other hydrological models may assist in reducing misclassification between wetland and upland classes.

The most applicable and simple analysis that can be done in the future is to integrate the new FRI wetland data into eCognition, once it is available. Assuming the new FRI wetland boundaries are more accurate than the current version, a rule could be developed that would not allow upland classes to be located within wetlands. This method was used in preliminary trials of this study, but was not used because the current FRI wetland boundaries were poorly delineated and too coarse. With the assumption of the new FRI having improved wetland boundaries, this application could potentially eliminate wetland samples being misclassified into upland classes.

CONCLUSION

This study showed that there is potential to increase the confidence level of classes used in current large area land classifications, such as in the OLCD. Hyperion's hyperspectral imagery for example, was capable of distinguishing among classes better than Landsat's currently used multispectral imagery. Hyperspectral imagery, however, is not yet practical for large area classifications because of its high cost, small image size, and lack of available software tools. In addition to improving the imagery, improving the way images are classified can also improve accuracy levels. Ecognition's object-oriented image classifier, for example, showed improvements over the traditional pixel-based classifier. The main finding of this study is that, although hyperspectral imagery can improve classifications, it is not necessary to wait for hyperspectral imagery to become economically feasible in order to improve classifications. For the present time, the most practical method for potentially improving large land cover classification accuracy, such as the OLCD, is to change from a pixel-based to an object-oriented image classifier.

LITERATURE CITED

Anonymous, N.D. 2006. VBA Programmer. http://www.vba-programmer.com. August 2, 2006.

Aardt, Jan. 2000. Spectral Separability among six southern tree species. Thesis, Virginia Polytechnic Institute and State university. 184 pp.

Aspinall J, Richard., W.A. Marcus, J.W. Boardman. 2002. Consideration in collecting, processing, and analysing high spatial resolution hypersprectral data for environmental investigations. Journal of Geographical Systems. Vol4 15-29. http://geography.uoregon.edu/amarcus/Publications/Aspinall_et%20_al_2002_JGS.pdf

Barry, Pamela 2001. EO-1/Hyperion Science Data User's Guide, Level 1_B. TRW Space, Defense & Information Systems. http://eo1.gsfc.nasa.gov/new/general/Disk2/HyperionScienceDataUsersGuide_public_L1B.pdf

Barry P,S., J. Pearlman. 2001. The EO-1 mission: Hyperion data. 12pp http://www.fas.org/irp/imint/hyperion.pdf. April 5, 2007.

Boyce, W.C. 2004. The Canadian SmallSAT Bus. 3pp. http://www.apegm.mb.ca/pdnet/papers/SmallSat.pdf. April 5 2007.

Canadian Space Agency. 2003. Earth and Environment: significant Canadian events and achievements report – 2003. 36 pp. http://www.space.gc.ca/asc/pdf/ceos_report2003.pdf

Chander G., B. Markham. 2003. Revised Landsat-5 TM radiometric calibration procedures and postcalibration dynamic ranges. IEEE Transactions on Geoscience and Remote Sensing. Vol.41:11 Part 2, pp 2674-2677.

Change, Kang-Tsung. 2005. Programming ArcObjects with VBA: a task-oriented approach. CRC Press LLC. 352pp.

Clark, M., D. Roberts, D. Clark. 2005. Hyperspectral discrimination of tropical rain forest tree species at leaf to crown scales. Remote Sensing of Environment. 96(3-4) 375-398.

Cihlar, J. 2000. Land cover mapping of large areas from satellites: status and research priorities. International Journal of Remote Sensing 21(6&7): 1093-1114.

Congalton, G. R., Green, K. 1999. Assessing the accuracy of remotely sensed data: principles and practices. Lewis Publishers. 139pp.

Environment Canada. 1995. Canadian Biodiversity Strategy: Canada's response to the convention on biological diversity. Biodiversity Convention Office, Hull, QC. 80p.

ESRI Forums, 2006. ESRI Developer Network Discussion Forums. Environmental Systems Research Institute, Inc. http://edn.esri.com/index.cfm?fa= forums. Gateway. Aug. 2, 2006.

European Space Agency. 2005. Proba: Project for on-board autonomy. http://www.esa.int/export/esaMI/Proba_web_site/ESAQ9KTHN6D_0.html. April 5, 2007.

Foster R. Jane, and Philip A. Townsend. 2004. Linking hyperspectral imagery and forest inventories for forest assessment in the central Appalachians. http://www.fs.fed.us/ne/newtown_square/publications/technical_reports/pdfs/20 04/316papers/FosterGTR316.pdf

Franklin, S. E., M.A. Wulder. 2002. Remote sensing methods in medium spatial resolution satellite data land cover classification of large areas. Progress in Physical Geography. Vol. 26(2) pp. 173-205.

Fiorella, M. and W.J. Ripple. 1993. Determining successional stage of temperate coniferous forests with Landsat satellite data. Photogrammetric Engineering & Remote Sensing. Vol. 59(2): 239-246.

Galvao, L., A. Formaggio, D. Tisot. 2005. Discrimination of sugarcane varieties in Southeastern Brazil with EO-1 Hyperion data. Remote Sensing of Environment. Vol. 94(2): 523-534.

Gillis, M. and Leckie, D. 1996. Forest inventory update in Canada. The Forestry Chronicle 72: 138-56

Gong, P., Ruiliang P., Bin Yu. 1997. Conifer species recognition: an exploratory analysis of in situ hyperspectral data. Remote Sensing of Environment. 62 (2) 189-200.

Goodchild, M.F., G.S. Biging, R.G. Congalton. P.G. Langley, N.R. Chrisman and F.W. Davis. 1994. Final Report of the accuracy assessment task forse. California Assembly Bill AB1580. National Center for Geographic Information and Analysis, UCSB.

Goodenough, D. G., A. Dyk, P. Bhogal, H. P. White. 2002. User Requirements Report for Forestry. Canadian Hyperspectral Users and Science Team, Canadian Space Agency. 15pp.

Goodenough D. G., A. S. Bhogal, A. Dyk, O. Niemann, T. Han, H. Chen, C. West, and

C. Schmidt, 2001. Calibration of forest chemistry for hyperspectral analysis. IGARSS 2001, Sydney, Australia, vol. 1, pp. 52-56, 2001.

Goodenough , D. G., A. S. Bhogal, A. Dyk, A. Hollinger, Z. Mah, K. O. Niemann, J. Pearlman, H. Chen, T. Han, J. Love, and S. McDonald. 2002. Monitoring Forests with Hyperion and ALI. in Proc. IGARSS 2002, Toronto, ON, Canada. http://rseng.cs.uvic.ca/DaveIEEEpub/IGARSS02_5.pdf

Han, T. Goodenough, D.G. Dyk, A. Love, J. 2002. Detection and correction of abnormal pixels in Hyperion images. Geoscience and Remote Sensing Symposium, 2002. IGARSS'02.2002 IEEE.

Huang, X., and J.R. Jensen. 1997. A machine learning approach to automated construction of knowledge bases for image analysis expert systems that incorporate GIS data. Photogrammetric Engineering and Remote Sensing 63(10):1185-1194.

Jensen, John R. 2005. Introductory digital image processing: a remote sensing perspective. 3rd ed. Pearson Prentice Hall, New Jersey. 526 pp.

Karteris, M.A. 1990. The utility of digital Thematic Mapper data for natural resources classification. International Journal of Remote Sensing 11(9): 1589-1598.

Lillesand, T., Kiefer, R., Chipman, J. 2004. Remote Sensing and Image Interpretation. John Wiley & Sons, Inc. 763 pp.

Lobo, A., Chic, O., Casterad, A. (1996): Classification of Mediterranean crops with multisensor data: per-pixel versus per-object statistics and image segmentation, International Journal of Remote Sensing, vol. 17: 2358-2400.

Loveland, T.R., Z. Zhiliang, D.O. Ohlen, J.F. Brown, B.C. Reed, and L. Yang. 1999. An analysis of the IGBP global land-cover characterization process. Photogrammetric Engineering and Remote Sensing. 65(9): 1021-1032.

MacDonald, Dettwiler and Associates Ltd. 2007. http://gs.mdacorporation.com. April 5, 2007.

Martin, M.E., S.D. Newman, J.D. Aber, and R.G. Congalton. 1998. Determining forest species composition using high spectral resolution remote Sensing data. Remote Sensing of Environment, 65 (3), pp. 249 - 254.

Moore, M.M., M.E. Bauer (1990). Classification of forest vegetation in North-Central Minnesota using Landsat Multispectral Scanner and Thematic Mapper data. Forest Science 36(2): 330-342.

NASA 2007. Landsat data continuation mission. http://ldcm.nasa.gov/.

Natural Resources Canada. 2003. Advanced Forest Technologies: Evaluation and
Validation of EO-1 for sustainable development (EVEOSD).
http://www.pfc.forestry.ca/aft/eveosd/EVEOSD-eo1/eo1_e.html. March 31,
2003.

Natural Resources Canada 2004. Earth observation for sustainable development of
forests (EOSD). http://www.pfc.forestry.ca/eosd/index_e.html. January 1, 2003.

Natural Resources Canada. 2004. Land cover map of Canada.
http://atlas.nrcan.gc.ca/site/english/maps/environment/forest/forestcanada/lan
dcover/1. May 4, 2004.

Ontario Ministry of Natural Resources. 2007. Managing Ontario's Forests: Forest
Resource Inventory.
http://ontariosforests.mnr.gov.on.ca/inventoryoverview.cfm#contents

Oruc, M., A. M. Marangoz, G. Buyksalih. 2004. Comparison of pixel- based
and object-oriented classification approaches using Landsat-7 ETM
spectral bands. In Proceedings of the ISRPS 2004 Annual Conference, Istanbul,
Turkey. July 19 - 23.

PCI Geomatics. 2003. Geomatica Software and eCognition to Assist National Wetland
Inventory. May 26, 203.
http://www.pcigeomatics.com/pressnews/2003_csa_nwi.html.

Pearson, Chip. 2005. Importing and exporting to text files. Pearson Software
Consulting. http://spreadsheets.about.com/gi/dynamic/offsite.htm?zi=
1/XJ&sdn=spreadsheets&zu=http%3A%2F%2Fwww.cpearson.com%2Fexcel%
2Fimptext.htm. Aug. 2, 2003. Last updated June 27, 2005.

Smith B, Randall. 2001. Introduction to Hyperspectral Imaging. TNTmips. 17pp.
http://www.microimages.com/getstart/pdf/hyprspec.pdf.

Spatial Mapping LTD. 2007. SPOT Raw Imagery Price List. 4pp.
http://www.resmap.com/pdf/spot5_pricelist.pdf.

Spectranalysis Inc. 1999. Ontario Land Cover Data Base: User's Manual. Ontario
Ministry of Natural Resources. Oakville, Ontario. 37pp.
http://geogratis.cgdi.gc.ca/download/ont_landcover/olcmanual.doc.

Spot Image 2006. http://www.spot.com/html/SICORP/_401_.php. April 5, 2007.

SPSS Inc. 2003. SPSS 12.0 for Windows.

Stehman S.V., T. L. Sohl, T. R. 2005. Loveland. An evaluation of sampling strategies to improve precision of estimates of gross change in land use and land cover. International Journal of Remote Sensing. 26: 4941-4957.

Stuffler, T. C. Kaufmann, S. Hofer, H. Mehl, G. Schreier, A. Mueller, G. Arnold, M. Landgemann, H. Bach, B. Doll, U. Benz, R. Haydn, F. Jung-Rothenhausler. 2004. The advanced hyperspectral mission EnMAP (Environmental Monitoring and analysis program) - Germany prepares for the future. 7pp. http://www.enmap.de/www/downloads/EnMAP_IAF-04_Paper.pdf

Thenkabail S.P, E.A. Enclona, M.S. Asheon, C. Legg, M.J De Dieu. 2004. Hyperion, IKONOS, ALI, and ETM+ sensors in the study of African rainforests. Remote Sensing of Environment. 90: 23-43.

Treitz, P. and P. Howarth. 2000. Integrating spectral, spatial, and terrain variables for forest ecosystem classification. Photogrammetric Engineering & Remote Sensing 66(3): 303-317.

United Nations. 1998. Kyoto protocol to the United Nations framework convention on climate change. http://unfccc.int/resource/docs/convkp/kpeng.pdf.

USGS. 2005. EO-1 User's Guide. http://eo1.usgs.gov/userGuide/1.html.

USGS. 2006. Landsat Satellites. http://landsat.usgs.gov/. April 5, 2007.

USGS 2007. Earth Observing 1 (EO-1): Hyperion Sensor. http://eo1.usgs.gov/hyperion.php. April 5, 2007.

Wolter, P.T., D.J. Mladenoff, G.E. Host and T.R. Crow. 1995. Improved forest classification in the northern lake states using multi-temporal Landsat imagery. Photogrammetric Engineering & Remote Sensing. 61(9): 1129-1143.

Wardoyo, W. and G.A. Jordan. 1996. Measuring and assessing management of forested landscapes. The Forestry Chronicle 72(6): 639-646.

Whiteside, T., and W. Ahmad. 2005. A comparison of object-oriented and pixel-based classification methods for mapping land cover in northern Australia. Proceedings of SSC2005 Spatial intelligence, innovation and praxis: The national biennial Conference of the Spatial Institute. September 2005: 1225-1231.

Wikipedia 2007. Box plot. http://en.wikipedia.org/wiki/Box_plot.

Wulder, M. 1998. A review of optical remote sensing techniques and applications for the assessment of forest inventory and biophysical parameters. Progress in physical geography vol22 no4 447-476

APPENDIX I
SUMMARY LIST OF THE LAND COVER CLASSES OF THE SECOND-EDITION
ONTARIO LAND COVER DATA BASE

Class Number	Class Name	Class Description
1	Water - Deep or Clear	Deep or clear waterbodies.
2	Water - Shallow or Sedimented	Shallow waterbodies and waterbodies with a high concentration of suspended sediment.
3	Settlement/Infrastructure	Clearings for human settlement and economic activity; major transportation routes.
4	Sand/Gravel/Mine Tailings	Beach deposits, aggregate quarries and sand dunes; mines and mine tailings.
5	Bedrock	Exposed bedrock, lacking vegetation cover.
6	Mudflats	Unvegetated coastal areas of the Hudson Bay-James Bay Lowlands, partly submerged at high tide.
7	Cutovers	Forest clearcuts estimated to be less than 10 years of age.
8	Burns	Forest burns estimated to be less than 10 years of age.
9	Regenerating Depletion	Old burns supporting very sparse vegetation.
10	Sparse Forest	A patchy or sparse forest canopy composed of coniferous or deciduous species or a combination of the two.
11	Deciduous Forest	Largely continuous forest canopy composed primarily of deciduous species.
12	Mixed Forest	Largely continuous forest canopy composed of both deciduous and coniferous species. In more northerly areas, a greater component of coniferous species can be expected; in more southerly areas, a greater component of deciduous species can be expected.
13	Coniferous Forest	Largely continuous forest canopy composed primarily of coniferous species
15	Intertidal Marsh	Coastal marshes of the Hudson Bay-James Bay Lowlands lying between the coastal mudflats and the supertidal zone.
16	Supertidal Marsh	Coastal marshes of the Hudson Bay-James Bay Lowlands lying inland of both the coastal mudflats and intertidal marshes, and subject to

		only exceptionally high tides.
17	Inland Marsh	Lakeshore and inland marshes of Southern Ontario.
18	Deciduous Swamp	Hardwood swamps of Southern Ontario occurring along rivers and in old lakebeds and other low-lying areas.
19	Coniferous Swamp	Swamps with dense conifer tree or shrub cover occurring in Southern Ontario.
20	Open Fen	Fens generally lacking tree cover that may support some shrub cover and tamarack. Open fens include fens with an open water surface, graminoid fens, pattern fens, and shrub-rich fens.
21	Treed Fen	Fens supporting a sparse to dense cover of trees or shrubs.
22	Open Bog	Bogs generally lacking tree cover.
23	Treed Bog	Bogs supporting a sparse to dense cover of trees.
24	Tundra Heath	Low tundra vegetation growing on slightly raised beach deposits and strand lines along the Hudson Bay coast.
25	Pasture	Open grassland with sparse shrubs in rural land.
28	Other	Landcover conditions not accurately defined by any other landcover class. This class includes the following: undefined clearings in disturbed areas; small, unburned areas within recent burns; and undefined transitional areas between classes, such as some wetland boundaries.
29	Cloud and Shadow	Areas of cloud or shadow on the satellite images.

APPENDIX II
EXAMPLE OF ERDAS MODEL USED TO SEPARATE BANDS
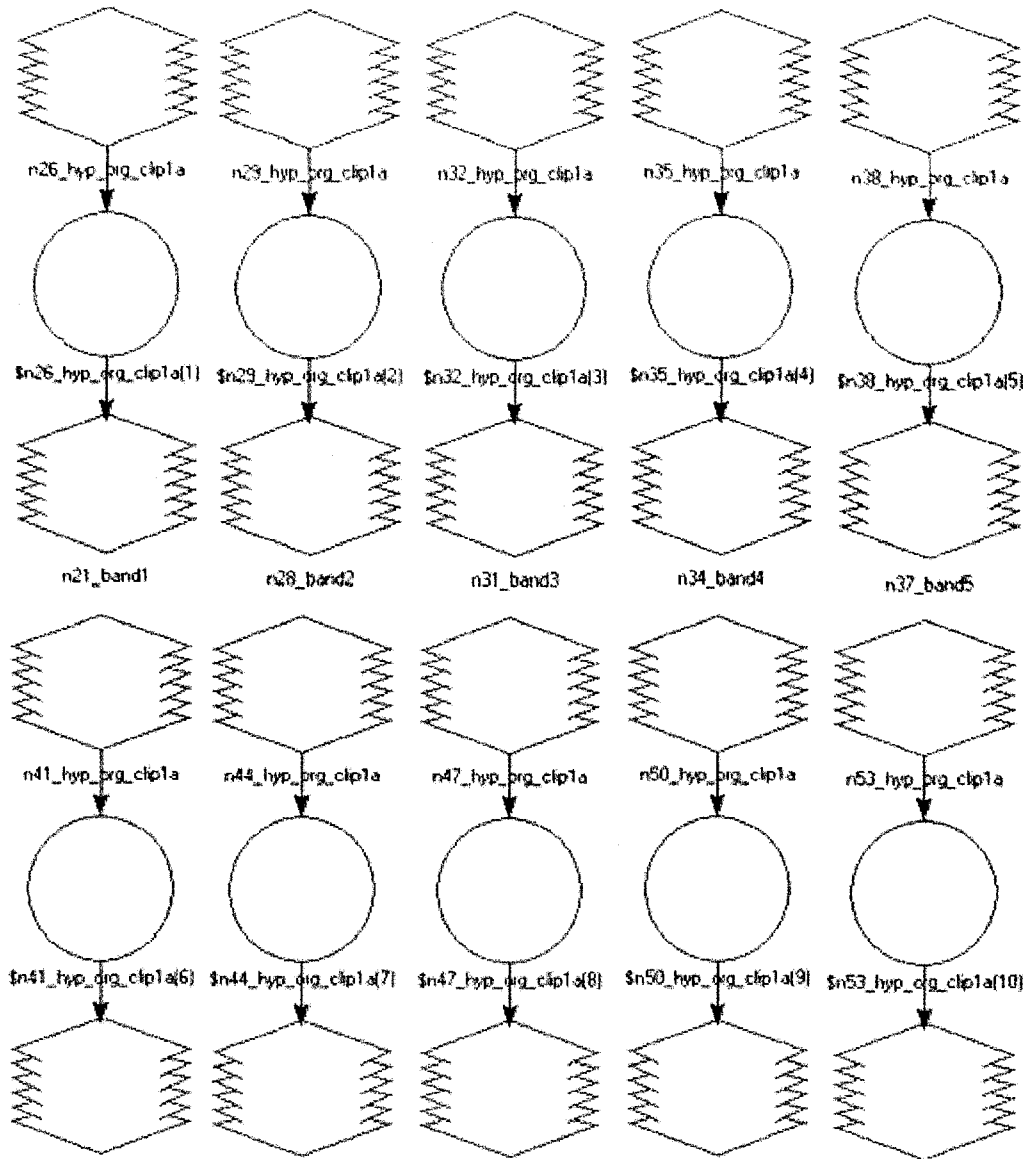
APPENDIX III
SCRIPT CONVERTING RASTER TO ASCII

```
Private Sub RastertoASCII_Click()
'Project Name:   Export multiple rasters to ascii
'Description:    Exports rasters to ascii by looping through
'                each raster layer in table of contents.
'Created by:     Jevon Hagens
'Last Updated:   August 2006
'Software:       Created in ArcMap 9.1


On Error GoTo Errorhandler
    '--Part 1: Get current map document
    Dim pMxDoc As IMxDocument
    Dim pMap As IMap
    Set pMxDoc = ThisDocument
    Set pMap = pMxDoc.FocusMap

    '--PART2: get folder name as path to save file in
    Dim strStartDir As String
    strStartDir = "C:\"
    Dim objSearchApp As Object
    Dim objFolder As Object
    Set objSearchApp = CreateObject("Shell.Application")
    Set objFolder = objSearchApp.BrowseForFolder _
                    (0, "Please choose folder to save file in:", 0)
    If objFolder Is Nothing Then
        MsgBox "You did not choose a folder"
        Exit Sub
    End If
    Dim strFolderName As String
    strFolderName = objFolder.Items.Item.Path

    '--Part3: loop through each raster layer and export as asii
    Dim indexRLayer As Integer
    For indexRLayer = 0 To pMap.LayerCount - 1 'loop
        Dim pRasterLayer As IRasterLayer
        Set pRasterLayer = pMap.Layer(indexRLayer)
        If Not TypeOf pRasterLayer Is IRasterLayer Then
            MsgBox "Please insert raster layers to export to ascii"
            Exit Sub
        End If
        Dim pRaster As IRaster
        Set pRaster = pRasterLayer.Raster
        'get name of raster (cut off .img at the end)
        Dim NameTemp As String
        NameTemp = pRasterLayer.Name
        Dim intName As Integer
        intName = Len(NameTemp)
        Dim Name As String
        Name = Left(NameTemp, intName - 4)
```

```
                'get rasterband collection
                Dim pRasterBandCol As IRasterBandCollection
                Set pRasterBandCol = pRaster
                Dim pRasterDSet As IRasterDataset
                'process band in each rasterlayer (only 1 anyways)
                Set pRasterDSet = pRasterBandCol.Item(0).RasterDataset
                'Set output file name
                Dim OutASCIIName As String
                OutASCIIName = strFolderName & "\" & Name & ".asc"
                'Export Raster
                Dim pRasterExportOp As IRasterExportOp
                Set pRasterExportOp = New RasterConversionOp
                pRasterExportOp.ExportToASCII pRasterDSet, OutASCIIName
        Next indexRLayer
        'display message when complete
        MsgBox "Processing Complete"
'--------Error Handling------------
Exit Sub                'Exit to avoid error handler
Errorhandler:                        'Error-handling routine
    MsgBox Str(Err.Number) & ": " & Err.Description, , "Error"
End Sub
```

APPENDIX IV
ILLUSTRATIONS OF PROCESS USED TO CORRECT ABNORMAL PIXELS

ArcMap document showing images loaded into the table of contents prior to running the script that converted each image into ASCII format
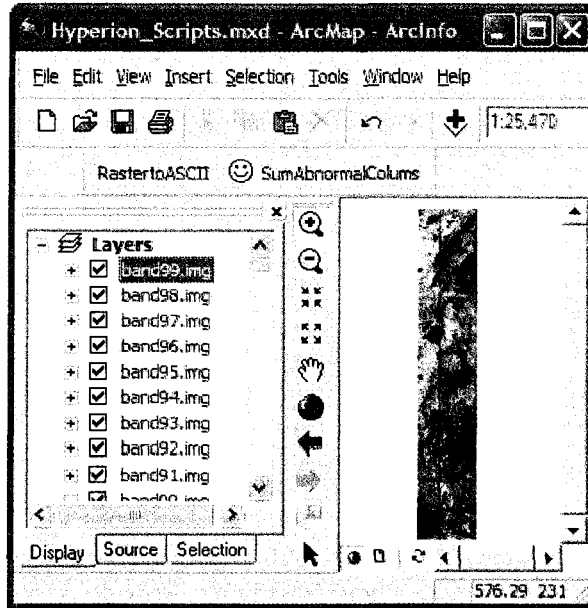
Band 12 showing script output of ASCII file (left) imported into Excel (right)
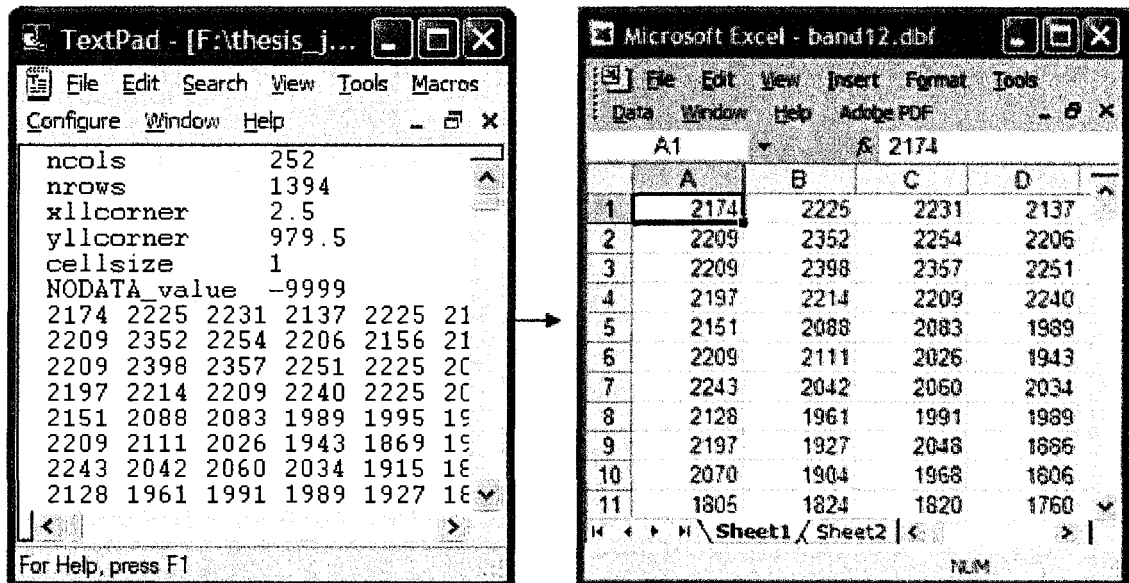
Band 91 DN values before (left) and after (right) abnormal pixel correction

	CK	CL	CM	C
1	3725	0	3647	
2	4537	0	4966	
3	5667	0	6143	
4	5055	0	5697	
5	5425	0	6691	
6	5759	0	5667	
7	4410	0	4199	
8	5901	0	4024	
9	6228	0	4870	
10	5000	0	4556	
11	5038	0	4322	

	CK	CL	CM	
1377	4797	5094	4957	
1378	4322	4498	4612	
1379	4501	4345	4406	
1380	4858	4509	4569	
1381	4623	4521	4661	
1382	4445	4406	4589	
1383	4092	4228	4251	
1384	4142	4186	4326	
1385	4169	3970	3986	
1386	4027	3697	3597	
1387	4221	4014	3910	

APPENDIX V
SCRIPT CONVERTING ASCII TO EXCEL

```
Public Sub ImportASCII_To_dbf()
'Project Name:  Import Ascii into Excel
'Description:   Imports ascii files created from ArcGIS, using
'               a space delimiter.  Deletes header info in first
'               six rows, then saves as .dbf based on name of image
'               each raster layer in table of contents.
'Created by:    Jevon Hagens
'Last Updated:  August 2006
'Software:      Created in Excel 2003


On Error GoTo EndMacro:
    '---part1: clear all cells
    'Cells.Select
    Cells.Delete|
    'set active cell to column1 row1
    Cells(1, 1).Select

    '---Part2: get file to import
    Dim FName As Variant
    FName = Application.GetOpenFilename _
        (filefilter:="ASCII Files(*.asc),*.txt,All Files (*.*),*.*")
    If FName = False Then
        MsgBox "You didn't select a file"
        Exit Sub
    End If

    '---Part3: Save application as .dbf using dynamic naming system
    'get length of FName string
    Dim intFName As Integer
    intFName = Len(FName)
    'get rid of .asc at end of string
    Dim FName2 As String
    FName2 = Left(FName, intFName - 4)
    'get length of FName2
    Dim intFName2 As Integer
    intFName2 = Len(FName2)
    'get index of "band" in string
    Dim intNameBand As Integer
    intNameBand = InStr(FName2, "band")
    'get final name
    Dim NameSave As String
    NameSave = Right(FName2, intFName2 - intNameBand + 1) & ".dbf"
    'get folder name as path to save file in
    Dim strStartDir As String
    strStartDir = "C:\"
    Dim objSearchApp As Object
    Dim objFolder As Object
    Set objSearchApp = CreateObject("Shell.Application")
    Set objFolder = objSearchApp.BrowseForFolder _
                (0, "Please choose folder to save file in:", 0)
```

```vba
        If objFolder Is Nothing Then
            MsgBox "You did not choose a folder"
            Exit Sub
        End If
        Dim strFolderName As String
        strFolderName = objFolder.Items.Item.Path


        '---PART4: Import file
        Dim RowNdx As Integer
        Dim ColNdx As Integer
        Dim TempVal As Variant
        Dim WholeLine As String
        Dim Pos As Integer
        Dim NextPos As Integer
        Dim SaveColNdx As Integer
        'set a space delimiter used to seperate columns
        Dim Sep As String
        Sep = " "
        Application.ScreenUpdating = False
        SaveColNdx = ActiveCell.Column
        RowNdx = ActiveCell.Row
        Open FName For Input Access Read As #1
        While Not EOF(1)
            Line Input #1, WholeLine
            If Right(WholeLine, 1) <> Sep Then
                WholeLine = WholeLine & Sep
            End If
            ColNdx = SaveColNdx
            Pos = 1
            NextPos = InStr(Pos, WholeLine, Sep)
            While NextPos >= 1
                TempVal = Mid(WholeLine, Pos, NextPos - Pos)
                Cells(RowNdx, ColNdx).Value = TempVal
                Pos = NextPos + 1
                ColNdx = ColNdx + 1
                NextPos = InStr(Pos, WholeLine, Sep)
            Wend
            RowNdx = RowNdx + 1
        Wend
        'delete first 6 rows
        Rows("1:6").Select
        'shift deleted rows up
        Selection.Delete Shift:=xlUp 'Rows must be selected
        'set active cell
        Cells(1, 1).Select
        'save application
        ActiveWorkbook.SaveAs Filename:=strFolderName & "\" & NameSave
        MsgBox "Process Complete"
EndMacro:
On Error GoTo 0
        Application.ScreenUpdating = True
        Close #1
End Sub
```

APPENDIX VI
SCRIPT CORRECTING ABNORMAL PIXELS

```
Public Sub PixelFix()
'Project Name:  Correct Hyperion Abnormal Pixels
'Description:   The program counts the number of pixels with values
'                  less then their left and right neighbors. Uses a
'                  threshold of 50% of the length to determin if a column
'                  is abnormal.  If a column is abnormal, strips of
'                  abnormal pixels greater then 5 pixels are replaced with
'                  the value of the ave of left and right neighbors
'Created by:    Jevon Hagens
'Last Updated:  August 2006
'Software:      Created in Excel 2003
On Error GoTo Errorhandler

    '---PART1: get last column and row index values
    ' ExcelLastCell is what Excel thinks is the last cell
    Dim ExcelLastCell As Range
    'xlLastCell is an object within excel
    Set ExcelLastCell = ActiveSheet.Cells.SpecialCells(xlLastCell)
    ' Determine the last row with data
    Dim intLastRow As Integer
    intLastRow = ExcelLastCell.Row
    Dim Row As Integer
    Row = ExcelLastCell.Row
    Do While Application.CountA(ActiveSheet.Rows(Row)) = 0 And Row <> 1
        Row = Row - 1
    Loop
    intLastRow = Row ' Row number
    'Determine the last column with data
    Dim intLastCol As Integer
    intLastCol = ExcelLastCell.Column
    Dim Col As Integer
    Col = ExcelLastCell.Column
    Do While Application.CountA(ActiveSheet.Columns(Col)) = 0 And Col <> 1
        Col = Col - 1
    Loop
    intLastCol = Col ' Column number

    '---PART2: Determine threshold values
    'min # of abnormal pixels in a column (50% of the length)
    Dim intThreshHold As String
    intThreshHold = intLastRow / 2
    'threshold for replacing strips
    'min # of consecutive abnormal pixels in a column
    Dim intThreshHoldStrip As String
    intThreshHoldStrip = 5
```

```vbnet
'--PART3: fix abnormal pixels
Dim strCellValue As String
Dim R As Integer
Dim C As Integer
For C = 1 To intLastCol
    Dim intCount As Integer
    intCount = 0
    'exclude first and last columns
    If C > 1 And C < intLastCol Then
        For R = 1 To intLastRow
            'set active cell
            Cells(R, C).Select
            'check if active cell is less then left and right cells
            If ActiveCell.Value < ActiveCell.Offset(0, -1) And _
                ActiveCell.Value < ActiveCell.Offset(0, 1) Then
                'count number of bad pixels in a column
                intCount = intCount + 1
            End If
        Next R
        'fix stripping in bad column
        If intCount > intThreshHold Then
            Dim R2 As Integer
            R2 = 1
            For R2 = 1 To intLastRow
                'set active cell
                Cells(R2, C).Select
                'count number of consicutive abnormal pixels
                'if pixel is abnormal (counting strips)
                If ActiveCell.Value < ActiveCell.Offset(0, -1) _
                    And ActiveCell.Value < ActiveCell.Offset(0, 1) Then
                    Dim intCount2 As Integer 'counter
                    intCount2 = 0
                    Dim R3 As Integer 'new row index
                    R3 = R2
                    'set active cell
                    Cells(R3, C).Select


                    'loop through and count number of consecutive bad pixels
                    Do Until (ActiveCell.Value >= ActiveCell.Offset(0, -1) _
                            Or ActiveCell.Value >= ActiveCell.Offset(0, 1)) _
                            Or R3 > intLastRow + 1
                        'set active cell
                        Cells(R3, C).Select
                        'count number of bad pixels in a column
                        intCount2 = intCount2 + 1
                        R3 = R3 + 1
                    Loop
                    'set count back one number
                    intCount2 = intCount2 - 1
```

```
                                'replace pixels if # bad pixels > threshold
                                If intCount2 > intThreshHoldStrip Then
                                    Dim R4 As Integer
                                    R4 = R2
                                    Dim intLastFix As Integer
                                    intLastFix = R2 - intCount2
                                    Do Until R4 = intLastFix
                                        'set active cell
                                        Cells(R4, C).Select
                                        'replace cell values
                                        ActiveCell.Value = CInt((ActiveCell.Offset(0, -1) + _
                                                    ActiveCell.Offset(0, 1)) / 2)
                                        R4 = R4 + 1
                                    Loop
                                End If
                            End If
                        Next R2
                    End If
                End If
            Next C
            'save workbook
            ActiveWorkbook.Save
            'display message when sucessfully completed
            MsgBox "Process Complete"

    '-------Error Handling------------
    Exit Sub                'Exit to avoid error handler
    Errorhandler:                       'Error-handling routine
        MsgBox Str(Err.Number) & ": " & Err.Description, , "Error"
    End Sub
```

APPENDIX VII
SCRIPT CONVERTING EXCEL TO ASCII

```
Public Sub Export_dbfToAscii()
'Project Name:   Export Excel(.dbf) to ascii
'Description:    Exports Excel grid to ascii format using a space
'                delimiter.
'Created by:     Jevon Hagens
'Last Updated:   August 2006
'Software:       Created in Excel 2003

    '---PART1: get name of file to export
    Dim intNameWBook As Integer
    intNameWBook = Len(ActiveWorkbook.Name)
    'get name of workbook without extension
    Dim strNameWBook As String
    strNameWBook = Left(ActiveWorkbook.Name, intNameWBook - 4)
    'get folder name of path to save file in
    Dim objSearchApp As Object
    Dim objFolder As Object
    Set objSearchApp = CreateObject("Shell.Application")
    Set objFolder = objSearchApp.BrowseForFolder _
                    (0, "Please choose folder to save file in:", 0)
    If objFolder Is Nothing Then
        MsgBox "You did not choose a folder"
        Exit Sub
    End If
    Dim strFolderName As String
    strFolderName = objFolder.Items.Item.Path
    'get final folder and path name
    Dim strAsciiFilePathName As String
    strAsciiFilePathName = strFolderName & "\" & strNameWBook & ".asc"

    'uses a space delimeter
    Dim Sep As String
    Sep = " "

    Dim WholeLine As String
    Dim FNum As Integer
    Dim RowNdx As Long
    Dim ColNdx As Integer
    Dim StartRow As Long
    Dim EndRow As Long
    Dim StartCol As Integer
    Dim EndCol As Integer
    Dim CellValue As String

    Application.ScreenUpdating = False
    On Error GoTo EndMacro:
    FNum = FreeFile
```

```
'export the entire worksheet
With ActiveSheet.UsedRange
     StartRow = .Cells(1).Row
     StartCol = .Cells(1).Column
     EndRow = .Cells(.Cells.Count).Row
     EndCol = .Cells(.Cells.Count).Column
End With

Open strAsciiFilePathName For Output Access Write As #FNum
'loop through each row and write each line
For RowNdx = StartRow To EndRow
     WholeLine = ""
     For ColNdx = StartCol To EndCol
          If Cells(RowNdx, ColNdx).Value = "" Then
              CellValue = ""
          Else
              CellValue = Cells(RowNdx, ColNdx).Text
          End If
          WholeLine = WholeLine & CellValue & Sep
     Next ColNdx
     WholeLine = Left(WholeLine, Len(WholeLine) - Len(Sep))
     Print #FNum, WholeLine
Next RowNdx

'display messagebox the finished
MsgBox "Process Complete"

'--------Error Handling------------
EndMacro:
On Error GoTo 0
Application.ScreenUpdating = True
Close #FNum
End Sub
```

APPENDIX VIII
SCRIPT SAVING EXCEL DOCUMENT TO DBF IV

```
Public Sub SaveAsdbfIV()
'Project Name:   Save as Excel(.dbfIV) format
'Description:    Save an existing Excel document as .dbf IV
'               dynamically based on previous workbook name
'Created by:     Jevon Hagens
'Last Updated:   August 2006
'Software:       Created in Excel 2003
    'get length of active workbook name
    Dim intFileLength As Integer
    intFileLength = Len(ActiveWorkbook.Name)
    'cut off .*** from filename
    Dim strFileName As String
    strFileName = Left(ActiveWorkbook.Name, intFileLength - 4)
    'dynamically save new file as dbfIV based on previous name
    ActiveWorkbook.SaveAs Filename:=ActiveWorkbook.Path & "\" & _
            strFileName, FileFormat:=xlDBF4
    ActiveWorkbook.Close
End Sub
```

APPENDIX IX
EXAMPLE OF ERDAS MODEL USED TO COMBINE CORRECTED BANDS
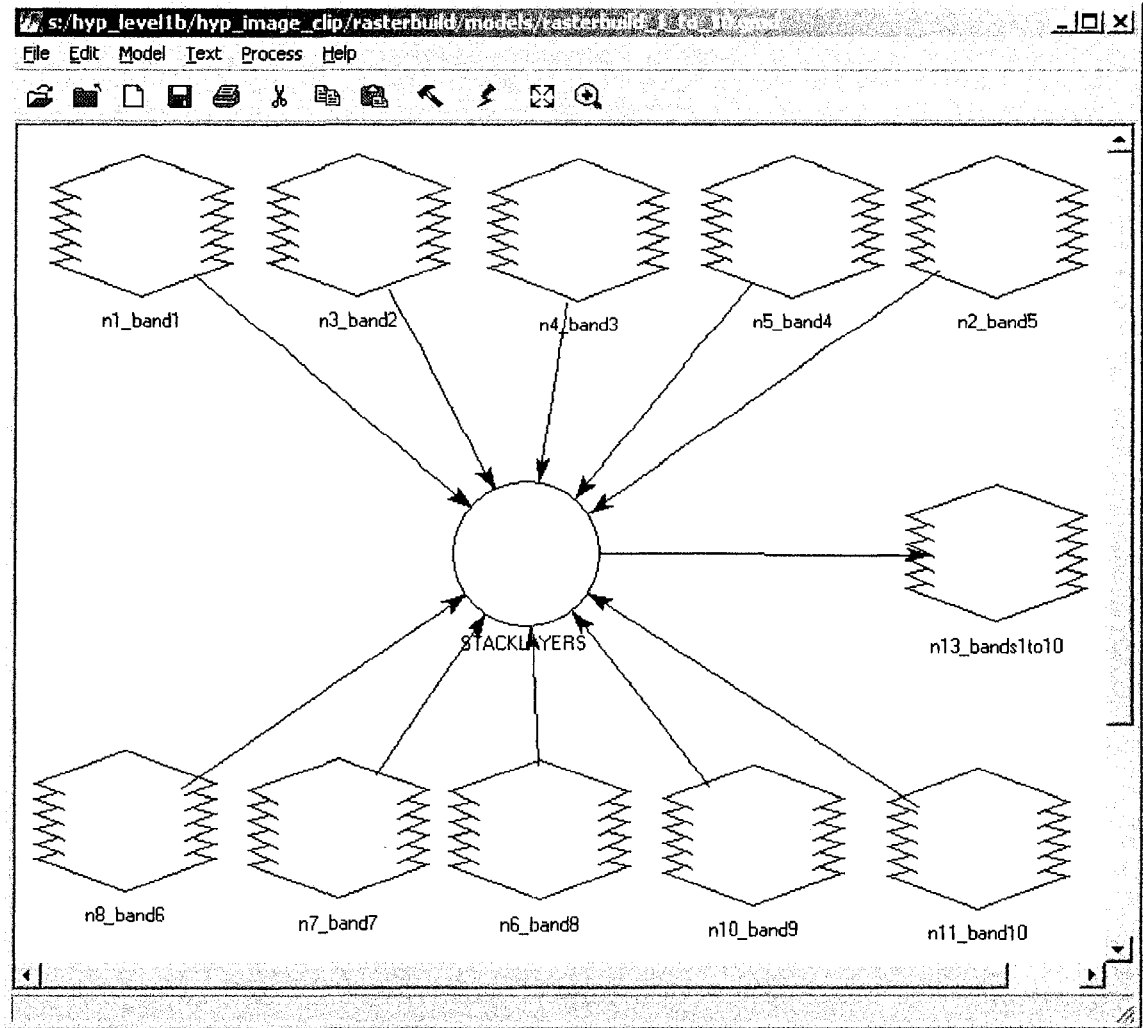
APPENDIX X
ERDAS MODEL USED TO CONVERT RAW LEVEL 1B HYPERION
DN VALUES TO ABSOLUTE RADIANCE

VNIR Bands / 40   SWIR Bands / 80

n13_hyp1b242_vnir_1to70   n4_hyp1b242_swir_71to242

$n13_hyp1b242_vnir_1to70 / 40 $n4_hyp1b242_swir_71to242 / 80

$n13_hyp1b242_vnir_1to70 $n4_hyp1b242_swir_71to242

n2_memory   n5_memory

STACKLAYERS

n9_hyp1b242_radcor
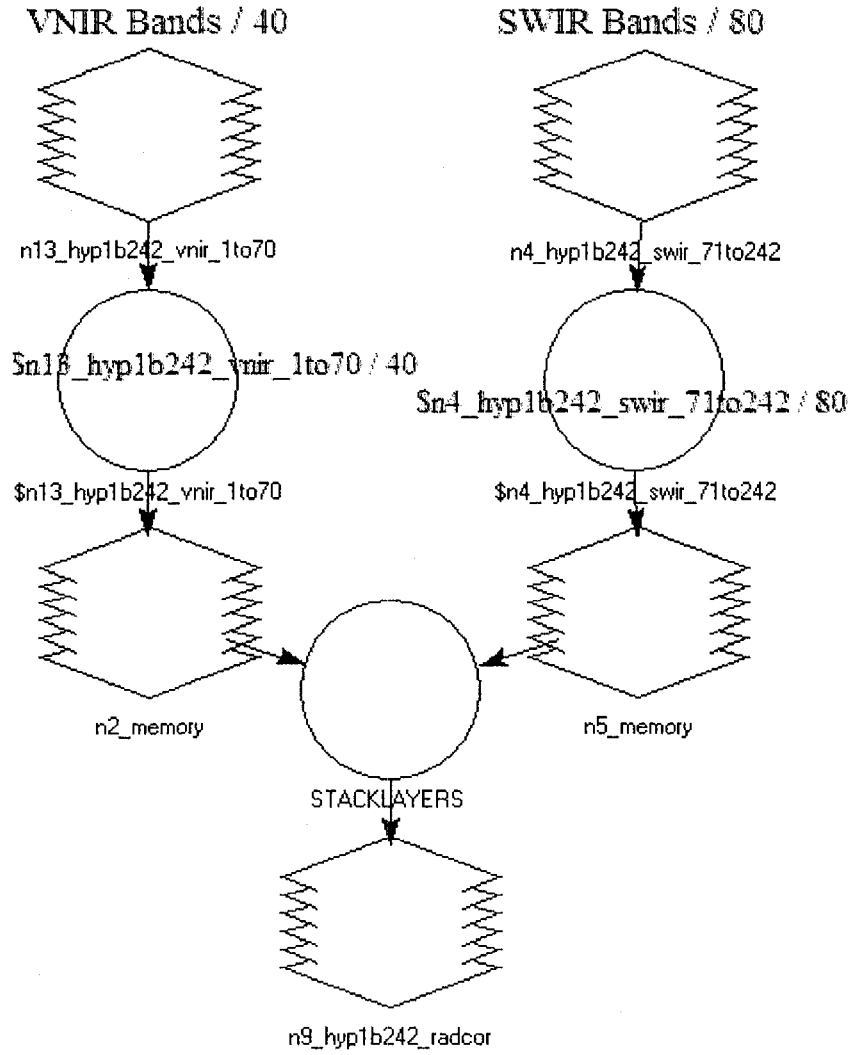
APPENDIX XI
ERDAS MODEL USED TO CONVERT RAW LEVEL 0 LANDSAT TM5
DN VALUES TO ABSOLUTE RADIANCE
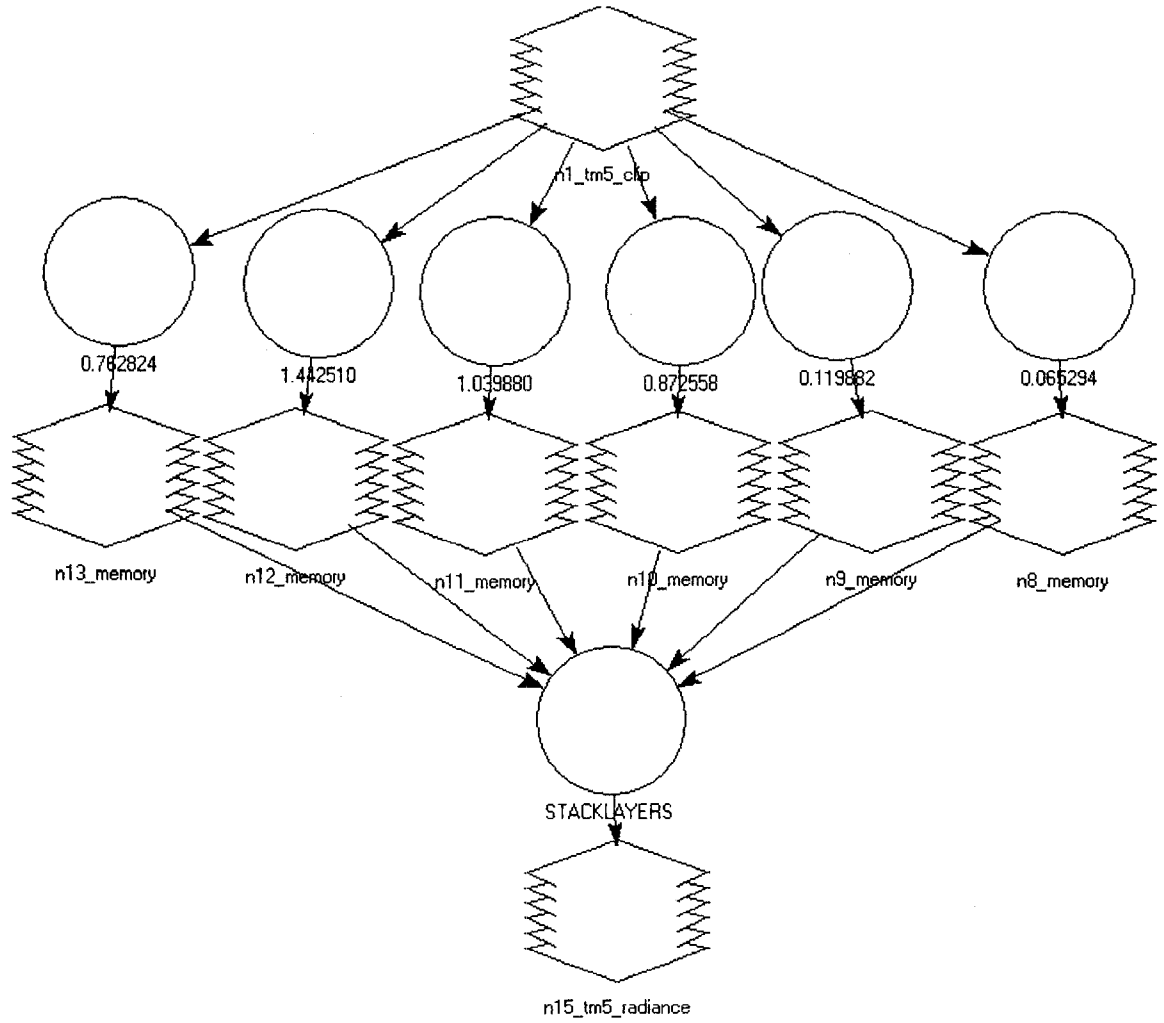
APPENDIX XII
AVERAGE WAVELENGTHS FOR ORGINAL 242 BAND
HYPERION IMAGE

Band	Average Wavelength (nm)	Band	Average Wavelength (nm)	Band	Average Wavelength (nm)	Band	Average Wavelength (nm)
1	355.59	33	681.20	57	925.41	97	1114.19
2	365.76	34	691.37	79	932.64	98	1124.28
3	375.94	35	701.55	58	935.58	99	1134.38
4	386.11	36	711.72	80	942.73	100	1144.48
5	396.29	37	721.90	59	945.76	101	1154.58
6	406.46	38	732.07	81	952.82	102	1164.68
7	416.64	39	742.25	60	955.93	103	1174.77
8	426.82	40	752.43	82	962.91	104	1184.87
9	436.99	41	762.60	61	966.11	105	1194.97
10	447.17	42	772.78	83	972.99	106	1205.07
11	457.34	43	782.95	62	976.28	107	1215.17
12	467.52	44	793.13	84	983.08	108	1225.17
13	477.69	45	803.30	63	986.46	109	1235.27
14	487.87	46	813.48	85	993.17	110	1245.36
15	498.04	47	823.65	64	996.63	111	1255.46
16	508.22	48	833.83	86	1003.30	112	1265.56
17	518.39	49	844.00	65	1006.81	113	1275.66
18	528.57	71	851.92	87	1013.30	114	1285.76
19	538.74	50	854.18	66	1016.98	115	1295.86
20	548.92	72	862.01	88	1023.40	116	1305.96
21	559.09	51	864.35	67	1027.16	117	1316.05
22	569.27	73	872.10	89	1033.49	118	1326.05
23	579.45	52	874.53	68	1037.33	119	1336.15
24	589.62	74	882.19	90	1043.59	120	1346.25
25	599.80	53	884.70	69	1047.51	121	1356.35
26	609.97	75	892.28	91	1053.69	122	1366.45
27	620.15	54	894.88	70	1057.68	123	1376.55
28	630.32	76	902.36	92	1063.79	124	1386.65
29	640.50	·55	905.05	93	1073.89	125	1396.74
30	650.67	77	912.45	94	1083.99	126	1406.84
31	660.85	56	915.23	95	1094.09	127	1416.94
32	671.02	78	922.54	96	1104.19	128	1426.94

Band	Average Wavelength (nm)	Band	Average Wavelength (nm)	Band	Average Wavelength (nm)	Band	Average Wavelength (nm)
129	1437.04	164	1790.19	199	2143.34	234	2496.39
130	1447.14	165	1800.29	200	2153.34	235	2506.48
131	1457.23	166	1810.38	201	2163.43	236	2516.59
132	1467.33	167	1820.48	202	2173.53	237	2526.68
133	1477.43	168	1830.58	203	2183.63	238	2536.78
134	1487.53	169	1840.58	204	2193.73	239	2546.88
135	1497.63	170	1850.68	205	2203.83	240	2556.98
136	1507.73	171	1860.78	206	2213.93	241	2566.98
137	1517.83	172	1870.87	207	2224.03	242	2577.08
138	1527.92	173	1880.98	208	2234.12		
139	1537.92	174	1891.07	209	2244.22		
140	1548.02	175	1901.17	210	2254.22		
141	1558.12	176	1911.27	211	2264.32		
142	1568.22	177	1921.37	212	2274.42		
143	1578.32	178	1931.47	213	2284.52		
144	1588.42	179	1941.57	214	2294.61		
145	1598.51	180	1951.57	215	2304.71		
146	1608.61	181	1961.66	216	2314.81		
147	1618.71	182	1971.76	217	2324.91		
148	1628.81	183	1981.86	218	2335.01		
149	1638.81	184	1991.96	219	2345.11		
150	1648.90	185	2002.06	220	2355.21		
151	1659.00	186	2012.15	221	2365.20		
152	1669.10	187	2022.25	222	2375.30		
153	1679.20	188	2032.35	223	2385.40		
154	1689.30	189	2042.45	224	2395.50		
155	1699.40	190	2052.45	225	2405.60		
156	1709.50	191	2062.55	226	2415.70		
157	1719.60	192	2072.65	227	2425.80		
158	1729.70	193	2082.75	228	2435.89		
159	1739.70	194	2092.84	229	2445.99		
160	1749.79	195	2102.94	230	2456.09		
161	1759.89	196	2113.04	231	2466.09		
162	1769.99	197	2123.14	232	2476.19		
163	1780.09	198	2133.24	233	2486.29		

APPENDIX XIII
AVERAGE WAVELENGTHS FOR 155 BAND HYPERION IMAGE
WITH BAD BANDS REMOVED

New Band	Average Wavelength (nm)	New Band	Average Wavelength (nm)	New Band	Average Wavelength (nm)	New Band	Average Wavelength (nm)	New Band	Average Wavelength (nm)
1	436.99	33	762.60	65	1073.89	97	1548.02	129	2092.84
2	447.17	34	772.78	66	1083.99	98	1558.12	130	2102.94
3	457.34	35	782.95	67	1094.09	99	1568.22	131	2113.04
4	467.52	36	793.13	68	1104.19	100	1578.32	132	2123.14
5	477.69	37	803.30	69	1114.19	101	1588.42	133	2133.24
6	487.87	38	813.48	70	1124.28	102	1598.51	134	2143.34
7	498.04	39	823.65	71	1134.38	103	1608.61	135	2153.34
8	508.22	40	833.83	72	1144.48	104	1618.71	136	2163.43
9	518.39	41	844.00	73	1154.58	105	1628.81	137	2173.53
10	528.57	42	854.18	74	1164.68	106	1638.81	138	2183.63
11	538.74	43	864.35	75	1174.77	107	1648.90	139	2193.73
12	548.92	44	874.53	76	1184.87	108	1659.00	140	2203.83
13	559.09	45	884.70	77	1194.97	109	1669.10	141	2213.93
14	569.27	46	894.88	78	1205.07	110	1679.20	142	2224.03
15	579.45	47	905.05	79	1215.17	111	1689.30	143	2234.12
16	589.62	48	915.23	80	1225.17	112	1699.40	144	2244.22
17	599.80	49	925.41	81	1235.27	113	1709.50	145	2254.22
18	609.97	50	922.54	82	1245.36	114	1719.60	146	2264.32
19	620.15	51	932.64	83	1255.46	115	1729.70	147	2274.42
20	630.32	52	942.73	84	1265.56	116	1739.70	148	2284.52
21	640.50	53	952.82	85	1275.66	117	1749.79	149	2294.61
22	650.67	54	962.91	86	1285.76	118	1759.89	150	2304.71
23	660.85	55	972.99	87	1295.86	119	1769.99	151	2314.81
24	671.02	56	983.08	88	1305.96	120	1780.09	152	2324.91
25	681.20	57	993.17	89	1316.05	121	1790.19	153	2335.01
26	691.37	58	1003.30	90	1326.05	122	2022.25	154	2345.11
27	701.55	59	1013.30	91	1336.15	123	2032.35	155	2355.21
28	711.72	60	1023.40	92	1497.63	124	2042.45		
29	721.90	61	1033.49	93	1507.73	125	2052.45		
30	732.07	62	1043.59	94	1517.83	126	2062.55		
31	742.25	63	1053.69	95	1527.92	127	2072.65		
32	752.43	64	1063.79	96	1537.92	128	2082.75		

APPENDIX XIV
NWST WETLAND SAMPLE TYPES

ES34 Treed Bog (Black spruce / sphagnum: organic soil)
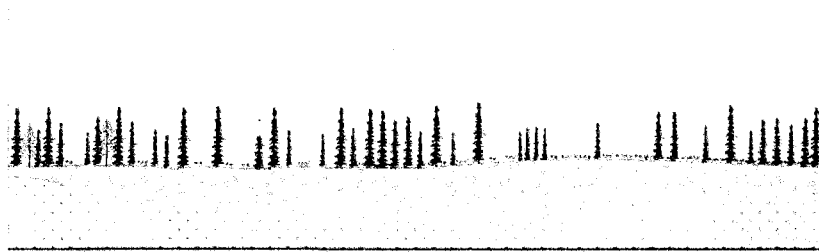
ES39 Open Bog (Ericaceus shrub / sedge / *sphagnum:* organic soil)
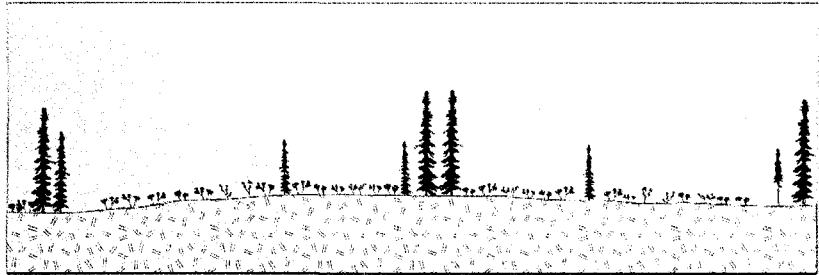
ES40 Treed Fen (Tamarack-black spruce / sphagnum: organic soil)
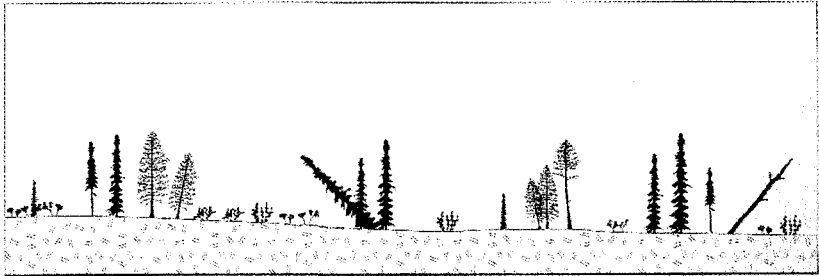
ES41 Open Poor Fen (Ericaceous shrub-sedge / sphagnum: organic soil)
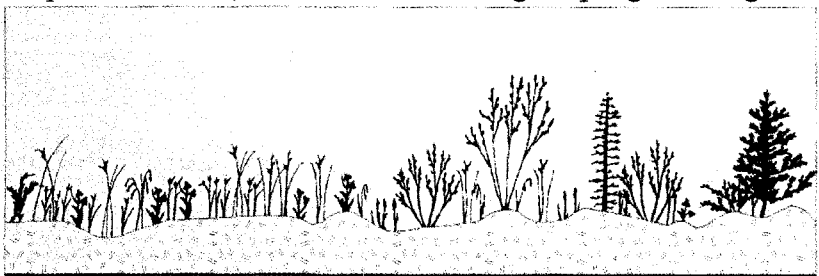
ES42 Open Moderately Rich Fen (Ericaceous shrub / sedge: organic soil)
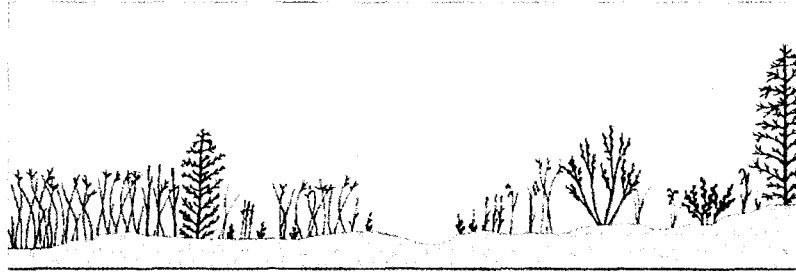
ES45 Shore Fen (Organic soil)

water

ES46 Meadow Marsh (Organic-mineral soil)

ES47 Sheltered Marsh (Emergent sedimentary peat substrate)
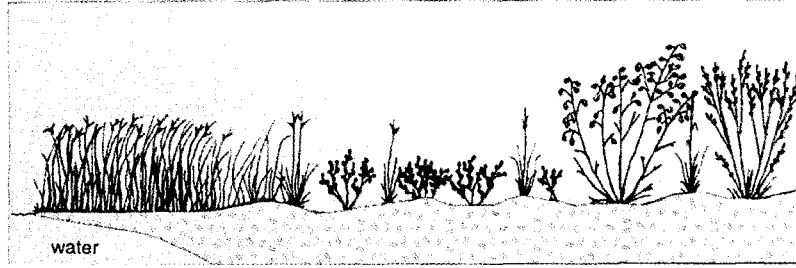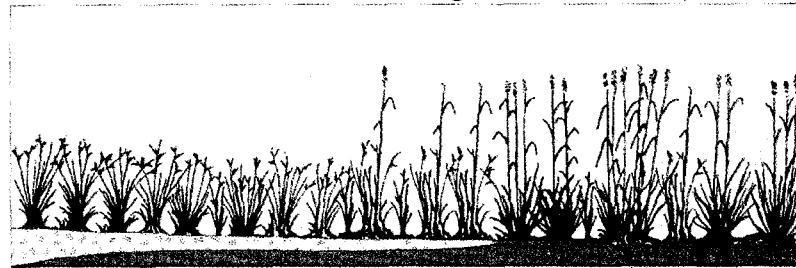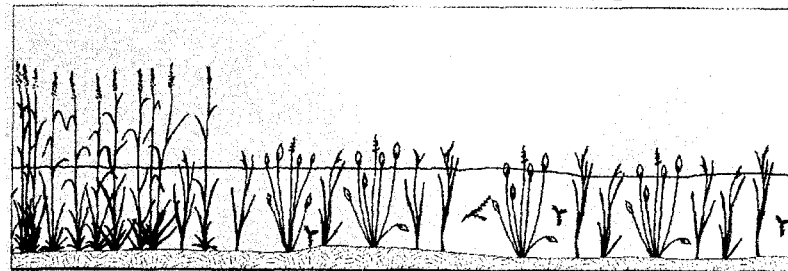

ES48 Exposed Marsh (Emergent mineral substrate)
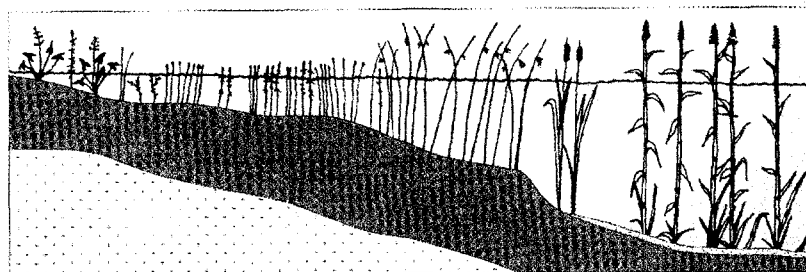
APPENDIX XV
TM PRINCIPAL COMPONENT IMAGES

PC1

PC2

PC3

PC4
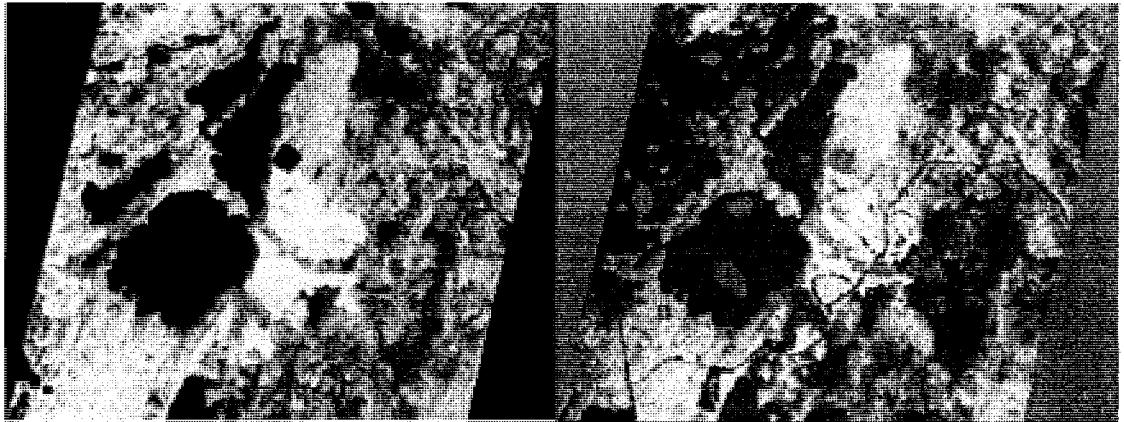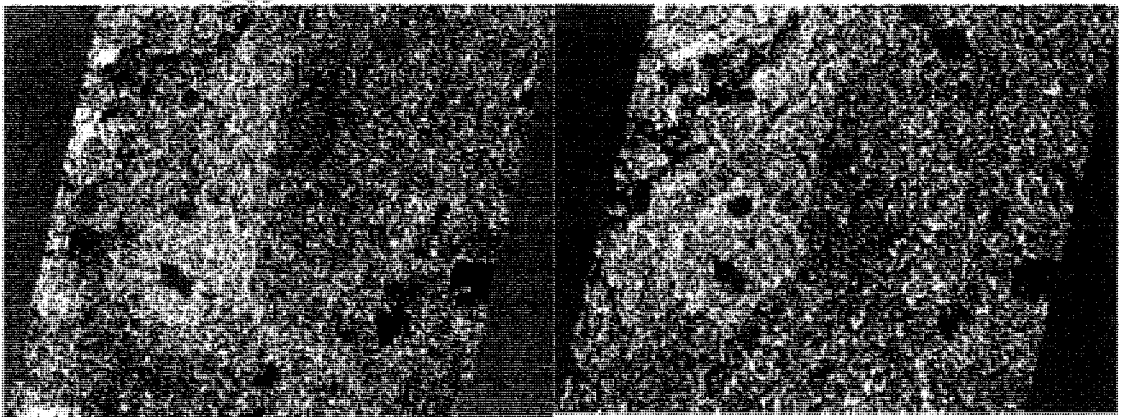
PC5

PC6

APPENDIX XVI
EIGEN MATRIX FROM HYPERION PCA

Band	PC 1	PC 2	PC 3	PC 4	PC 5	PC 6	...	PC 155
1	0.025	0.035	-0.176	-0.127	0.030	0.029	...	-0.234
2	0.020	0.037	-0.142	-0.103	0.025	0.020	...	-0.236
3	0.019	0.038	-0.133	-0.097	0.024	0.015	...	-0.996
4	0.021	0.038	-0.145	-0.105	0.026	0.020	...	-0.689
5	0.020	0.041	-0.134	-0.097	0.025	0.017	...	0.100
6	0.020	0.040	-0.135	-0.096	0.024	0.019	...	0.556
7	0.019	0.044	-0.125	-0.090	0.023	0.015	...	0.106
8	0.020	0.042	-0.125	-0.090	0.023	0.016	...	0.120
9	0.025	0.043	-0.132	-0.094	0.025	0.016	...	0.322
10	0.032	0.037	-0.142	-0.101	0.026	0.018	...	0.701
11	0.034	0.035	-0.131	-0.094	0.025	0.014	...	0.828
12	0.038	0.036	-0.136	-0.098	0.027	0.014	...	0.537
13	0.038	0.036	-0.133	-0.096	0.026	0.014	...	0.506
14	0.036	0.042	-0.136	-0.097	0.028	0.017	...	0.905
15	0.034	0.048	-0.141	-0.101	0.029	0.020	...	-0.992
16	0.032	0.052	-0.137	-0.097	0.028	0.020	...	-0.759
17	0.032	0.055	-0.140	-0.099	0.029	0.021	...	-0.742
18	0.031	0.056	-0.135	-0.095	0.028	0.020	...	0.177
19	0.028	0.059	-0.125	-0.088	0.026	0.018	...	-0.237
20	0.028	0.061	-0.125	-0.088	0.026	0.019	...	0.055
21	0.027	0.063	-0.123	-0.085	0.026	0.018	...	0.269
22	0.026	0.065	-0.119	-0.083	0.025	0.016	...	-0.429
23	0.025	0.066	-0.120	-0.083	0.024	0.016	...	0.813
24	0.022	0.067	-0.106	-0.074	0.022	0.011	...	-1.099
25	0.023	0.069	-0.106	-0.073	0.021	0.010	...	0.678
26	0.025	0.069	-0.108	-0.074	0.022	0.011	...	-0.124
27	0.036	0.061	-0.117	-0.079	0.024	0.013	...	-2.748
28	0.066	0.023	-0.098	-0.072	0.022	-0.001	...	0.407
29	0.086	-0.013	-0.074	-0.062	0.013	-0.023	...	1.438
30	0.104	-0.051	-0.043	-0.048	0.002	-0.053	...	-0.383
31	0.117	-0.078	-0.018	-0.039	-0.005	-0.075	...	1.104
32	0.126	-0.093	-0.002	-0.035	-0.008	-0.084	...	-2.534
33	0.130	-0.101	0.007	-0.033	-0.012	-0.096	...	0.726
34	0.127	-0.098	0.004	-0.028	-0.013	-0.093	...	0.400
35	0.128	-0.097	0.008	-0.029	-0.011	-0.090	...	-0.204
36	0.128	-0.096	0.005	-0.031	-0.010	-0.088	...	-0.144
37	0.129	-0.096	0.010	-0.027	-0.011	-0.089	...	-0.239
38	0.126	-0.091	0.002	-0.033	-0.008	-0.079	...	-0.559
39	0.125	-0.090	0.001	-0.031	-0.009	-0.080	...	0.231
40	0.125	-0.091	0.010	-0.024	-0.011	-0.083	...	0.246
41	0.127	-0.091	0.011	-0.024	-0.010	-0.083	...	0.015

Band	PC 1	PC 2	PC 3	PC 4	PC 5	PC 6	...	PC 155
42	0.127	-0.090	0.009	-0.026	-0.009	-0.081	...	0.088
43	0.127	-0.088	0.008	-0.026	-0.009	-0.080	...	0.064
44	0.128	-0.090	0.016	-0.021	-0.010	-0.082	...	-0.069
45	0.126	-0.086	0.008	-0.025	-0.008	-0.076	...	-0.110
46	0.125	-0.083	0.003	-0.030	-0.006	-0.067	...	-0.470
47	0.124	-0.081	-0.001	-0.030	-0.006	-0.066	...	0.250
48	0.124	-0.078	-0.012	-0.036	-0.004	-0.061	...	0.132
49	0.118	-0.069	-0.046	-0.057	0.001	-0.047	...	0.357
50	0.120	-0.072	0.005	-0.007	-0.001	0.033	...	0.582
51	0.098	-0.060	0.020	0.008	-0.003	0.042	...	-0.087
52	0.094	-0.051	-0.022	-0.018	0.003	0.048	...	0.154
53	0.105	-0.054	-0.033	-0.022	0.004	0.049	...	0.282
54	0.105	-0.055	0.003	0.003	-0.001	0.037	...	0.208
55	0.106	-0.057	0.041	0.029	-0.006	0.026	...	-0.050
56	0.104	-0.055	0.032	0.023	-0.004	0.027	...	-0.135
57	0.107	-0.056	0.027	0.019	-0.003	0.031	...	-0.137
58	0.107	-0.055	0.024	0.017	-0.002	0.032	...	-0.141
59	0.104	-0.052	0.011	0.007	0.000	0.032	...	-0.041
60	0.104	-0.052	0.012	0.008	0.000	0.032	...	-0.037
61	0.106	-0.053	0.004	0.002	0.001	0.036	...	-0.066
62	0.107	-0.054	0.005	0.004	0.001	0.037	...	-0.174
63	0.110	-0.054	0.010	0.007	0.001	0.038	...	-0.291
64	0.109	-0.054	0.011	0.007	0.001	0.038	...	-0.090
65	0.109	-0.053	0.007	0.005	0.002	0.040	...	-0.112
66	0.111	-0.053	0.002	0.001	0.003	0.043	...	0.031
67	0.107	-0.051	0.011	0.008	0.001	0.040	...	-0.183
68	0.107	-0.050	0.023	0.016	0.000	0.040	...	-0.357
69	0.108	-0.046	-0.004	-0.003	0.004	0.056	...	-0.180
70	0.105	-0.043	-0.013	-0.005	0.003	0.065	...	0.163
71	0.097	-0.038	0.016	0.018	-0.001	0.047	...	0.069
72	0.094	-0.031	0.011	0.016	-0.001	0.046	...	0.049
73	0.090	-0.025	0.022	0.025	-0.002	0.038	...	0.064
74	0.093	-0.023	0.020	0.023	-0.001	0.038	...	0.089
75	0.092	-0.021	0.023	0.025	-0.002	0.036	...	0.123
76	0.092	-0.019	0.025	0.027	-0.002	0.036	...	0.174
77	0.094	-0.018	0.021	0.024	-0.001	0.039	...	0.214
78	0.092	-0.016	0.011	0.017	0.001	0.041	...	0.311
79	0.094	-0.017	0.025	0.027	-0.001	0.039	...	0.270
80	0.095	-0.018	0.026	0.028	-0.001	0.039	...	0.202
81	0.097	-0.019	0.014	0.020	0.001	0.042	...	0.304
82	0.098	-0.018	0.008	0.016	0.002	0.043	...	0.293
83	0.098	-0.018	0.009	0.016	0.002	0.043	...	0.323
84	0.101	-0.018	0.005	0.015	0.003	0.045	...	0.464
85	0.100	-0.019	0.014	0.021	0.001	0.041	...	0.446

Band	PC 1	PC 2	PC 3	PC 4	PC 5	PC 6	...	PC 155
86	0.100	-0.017	0.014	0.021	0.001	0.042	...	0.343
87	0.100	-0.014	0.016	0.023	0.001	0.043	...	0.280
88	0.098	-0.010	0.018	0.025	0.001	0.042	...	0.154
89	0.093	-0.005	0.019	0.027	0.000	0.040	...	0.153
90	0.092	0.001	0.018	0.026	0.000	0.041	...	-0.042
91	0.096	0.001	0.035	0.040	-0.002	0.046	...	-0.154
92	0.055	0.098	-0.006	0.014	0.005	0.010	...	0.241
93	0.058	0.096	-0.001	0.017	0.005	0.011	...	0.221
94	0.059	0.094	0.022	0.033	0.001	0.003	...	0.159
95	0.063	0.092	0.027	0.037	0.001	0.005	...	0.148
96	0.067	0.086	-0.002	0.018	0.005	0.015	...	0.152
97	0.069	0.081	-0.001	0.019	0.004	0.016	...	0.054
98	0.068	0.075	-0.002	0.018	0.004	0.018	...	0.093
99	0.071	0.072	-0.004	0.017	0.004	0.020	...	0.093
100	0.070	0.070	0.010	0.027	0.002	0.018	...	-0.202
101	0.073	0.070	0.010	0.027	0.003	0.021	...	-0.073
102	0.072	0.066	0.006	0.023	0.003	0.021	...	0.052
103	0.073	0.064	0.022	0.035	0.001	0.019	...	0.001
104	0.074	0.063	0.013	0.030	0.002	0.025	...	-0.181
105	0.073	0.060	0.013	0.029	0.002	0.026	...	-0.265
106	0.078	0.063	0.017	0.032	0.002	0.026	...	-0.177
107	0.078	0.062	0.016	0.032	0.002	0.027	...	-0.262
108	0.077	0.061	0.014	0.030	0.002	0.026	...	-0.356
109	0.078	0.060	0.008	0.026	0.003	0.028	...	-0.305
110	0.077	0.060	0.015	0.031	0.002	0.024	...	-0.350
111	0.078	0.061	0.019	0.034	0.001	0.024	...	-0.525
112	0.076	0.061	0.016	0.031	0.001	0.024	...	-0.173
113	0.075	0.061	0.020	0.034	0.001	0.023	...	-0.151
114	0.076	0.063	0.016	0.030	0.001	0.023	...	0.016
115	0.077	0.066	0.004	0.022	0.003	0.026	...	0.070
116	0.078	0.071	0.025	0.038	0.001	0.021	...	-0.100
117	0.075	0.073	0.038	0.047	-0.001	0.017	...	-0.168
118	0.072	0.073	0.022	0.036	0.001	0.019	...	-0.401
119	0.071	0.073	0.014	0.029	0.002	0.020	...	-0.472
120	0.068	0.079	0.069	0.069	-0.006	0.008	...	-0.963
121	0.066	0.079	0.088	0.082	-0.010	0.005	...	-0.844
122	0.030	0.151	0.027	0.026	-0.001	-0.066	...	-0.215
123	0.029	0.156	0.061	0.053	-0.005	-0.063	...	-0.576
124	0.031	0.181	0.063	0.025	-0.004	-0.040	...	0.419
125	0.023	0.203	0.138	0.041	-0.015	-0.064	...	1.196
126	0.053	0.155	-0.040	-0.015	0.010	-0.055	...	0.774
127	0.050	0.150	-0.007	0.010	0.005	-0.056	...	0.725
128	0.039	0.146	0.050	0.040	-0.002	-0.037	...	0.811
129	0.041	0.144	0.048	0.038	-0.001	-0.033	...	0.928

Band	PC 1	PC 2	PC 3	PC 4	PC 5	PC 6	...	PC 155
130	0.049	0.141	0.031	0.032	0.001	-0.027	...	0.245
131	0.049	0.131	0.020	0.024	0.002	-0.023	...	0.122
132	0.047	0.126	-0.008	0.000	0.006	-0.003	...	0.710
133	0.049	0.131	-0.004	0.003	0.006	-0.003	...	0.731
134	0.051	0.117	0.013	0.027	0.001	-0.017	...	-0.328
135	0.050	0.118	0.031	0.041	-0.002	-0.022	...	-0.655
136	0.045	0.140	0.081	0.061	-0.004	-0.027	...	-0.589
137	0.045	0.136	0.080	0.061	-0.004	-0.025	...	-0.607
138	0.052	0.101	-0.017	0.005	0.007	0.002	...	-0.333
139	0.049	0.095	-0.001	0.016	0.004	0.000	...	-0.409
140	0.046	0.110	0.073	0.061	-0.004	-0.021	...	0.337
141	0.047	0.109	0.065	0.056	-0.003	-0.017	...	0.344
142	0.058	0.100	-0.021	0.005	0.006	0.007	...	0.001
143	0.060	0.104	-0.013	0.010	0.005	0.005	...	0.041
144	0.045	0.109	0.093	0.072	0.012	-0.026	...	-0.564
145	0.046	0.104	0.054	0.041	0.019	-0.018	...	-0.175
146	0.048	0.095	-0.007	0.009	0.002	-0.006	...	0.405
147	0.050	0.095	-0.037	-0.012	0.005	0.000	...	0.594
148	0.044	0.096	0.030	0.034	-0.001	-0.017	...	-0.022
149	0.039	0.107	0.091	0.076	-0.009	-0.039	...	-0.229
150	0.047	0.115	0.026	0.035	-0.007	-0.023	...	-0.381
151	0.050	0.110	-0.027	-0.002	-0.001	-0.011	...	-0.164
152	0.050	0.094	-0.088	-0.049	0.017	0.014	...	-0.065
153	0.043	0.100	-0.037	-0.014	0.011	-0.001	...	-0.170
154	0.043	0.091	-0.091	-0.035	-0.079	0.012	...	-0.321
155	0.043	0.099	-0.092	-0.028	-0.118	0.009	...	-0.448

APPENDIX XVII
FIRST SIX HYPERION PRINCIPAL COMPONENT IMAGES

PC1

PC2

PC3

PC4
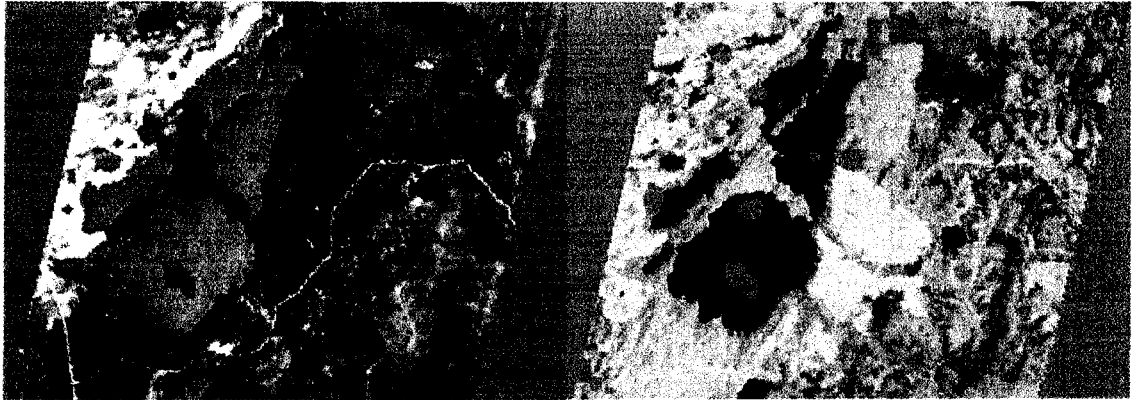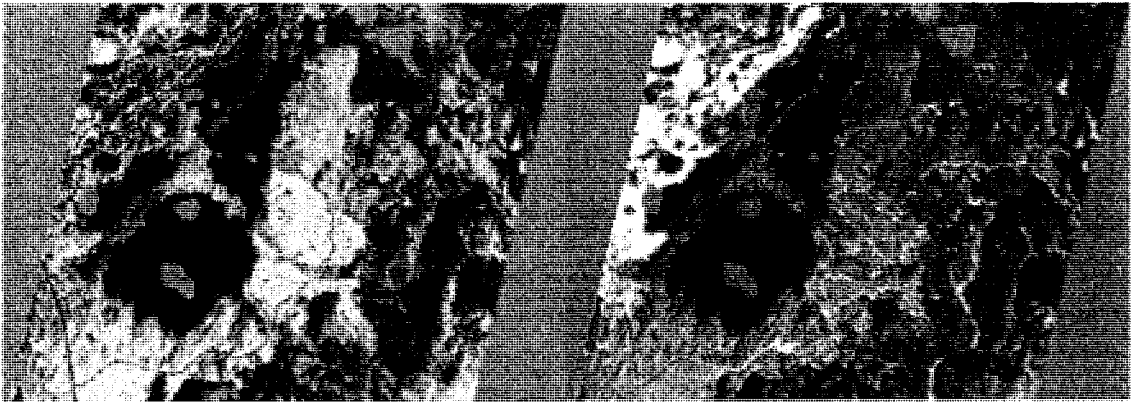
PC5

PC6

APPENDIX XVIII
POOLED WITHIN-GROUPS CORRELATION MATRIX SHOWING AVERAGE CORRELATIONS BETWEEN HYPERION'S FIRST 19 BANDS

Band	1	2	3	4	5	6	7	8	9	10	11	12	13	14	15	16	17	18	19
1	1.00	0.72	0.75	0.75	0.74	0.72	0.73	0.72	0.72	0.70	0.67	0.65	0.64	0.65	0.65	0.65	0.64	0.63	0.62
2	0.72	1.00	0.82	0.84	0.83	0.82	0.81	0.82	0.82	0.80	0.76	0.74	0.73	0.74	0.75	0.74	0.73	0.72	0.70
3	0.75	0.82	1.00	0.89	0.88	0.86	0.86	0.86	0.86	0.83	0.79	0.77	0.76	0.77	0.78	0.77	0.76	0.76	0.74
4	0.75	0.84	0.89	1.00	0.91	0.90	0.90	0.90	0.89	0.86	0.81	0.80	0.79	0.81	0.82	0.82	0.81	0.81	0.79
5	0.74	0.83	0.88	0.91	1.00	0.93	0.93	0.92	0.91	0.88	0.83	0.81	0.81	0.84	0.85	0.85	0.84	0.84	0.83
6	0.72	0.82	0.86	0.90	0.93	1.00	0.94	0.94	0.93	0.87	0.83	0.81	0.80	0.83	0.86	0.87	0.87	0.87	0.86
7	0.73	0.81	0.86	0.90	0.93	0.94	1.00	0.95	0.94	0.89	0.84	0.82	0.82	0.85	0.88	0.90	0.89	0.89	0.88
8	0.72	0.82	0.86	0.90	0.92	0.94	0.95	1.00	0.95	0.91	0.86	0.85	0.85	0.88	0.90	0.91	0.91	0.91	0.90
9	0.72	0.82	0.86	0.89	0.91	0.93	0.94	0.95	1.00	0.95	0.92	0.91	0.90	0.92	0.93	0.93	0.92	0.92	0.90
10	0.70	0.80	0.83	0.86	0.88	0.87	0.89	0.91	0.95	1.00	0.97	0.96	0.96	0.96	0.95	0.93	0.90	0.89	0.86
11	0.67	0.76	0.79	0.81	0.83	0.83	0.84	0.86	0.92	0.97	1.00	0.98	0.98	0.96	0.94	0.91	0.88	0.86	0.83
12	0.65	0.74	0.77	0.80	0.81	0.81	0.82	0.85	0.91	0.96	0.98	1.00	0.98	0.97	0.94	0.91	0.88	0.86	0.83
13	0.64	0.73	0.76	0.79	0.81	0.80	0.82	0.85	0.90	0.96	0.98	0.98	1.00	0.98	0.95	0.92	0.90	0.88	0.84
14	0.65	0.74	0.77	0.81	0.84	0.83	0.85	0.88	0.92	0.96	0.96	0.97	0.98	1.00	0.98	0.96	0.93	0.92	0.89
15	0.65	0.75	0.78	0.82	0.85	0.86	0.88	0.90	0.93	0.95	0.94	0.94	0.95	0.98	1.00	0.98	0.97	0.96	0.94
16	0.65	0.74	0.77	0.82	0.85	0.87	0.90	0.91	0.93	0.93	0.91	0.91	0.92	0.96	0.98	1.00	0.98	0.98	0.97
17	0.64	0.73	0.76	0.81	0.84	0.87	0.89	0.91	0.92	0.90	0.88	0.88	0.90	0.93	0.97	0.98	1.00	0.98	0.98
18	0.63	0.72	0.76	0.81	0.84	0.87	0.89	0.91	0.92	0.89	0.86	0.86	0.88	0.92	0.96	0.98	0.98	1.00	0.98
19	0.62	0.70	0.74	0.79	0.83	0.86	0.88	0.90	0.90	0.86	0.83	0.83	0.84	0.89	0.94	0.97	0.98	0.98	1.00

APPENDIX XIX
POOLED WITHIN-GROUPS CORRELATION MATRIX SHOWING AVERAGE
CORRELATIONS BETWEEN SELECTED BANDS IN DFA STEP 16
USED IN LEVEL 1 CLASSIFICATION

Band Number	7	14	26	27	28	31	40	57	82	84	86	89	92	114	120	138
7	1.00	0.85	0.82	0.78	0.49	0.12	0.11	0.18	0.29	0.30	0.30	0.33	0.64	0.53	0.54	0.62
14	0.85	1.00	0.74	0.82	0.76	0.42	0.39	0.45	0.54	0.54	0.55	0.56	0.66	0.65	0.64	0.62
26	0.82	0.74	1.00	0.92	0.49	0.04	0.06	0.16	0.29	0.30	0.30	0.35	0.80	0.60	0.65	0.77
27	0.78	0.82	0.92	1.00	0.74	0.32	0.33	0.41	0.52	0.53	0.53	0.56	0.82	0.73	0.74	0.78
28	0.49	0.76	0.49	0.74	1.00	0.82	0.82	0.84	0.86	0.86	0.86	0.84	0.59	0.75	0.68	0.52
31	0.12	0.42	0.04	0.32	0.82	1.00	0.99	0.96	0.90	0.90	0.89	0.86	0.30	0.60	0.50	0.23
40	0.11	0.39	0.06	0.33	0.82	0.99	1.00	0.97	0.91	0.91	0.90	0.87	0.32	0.62	0.52	0.25
57	0.18	0.45	0.16	0.41	0.84	0.96	0.97	1.00	0.96	0.96	0.96	0.93	0.44	0.72	0.63	0.37
82	0.29	0.54	0.29	0.52	0.86	0.90	0.91	0.96	1.00	0.99	0.99	0.98	0.61	0.85	0.77	0.54
84	0.30	0.54	0.30	0.53	0.86	0.90	0.91	0.96	0.99	1.00	0.99	0.98	0.62	0.86	0.78	0.55
86	0.30	0.55	0.30	0.53	0.86	0.89	0.90	0.96	0.99	0.99	1.00	0.99	0.63	0.86	0.78	0.55
89	0.33	0.56	0.35	0.56	0.84	0.86	0.87	0.93	0.98	0.98	0.99	1.00	0.68	0.89	0.83	0.61
92	0.64	0.66	0.80	0.82	0.59	0.30	0.32	0.44	0.61	0.62	0.63	0.68	1.00	0.90	0.92	0.92
114	0.53	0.65	0.60	0.73	0.75	0.60	0.62	0.72	0.85	0.86	0.86	0.89	0.90	1.00	0.96	0.85
120	0.54	0.64	0.65	0.74	0.68	0.50	0.52	0.63	0.77	0.78	0.78	0.83	0.92	0.96	1.00	0.87
138	0.62	0.62	0.77	0.78	0.52	0.23	0.25	0.37	0.54	0.55	0.55	0.61	0.92	0.85	0.87	1.00

APPENDIX XX
SPSS OUTPUT FOR LEVEL 1 DISCRIMINANT FUNCTION ANALYSIS USING HYPERION IMAGERY

Wilks' Lambda

Test of Function(s)	Wilks' Lambda	Chi-square	df	Sig.
1 through 7	.000	6865.707	245	.000
2 through 7	.004	4810.360	204	.000
3 through 7	.038	2838.419	165	.000
4 through 7	.208	1366.980	128	.000
5 through 7	.529	554.451	93	.000
6 through 7	.709	299.709	60	.000
7	.867	123.832	29	.000

Eigenvalues

Function	Eigenvalue	% of Variance	Cumulative %	Canonical Correlation
1	9.603[a]	38.5	38.5	.952
2	8.634[a]	34.6	73.2	.947
3	4.421[a]	17.7	90.9	.903
4	1.543[a]	6.2	97.1	.779
5	.340[a]	1.4	98.5	.504
6	.224[a]	.9	99.4	.428
7	.153[a]	.6	100.0	.364

a. First 7 canonical discriminant functions were used in the analysis.

APPENDIX XXI
STANDARDIZED CONICAL DISCRIMINANT FUNCTION COEFFICIENTS
FOR HYPERION LEVEL 1 CLASSIFICATION

Band	Function			
Number	1	2	3	4
3	0.20	-0.06	0.36	0.23
6	-0.37	-0.16	-0.14	0.25
7	-0.20	-0.23	0.49	0.27
11	0.04	-0.64	0.49	-0.95
12	-0.89	0.29	-0.34	-0.71
14	0.22	0.46	-0.29	0.50
17	0.03	-0.13	-0.90	1.17
26	0.75	0.49	1.37	-0.14
27	-0.32	0.89	-1.24	-0.28
28	0.97	-2.08	-0.47	0.31
31	0.50	2.12	0.81	-3.33
32	2.81	-0.02	0.34	-0.48
33	1.47	0.60	0.93	-0.88
34	0.21	-1.37	1.33	3.13
44	-2.82	0.26	-1.61	0.21
47	-1.15	-0.22	-0.33	0.91
50	-0.11	-0.44	0.16	0.24
57	0.19	-0.76	1.09	0.92
62	-0.53	0.50	-0.86	-1.89
69	-0.07	-0.65	0.59	0.79
74	-0.18	0.15	0.75	1.61
77	0.11	-0.86	0.96	0.83
79	-0.36	-0.52	0.76	2.55
82	-1.78	-1.26	0.31	2.00
84	-0.23	2.07	-1.98	-1.21
86	0.00	2.18	-2.27	-2.38
88	0.48	1.09	-1.35	-1.90
89	1.18	0.78	-0.07	-0.42
92	-0.61	-0.19	0.21	-0.67
97	-0.16	0.33	0.18	1.08
111	0.73	-1.12	0.53	-0.72
114	-0.58	-1.14	0.69	0.15
120	0.73	-0.31	0.01	-0.16
136	0.28	-0.18	0.26	0.03
138	0.66	0.19	-0.09	-0.42

APPENDIX XXII
SPSS OUTPUT FOR LEVEL 2 DISCRIMINANT FUNCTION ANALYSIS
SEPARATING BLACK SPRUCE AND JACK PINE

Wilks' Lambda

Test of Function(s)	Wilks' Lambda	Chi-square	df	Sig.
1	.165	403.259	22	.000

Eigenvalues

Function	Eigenvalue	% of Variance	Cumulative %	Canonical Correlation
1	5.051[a]	100.0	100.0	.914

a. First 1 canonical discriminant functions were used in the analysis.

Function 1 standardized conical DF coefficients

Band	Coefficient	Band	Coefficient
7	0.422	68	-1.492
8	-0.578	73	1.255
10	0.588	90	-1.090
14	0.687	94	0.964
17	0.535	96	0.834
25	-0.631	110	-1.074
40	-2.766	125	0.283
41	2.289	128	-0.352
52	-0.330	138	-0.468
56	-0.687	149	-0.255
59	2.147	153	0.278

APPENDIX XXIII
SPSS OUTPUT FOR LEVEL 2 DISCRIMINANT FUNCTION ANALYSIS
SEPARATING SPARSE AND DENSE DECIDUOUS

Wilks' Lambda

Test of Function(s)	Wilks' Lambda	Chi-square	df	Sig.
1	.192	280.154	17	.000

Eigenvalues

Function	Eigenvalue	% of Variance	Cumulative %	Canonical Correlation
1	4.222[a]	100.0	100.0	.899

a. First 1 canonical discriminant functions were used in the analysis.

Function 1 standardized conical discriminant function coefficients for all selected stepwise bands

Band	Function 1	Band	Function 1
7	-.342	110	-.879
23	-.278	113	.809
67	-1.504	115	.857
77	2.445	120	.415
79	1.727	130	.499
80	-1.230	137	-.242
90	-.819	138	-.873
99	-.467	139	.502
104	-.514		

APPENDIX XXIV
FINAL (LEVEL 2) CLASSIFIED LANDSAT IMAGE USING A PIXEL-BASED
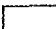SUPERVISED CLASSIFIER WITH SIX BANDS

Legend

Cloud/Background
Water
Wetland
Black Spruce
Jack Pine
Mixedwood
Dense Deciduous
Sparse Deciduous
Cut

XXV
FINAL (LEVEL 2) CLASSIFIED HYPERION IMAGE USING A PIXEL-BASED SUPERVISED CLASSIFIER WITH STEPWISE DFA BANDS
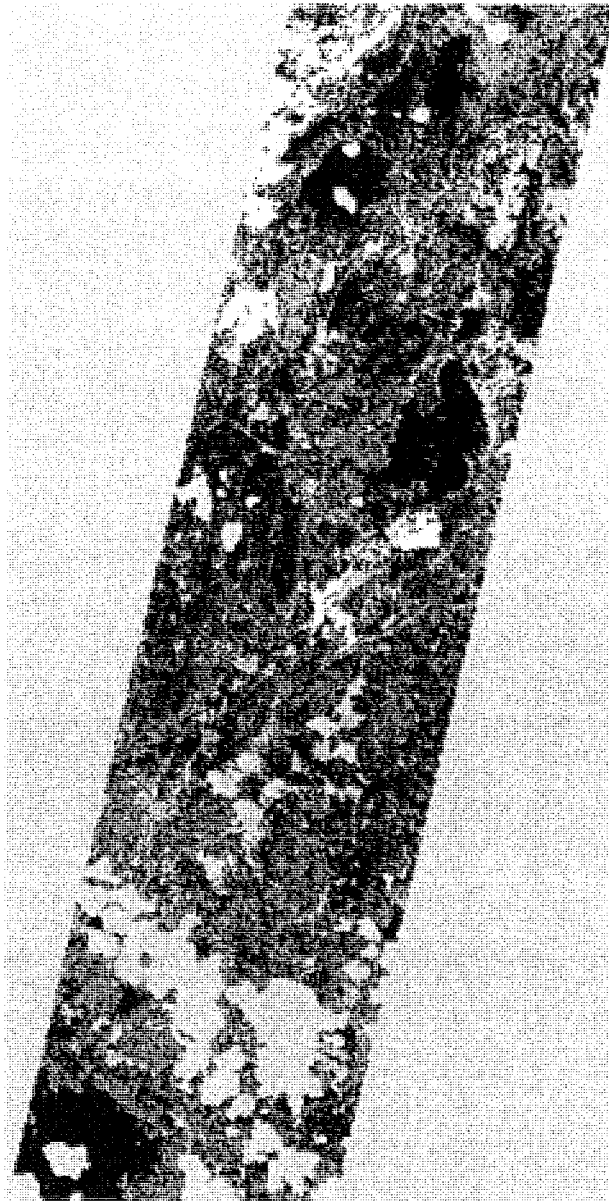
Legend
- Cloud/Background
- Water
- Wetland
- Black Spruce
- Jack Pine
- Mixedwood
- Dense Deciduous
- Sparse Deciduous
- Cut

APPENDIX XXVI
FINAL CLASSIFIED LANDSAT IMAGE USING AN OBJECT-ORIENTED
SUPERVISED CLASSIFIER WITH SIX BANDS

XXVII
FINAL CLASSIFIED HYPERION IMAGE USING AN OBJECT-ORIENTED
SUPERVISED CLASSIFIER WITH STEPWISE DFA BANDS